International Elective Master Course Module

Nonlinear Analysis of Structures: Wind Induced Vibrations

Edited by:

Victor Vîlceanu

Dr. Lars Abrahamczyk

Prof. Dr. Guido Morgenthal

Bauhaus-University Weimar

In part of the Erasmus+ SP Project Forecast Engineering

Bauhaus-Universität Weimar

International Elective Master Course Module

Nonlinear Analysis of Structures: Wind Induced Vibrations

Edited by:

Victor Vîlceanu
Dr. Lars Abrahamczyk
Prof. Dr. Guido Morgenthal

2019

The creation of these resources has been funded by the ERASMUS+ grant program of the European Union under grant no. 2016-1-DE01-KA203-002905. Neither the European Commission nor the project's national funding agency DAAD are responsible for the content or liable for any losses or damage resulting of the use of these resources.

Published by: Bauhaus-Universität Weimar, Institute of Civil Engineering, Weimar, Germany

Cover page is a photo of a project model in the wind tunnel facility of Bauhaus-Universität Weimar.

Participants of the International Elective Master Course Module:

Bauhaus-Universität Weimar

First Name	Last Name	Home Country
Alok	Sharma	India
Ahmed Adel	Ismael Elsayed Ali	Egypt
Deeya	George	India
Hermann Mauricio	Lino Wilde	Bolivia
Islam	Abdou	Egypt
Mena Michael	Zaki Abdelnour	Egypt
Reyadh	Othman	Yemen
Shèrif	Abdelghany	Egypt

Josip Juraj Strossmayer University of Osijek

First Name	Last Name	Home Country
Ana	Perić	Croatia
Benjamin	Pervan	Croaita
Dorotea	Markasović	Croatia
Ivan	Vrdoljak	Croatia
Sarah	Šćurla	Croatia
Tin	Vujčić	Croatia

Universidade de Aveiro

First Name	Last Name	Home Country
Afonso	Soares	Portugal
Diego	Mendes	Portugal
Heliodoro Daniel	Almeida Ribeiro	Portugal
Leonor	Vaz	Portugal
Rafaela	Caetano de Almeida	Portugal
Ranieri Couto	Terra	Portugal

University of Ljubljana

First Name	Last Name	Home Country
Amel	Emkić	Bosnia-Herzegovina
Jernej	Gortnar	Slovenia
Maša	Rebernik	Slovenia

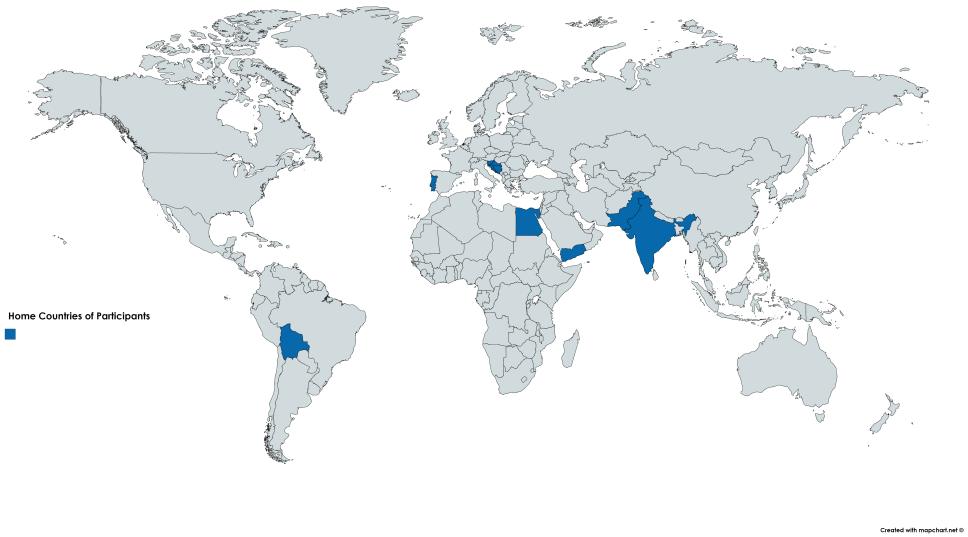

Contents

List of Tables

Foreword

The proceedings at hand are the result of the International Master Course Module: "Nonlinear Analysis of Structures: Wind Induced Vibrations" held at the Faculty of Civil Engineering at Bauhaus-University Weimar, Germany in the summer semester 2019 (April - August). This material summarizes the results of the project work done throughout the semester, provides an overview of the topic, as well as impressions from the accompanying programme.

This master course was part of the Erasmus+ Strategic Partnership, formed with partner universities from Weimar, Aveiro, Osijek, Budapest and Ljubljana. The selected students from the partner universities worked together in an international course during one semester from abroad. The Erasmus+ SP project partners are grateful for the sponsorship from the European Union by the grant no. 2016-1-DE01-KA203-002905. The succesful course in 2019 and its report would not have been possible without this generous financial support.

I. Forecast Engineering: From Past Design to Future Decisions

Erasmus+ Strategic Partnerships - Cooperation for Innovation and the Exchange of good practices

https://www.uni-weimar.de/bauing/erasmus-sp

A. *Concept*

Current and future engineering practices need highly qualified engineers trained in advanced topics of structural engineering, by using modern technologies and by developing good transversal competencies. Additionally, previous acquired knowledge and conducted experimental tests have to be collected, provided and made available and accessible to the scientific community. New forms of cooperation and training have been introduced to address this issue.

In part of the succesfully established Erasmus+ Strategic Partnership project, partners from civil engineering faculties and chairs at the Universities of Osijek, Aveiro, Ljubljana and Budapest (Fig.1) possess diverse expertise, capacities and information from many past and current research projects that leads to innovative opportunities in research and education. The aim is to help shape innovative developments in civil engineering in intercultural exchange and to promote the specialist, social and language skills of excellent junior staff.

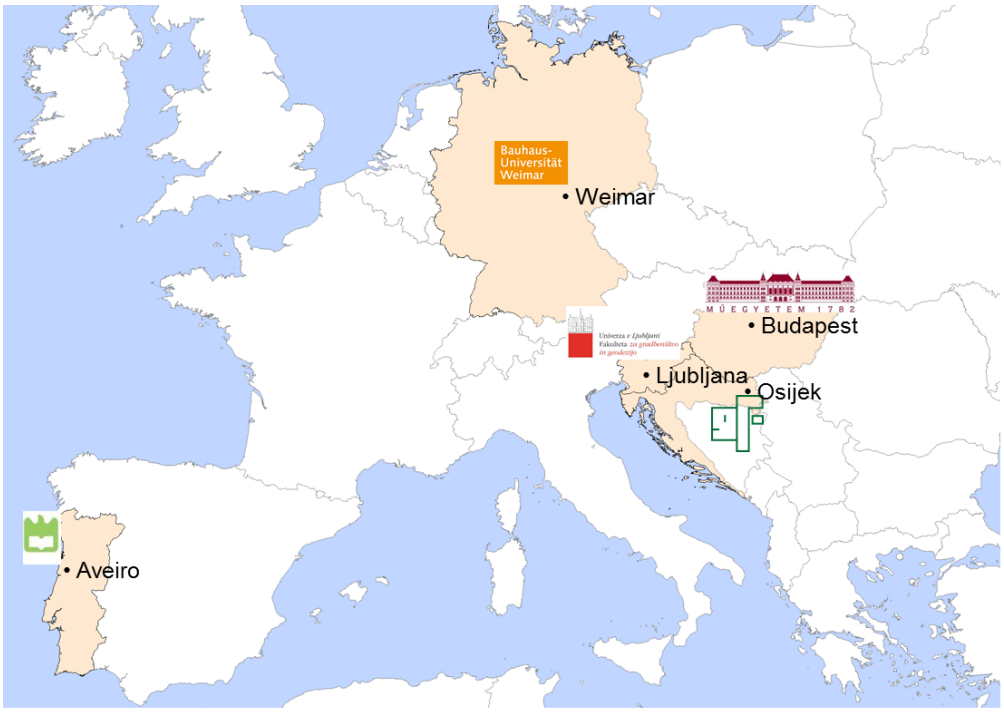

Figure 1. Project Partners of the Erasmus+ Strategic Partnership

As part of the programme Erasmus + and Key Action II: Strategic Partnerships, Bauhaus-University Weimar (Germany) worked together with the Universidade de Aveiro (Portugal), University of Osijek (Croatia), University of Ljubljana (Slovenia) and Budapest University of Technology and Economics (Hungary) for a strategic footing in structural engineering programmes. At the center of international cooperation was the exchange of technical competencies in the areas of earthquake engineering, steel and bridge construction, mathematical models and structural analysis.

The range of measures is diverse and spans the faculties of Civil Engineering and Media of the Bauhaus-University Weimar. Research and study visits, summer schools, tele-teaching events and guest lecturerships were planned. Particular attention was paid to interdisciplinary research and the promotion of master and doctoral students.

Erasmus+ is the education, youth and sport program of the European Union. Erasmus+ brings together existing EU programs for lifelong learning, youth and sport, as well as European cooperation programs in higher education. The seven-year program aimed to enhance skills and employability and to promote the modernization of education, training, child and youth services.

B. Objective

The project Erasmus+ Strategic Partnership through its partner institutions has established an International Elective Master course module (IntEIM) for M.Sc. students. New procedures were introduced to achieve the objective of the project and to bundle the capacities from its partners. The project benefited from the recently conducted research projects and ensured demands on high quality education and link to current research topics.

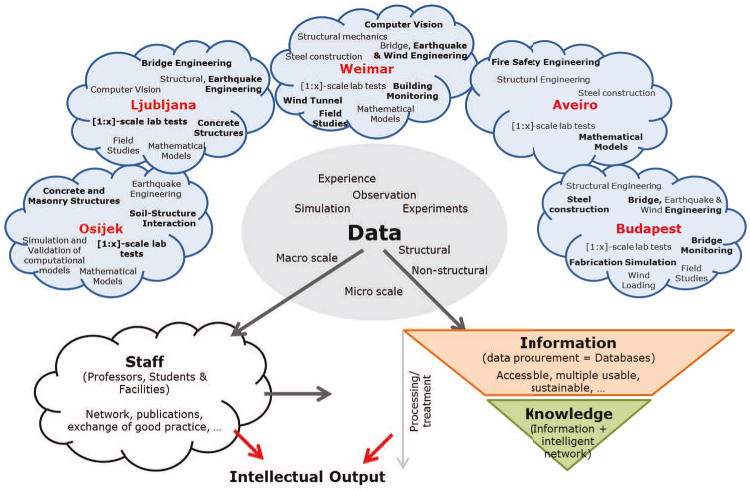

Figure 2. Competencies and Network of the Project Partners

The IntEIM course module for M.Sc.students arranged a blind test competition for international teams composed by the strategic partners. The project teams were requested to compare the results from the experiments with numerical techniques. The objective is to develop a framework of best practice through the establishment of networks. The participating students were working together in interdisciplinary teams to increase their knowledge and understanding of the topic.

The conduction of the learning & teaching activity was arranged in 3 phases:

- Kick-off meeting: All participants came together to be introduced into the project topics, to compose the teams and create networks for the virtual activities (Group of 5, respectively 6 students). The participatns attended the lectures and seminars to be introduced into the background of the project. This time frame was from April 7th to 12th, 2019 at Bauhaus-University in Weimar.
- Independent work was done over the semester, supported regularly by flipped classes and video-meetings.
- Project closing week: All the participants came together for a second week to present and compare the achieved results with the experimental tests, as well as to finalize the reports. The time frame was from August 12th to 16th, 2019 at Bauhaus-University in Weimar.

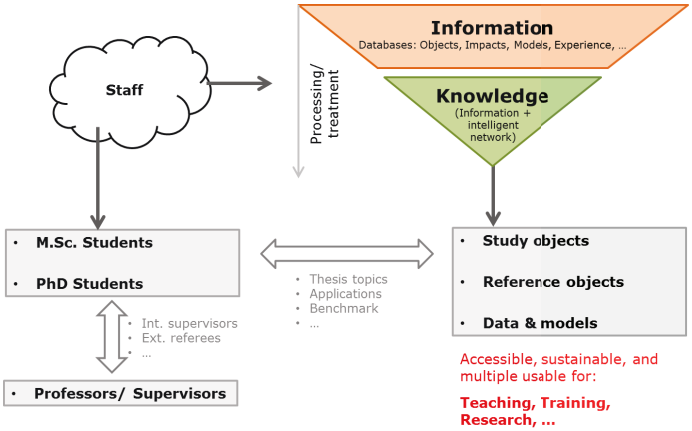

Figure 3. Competencies and Network of the Project Partners

II. IntEIMsc Course Description

A. General Information

International Elective Master Course Module (IntEIMsc) "Nonlinear Analysis of Structures: Wind Induced Vibrations" was a course of Graduate University Study Programme in Civil Engineering. The teaching activity & the course learning coordinator was Professor Guido Morgenthal (Chair of Modeling and Simulation of Structures) and the chair assistants, Dr. Tajammal Abbas, Igor Kavrakov, Samir Chawdhury, Luis Federico Vilchez, Samuel Gebretensaye and Victor Vilceanu. The course language was English and it was delivered with two weeks of lectures, project work and practice hours. By successful completion of the course the student was awarded with 6 ECTS credits. The course was established within the "Erasmus+", "Cooperation for innovation and the exchange of good practices", "Strategic partnerships in higher education", "Development of innovation" project entitled "Forecast Engineering: From Past Design to Future Decisions (Project reference: 2016-1-DE01-KA203-002905). The course was taught at the Faculty of Civil Engineering at the Bauhaus-University of Weimar. The course introduced a state-of-the-art education, by complying with the objective of the project.

B. Outline

Wind Engineering is a particular field of Civil Engineering that evaluates the resistance of structures caused by wind loads. Bridges, high-rise buildings, chimneys and telecommunication towers might be susceptible to wind vibrations due to their increased flexibility, therefore a special design is carried for this aspect. Advancement in technology and scientific studies permit us doing research at small scale for more accurate analyses. Therefore scaled models of real structures are built and tested for various construction scenarios. These models are placed in wind tunnels where experiments are conducted to determine parameters such as: critical wind speeds for bridge decks, static wind coefficients and forces for buildings or bridges. The objective of the course was to offer insight to the students into the assessment of long-span cable-supported bridges and high-rise buildings under wind excitation. The participating students worked in interdisciplinary teams to increase their knowledge in the understanding and influences on the behaviour of wind-sensitive structures. The students shared their experiences and established their network. At the end of the course all international project teams had to present the achieved results as well as to submit a final report. Both were used for the final evaluation.

The set up project dealt with wind tunnel experiments from which data was extracted to compare with the data given by wind-structure interaction CFD technique (CFD-computational fluid dynamics). Such pedagogical approach did not exist at any master course from the involved partners, therefore it enhanced the quality and attractiveness of the course. The Intellectual Output, carried out by the Bauhaus-University Weimar, created a network for the participating M.Sc. students, shared current state of best practice and achieved results among all participants. Bauhaus-University Weimar supported the establishment of the project by the E-learning lab and in cooperation with the Chair of Instructional Design. Course materials were additionally prepared, the results were treated for the supplementation into the database and students results were summarized for a final publication.

C. Pre-requisites

Students were selected based on the prior knowledge of Structural Dynamics, Structural Analysis, Fluid Mechanics, as well as construction and building of materials. English language of at least A2 level was mandatory.

D. Syllabus

The course was taught using lectures, seminars, workshops, laboratory experiments, distance education, individual and group assignments, multimedia, internet and mentoring.

The course was delivered in three main parts:

- First part or introductory week was the kick-off meeting. It was comprised of lectures, exercises and team building measures. This part was conducted from April 8th to 12th 2019. The aim of first part was to introduce the project itself, to compose the international teams (group of 5,6 students), to present and explain the experimental facilities, to explain the necessary background and advanced topics for project completion.
- Second part was the independent or project group work over the whole summer semester (April-August). Groups of 5 or 6 students were assembled from different partner universities. Groups were assigned at the beginning of the course (8th of April). Group assignments were handed over to the students at the end of the course (on April 12th). The international teams had to independently work on the given tasks using virtual communication technologies. Further new solving strategies were discussed with the learning & teaching activity coordinator and

the partner assistants, together.The topics required for all the groups to build scaled models and to test at the wind tunnel to be later compared with the CFD numerical techniques.
- Third part consisted in project closure from August 12th to 16th, 2019. The project closing was composed of group work and presentation by the participants. The aim was to do the blind test competition (comparison between numerical and experimental data), to present the project teams and to discuss the results, to finalize in form of a report, to supply the used material and results for future generations and further applications for consideration into the project database.

E. Intended Learning Outcomes

Upon successful completion of this course the participant was able to:
- Use specialized advanced software
- Assess long-span bridges and high-rise buildings under wind excitation
- Describe the expected behaviour and results of an experiment
- Work in an international group and practice their management, presentation and language skills

F. Assessment Criteria

The students were required for class attendance and participation, group project work, report and presentation. Upon successful completion of the report (60 %), presentation (30 %) and by additionally verifying the literacy (10 %) the students were awarded with the grade (1-5) and 6 ECTS credit certificate if they succeeded with no less than 60 %. Attained points (percentages) in relation to grades: 90 - 100 % excellent (1); 80 - 89 % very good (2); 70 - 79 % good (3); 60 - 69 % sufficient (4); 0 - 59 % insufficient (5).

G. Monitoring and evaluation of learning outcomes

Monitoring and evaluation of learning outcomes was achieved through individual assessment criteria and class attendance and participation. Each participant had to complete a survey form, a questionnaire sent by e-mail with following content:
- Quality of counselling and accessibility of information
- General procedure of the activity
- Content
- Problems encountered

H. Monitoring and evaluation

Monitoring and evaluation of the course workload were assigned through learning outcomes, with respect to teaching methodology and assessment criteria. A short report was directed by the coordinator which included feedback from the course coordinator to the participants with following content:
- Learning outcomes
- Achieved/trained competencies
- Benefits for the lecturer

Table I
TIME SCHEDULE OF THE FIRST WEEK OF THE ERASMUS WIND COURSE - APRIL 2019

Hours	**Sunday (7/04)**	**Monday (8/04)**	**Tuesday (9/04)**	**Wednesday (10/04)**	**Thursday (11/04)**	**Friday (12/04)**
9:15 - 10:45		Lecture - Wind Induced Vibrations (Room 101, M7b)	Wind Tunnel Introduction (-1 Story, M7b)	Finite Element Method (Sofistik) for bridge modeling (Luna Blue M7b)	Seminar Wind-structure solver (M13A, Computer pool)	Project Work (M13A, Computer pool)
10:45 - 11:00	Coffee break					
11:00 - 12:30		Lecture - Wind Induced Vibrations Room 101, M7b	Workshop - Introduction (Belvedere Allee 1b)	Finite Element Method (Sofistik) for bridge modeling (Luna Blue M7b)	Seminar Wind-structure solver (M13A, Computer pool)	Project Work (M13A, Computer pool)
12:30 - 13:30	Lunch break					
13:30 - 15:00	Weimar City Tour (Wielandplatz)	Lecture - Wind Induced Vibrations and Structural Dynamics (Room 101, M7b)	Introduction to CFD Wind-structure solver (M13A, Computer pool)	Seminar Wind-structure solver (M13A, Computer pool)	Project Work (M13A, Computer pool)	Project Work (M13A, Computer pool)
15:00 - 15:15	Coffee break					
15:15 - 16:45		Projects description Room 101, M7b	Introduction to CFD Wind-structure solver (M13A, Computer pool)	Seminar Wind-structure solver (M13A, Computer pool)	Project Work (M13A, Computer pool)	Project Work (M13A, Computer pool)
19:00 - 22:00			Barbecue (Projekt Eins, Schutzengasse)			

Table II
TIME SCHEDULE OF THE SECOND WEEK OF THE ERASMUS WIND COURSE - AUGUST 2019

Hours	**Monday (12/08)**	**Tuesday (13/08)**	**Wednesday (14/08)**	**Thursday (15/08)**	**Friday (16/08)**
9:15 - 10:45	Status Presentation (Luna Blue, M7b)	CFD Post-processing (Computer Pool, M13A)	Project Work (Computer Pool, M13A)	Presentation Practice Session (Computer Pool, M13A)	Preparation final report (Computer pool, M13A)
10:45 - 11:00	Coffee break				
11:00 - 12:30	Wind Tunnel Experiments (-1 Story, M7b)	CFD Post-processing (Computer Pool, M13A)	Project Work (Computer Pool, M13A)	Preparation Final Report (Computer pool,M13A)	Final Presentations (Lecture Hall C, M13C)
12:30 - 13:30	Lunch break				
13:30 - 15:00	Wind Tunnel Experiments (-1 Story, M7b)	CFD Post-processing (Computer pool, M13A)	Preparation Final Report (Computer pool, M13A,)	Preparation Final Report & Presentation (M13A, Computer pool)	Submitting Final Report (Computer pool, M13A)
15:00 - 15:15	Coffee break				
15:15 - 16:45	Wind Tunnel Experiments -1 Story, M7b	CFD Post-processing (Computer pool, M13A)	Preparation Final Report (Computer pool, M13A)	Preparation Final Report & Presentation (Computer pool, M13A)	Submitting Final Report (Computer pool, M13A)
19:00 - 22:00	Team Building: Sport & BBQ, (Falkenburg, University Sport Centre)				

III. PROJECT ASSIGNMENT 1

Study of wind loading on high-rise building: Burj Khalifa

(a) Study and literature review about Burj Khalifa case (geometry, material properties, design, building conditions).
(b) Build an equivalent FEM model (Sofistik).
(c) Modelling and simulation of the cross-section at the base in VXflow and determine the static wind coefficients and check at different angles of attack.
(d) Build the corresponded cross-section using 3D printer (.STL format) for experimental tests in the Wind Tunnel and measure time-history for different angles of attack.
(e) Modelling and simulation of the building in multi-slice simulation (both static and dynamic tests) in VXflow and determination of the base force.
(f) Build a scale model of the high-rise building and measure the time-history of the base force (spectral distribution).
(g) Results comparison between numerical and experimental procedures.
(h) Submission of the reports and presentation of the results.

Burj Khalifa (Source image: https://en.wikipedia.org/wiki/File:Burj Khalifa building)

Following report with the pages from 1 to 47 correspond to pages 19 to 65 of the report at hand

Project report

Study of Wind Loading on High-Rise Building: Burj Khalifa

Submitted by

George, Deeya, Student at Bauhaus University, Germany;
Mendes, Diego, Student at Aveiro University, Portugal;
Rebernik, Masa, Student at Ljubljana University, Slovenia;
Abdelnour, Mena, Student at Bauhaus University, Germany;
Scurla, Sarah, Student at J.J.Strossmayer University, Croatia;
Vujcic, Tin, Student at J.J.Strossmayer University, Croatia

BAUHAUS-UNIVERSITÄT WEIMAR

Faculty of Civil Engineering

Table of Contents

page

1 Abstract

High-rise buildings are susceptible to wind vibrations due to their large slenderness and flexibility, therefore special attention must be given to evaluate the resistance of the structure against the wind loads. The aim of this project is to provide insights into the assessment of high-rise buildings under wind excitations. To this end, a number of case studies have been selected to preform experimental and computational fluid dynamics (CFD) studies of wind-structure interaction. The outcome of these studies if to quantify the aerodynamic forces and to validate the numerical simulations using experimental methods at the wind tunnel facility at Bauhaus-University.

2 Introduction

2.1 Motivation

To the course of "Nonlinear Analysis of Structures Wind Induced Vibrations" taught in Bauhaus University in Weimar, the group was given the opportunity to work with the iconic building: Burj Khalifa, situated in Dubai – the tallest building in the World. From the beginning, the most challenging tasks, was to deal with the wind loads, due to the tower's dimensions, such as its height, slenderness and aesthetics.

The overarching aim of the project is to consider the behavior of the structures due to the wind loads. Two methods were used to achieve the purpose of the study; Wind tunnel test and Computational Fluid Dynamics (CFD) simulations. Additionally, the response of the structure due to the Vortex Induced Vibration (VIV), shown in Figure 1, was investigated and the possibility to reduce its effects on future high rise buildings.

From the literature, it was understood that the shape of the structure was chosen as a "Y" shape in plan, as illustrated in Figure 2, to reduce the wind effects on the structure, moreover the spiral shape of the structure was adopted to break the correlation between the wind forces along the elevation of the structure, refer to Figure 3.

Finally, the procedures and the limitations of producing the study models that could capture the real building phenomena were discussed to acknowledge the reliability and the accuracy of both wind tunnel test models and CFD models. Since the methodology/approach that is used in each of the methods are totally different, in addition to which method will capture to efficient to capture the different structural features to resist against wind loads.

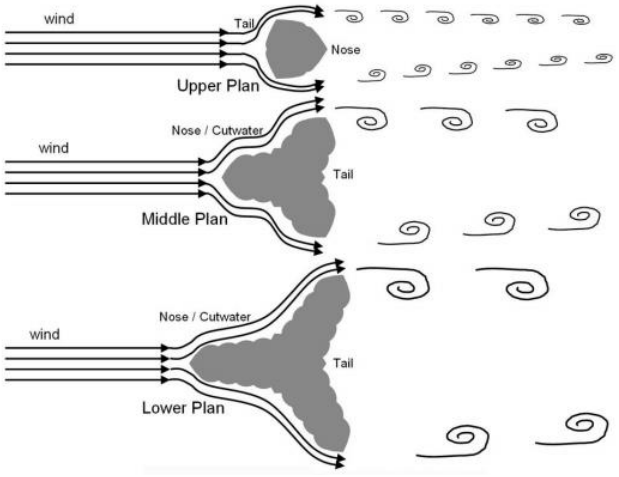

Figure 1 : Vortex Shedding Behaviour

[Source: "Burj Dubai: Engineering the World's Tallest Building"]

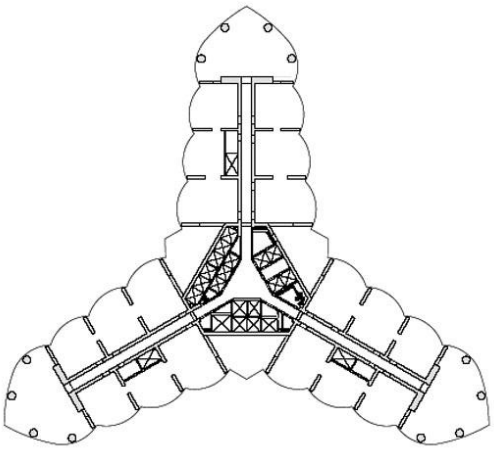

Figure 2 : Base Cross Section

[Source: https://csengineermag.com]

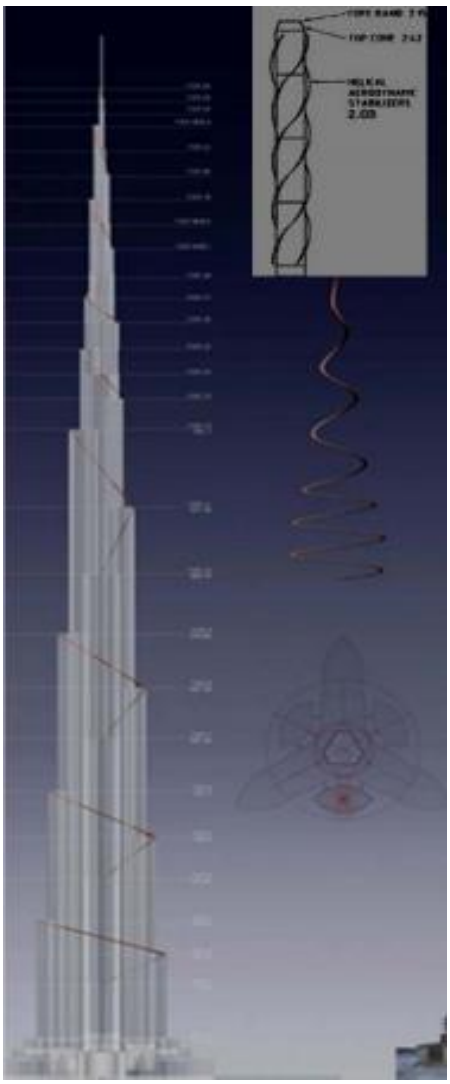

Figure 3 : Tower Spiral Shape

[Source: A. Abdelrazaq, Validating the Structural Behaviour and Response of Burj Khalifa]

2.2 Objectives

In order to develop the project accordingly, a few tasks were imposed so that the structure could be properly studied. Two studies divided in two parts, experimental and numerical, which were after compared in order to test whether the CFD study (numerical part) is suitable enough to substitute the Wind Tunnel Test in future designs, which represents a significant monetary cost.

The division of the study was according the following list:

1. Experimental Tests (Wind Tunnel Tests):
    a. Static study with constant cross-section, which corresponds to the largest cross section, where it is located at the base of the tower. The result of the study, after processing the measurements, is the aerodynamic coefficients of the cross-section which are drag coefficient, lift coefficient and moment coefficient.
    b. Static study with varying cross-sections, using the exact shape of the tower, reflecting the setbacks and cross sectional changes along the height of the tower. The result of

the study is the base forces at the base of the model, which are shear forces in both horizontal directions, torsion and overturning moment.

2. Numerical Simulations (CFD) using VXflow software:
    a. Static study with constant cross-section, corresponding to the same cross section used in the wind tunnel test, and the coefficients are calculated directly from the software used for the simulation.
    b. Static study with varying cross-sections. Only 7 slices (slice means cross-section in the used software language), corresponding to 7 different cross sections along the height of the tower.
    c. Dynamic study with varying cross-sections. Only 7 slices as previous were used and the results where the critical flutter speed of the different slices.
3. Comparison of the wind coefficients and base forces from the experiments and CFD simulations.
4. Discussion about the reliability of each method and whether the results are realistic corresponding to the real behavior of the structure.

3 Methodology

The study wind tunnel tests were performed in the wind tunnel test facility at Bauhaus University shown in Figure 4, which has the following characteristics:

- Low-speed wind tunnel Göttingen type: Wind-speed: $U = 1 - 30\ m/s$
- Open and a closed measuring
- Degree of turbulence: 0.5% (closed measuring section)
  0.8% (open measuring section)
- Measuring section: W m

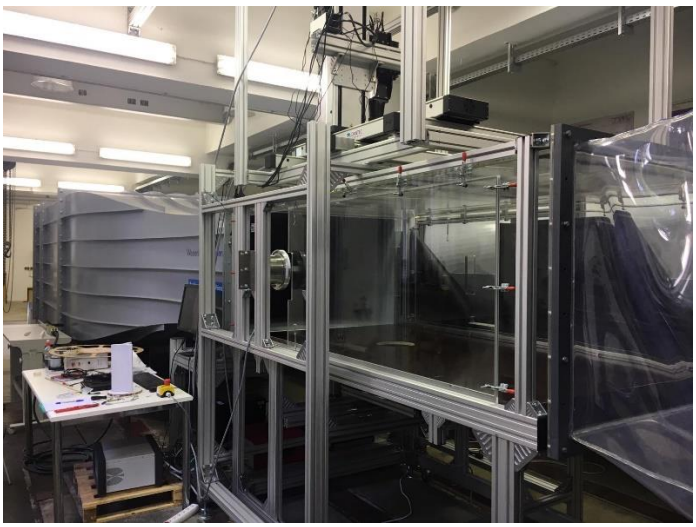

Figure 4 : Wind Tunnel Facility at Bauhaus University

Each model is fixed so that the base of the model is at the same level with the wind tunnel floor, then from beneath the model a senor is attached to the base which measures forces acting on the model when the test starts. Then, the data obtained from the sensor is processed and the start of the signal is removed to avoid any the fluctuations at the beginning of the recording. Finally, the average of each

record is obtained corresponding to the forces at the base and in the case of the constant cross-section the aerodynamic coefficients are calculated and compared to the corresponding case of the CFD simulations, however in the case of the varying cross section the forces are scaled up and compared to the corresponding forces of the CFD simulations.

The CFD simulations where performed using VXflow Software shown in Figure 5. VXflow is a flow solver based on the Vortex Particle Method. Using the software post processing tools, the aerodynamic coefficients are calculated for the case of the constant cross section and in the case of the multi-slice, the forces where directly extracted from the output files of the calculations.

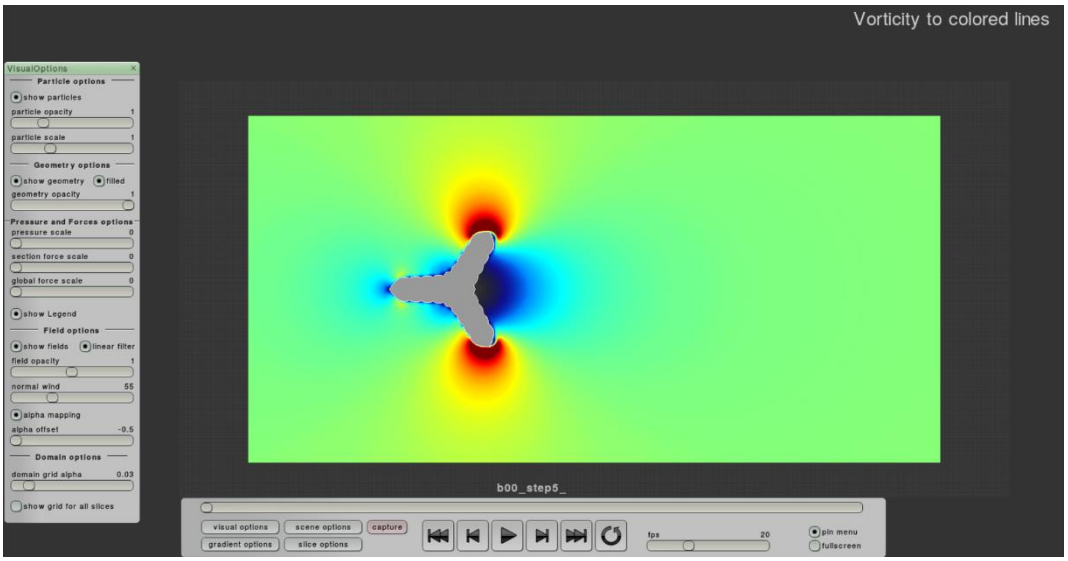

Figure 5 : User Interface in VXflow

4 Literature Review

4.1 Geometry of the Tower Facts

Burj Khalifa is considered as the tallest building in the world with a height of 828 meter. The tower is built using high-performance concrete with around 600 m above the ground level and the remaining meters are of steel construction. Tower's shape was chosen as 'Y' shape in plan, as shown in
Figure 6, to reduce the effect of the wind forces on the structure, as a consequence of that, the buttressed core structural system was the ideal option with the addition of 3 wings of shear walls. With the given structural system the tower structural behavior was extremely stiff laterally and torsionally.

Additionally, by reducing the cross section of the tower with creating setbacks at certain heights, two objectives were reached: first, the spiral stepping pattern of the tower like using spiral shape in chimney to break the correlation between the wind forces along the height of the tower; second, the building setbacks pattern is achieved by using both walls and columns which results in a steady load path and consequently the structural difficulties of column transfers were eliminated.

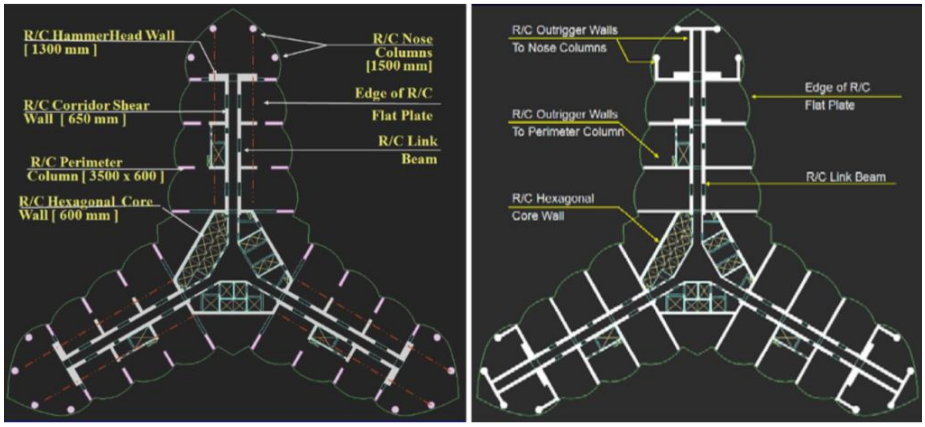

Figure 6 : Tower Structural System

[Source: A. Abdelrazaq, Validating the Structural Behavior and Response of Burj Khalifa]

Moreover, due to the usage of high-performance concrete resulted in a limitation of the movement along the height of the tower, especially with the reduction of the cross sections. Also the pump ability and using slip- and climb-form technology integrated with the advantage of the high-performance concrete results into far more construction speed compared to the steel structure.

4.2 Tower Wind Studies

The design team of the tower broadly studied the wind load effects on the tower through a large number of wind tunnel tests on small-scaled model of the tower. By doing the tests for different types of model: rigid-model force balance, aero-elastic model; in addition to pressure measurements, the behavior of the structure under the wind forces was extensively understood.

Wind-induced vibrations was a matter of concern, to avoid the formation of vortex shedding refer to Figure 7, which could set the whole structure in undesired vibrations and large displacement.

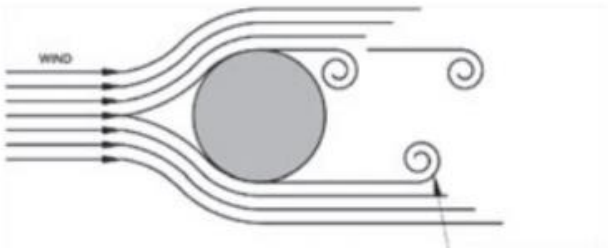

Figure 7 : Representation of a Vortex on a Circular Shape

[Source: “Burj Dubai: Engineering the World’s Tallest Building”]

4.2.1 Observed Wind Phenomena

According to “Bringing to i fe the World’s Tallest Structure” article, by Jonathan Weigand, aero-elasticity refers to the science of studying inertial, dynamic, and aero-dynamic forces. The design team performed many static wind tunnel tests to obtain roughly the dynamic reaction of the tower due to the acting wind loads which were used to obtain the stiffness, shape proportions.

Additionally, the responses of the structure from different directions could be identified, for example and as shown in Figure 8, the higher and lower wind impact effect could be selected which later contributed to the decision of choosing the tower orientation.

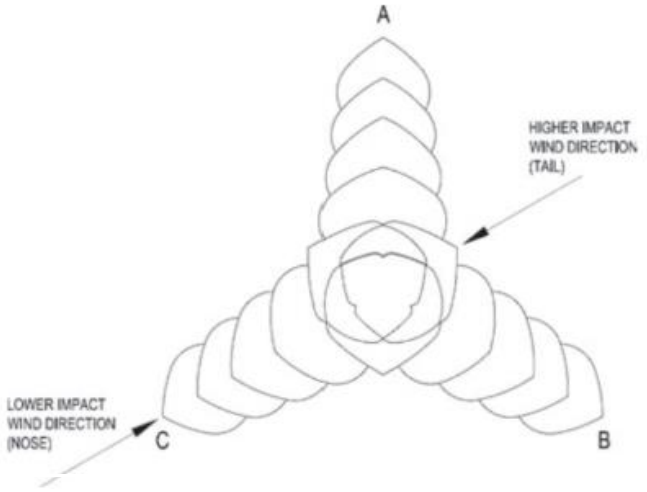

Figure 8 : Representation of the Most and Least wind effects
[Source: "Burj Dubai: Engineering the World's Tallest Building"]

Engineers, finally, used the wind tunnel data, the shape was optimized and refined in the spiral shape as shown previously to reduce both wind effects.

4.2.2 Tower Mode Shapes and Frequencies

Through finite element model, the designers calculated the critical model shapes of the tower and the corresponding structural periods, which were 11.3 seconds for the first model (lateral sway), 10.2 seconds for the second model (perpendicular lateral sway) and the fifth mode (torsion) is 4.3 seconds.

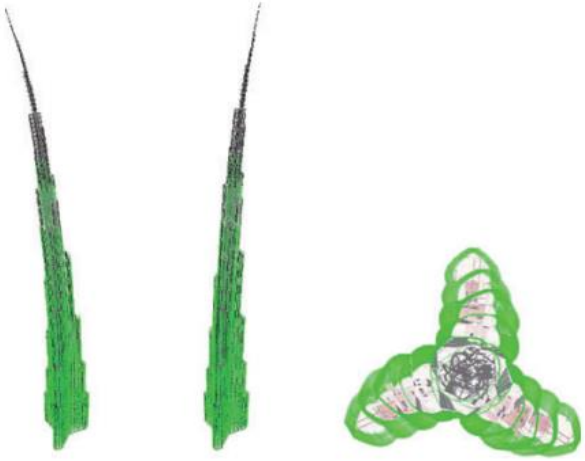

Figure 9 : Dynamic mode shapes
[Source: "Burj Dubai: Engineering the World's Tallest Building"]

4.2.3 Design Wind Speed

According to the article "Burj Dubai Tower" by Peter A Irwin and William F Baker, quotes that the wind speed of 55 m/s is a reliable value, thus this is the used wind speed for the CFD simulations.

5 Static Study of Section Model

As a first step to investigate the tower against wind loads effects, a base cross-section is chosen to be studied as shown in Figure 10. The purpose is to inspect the chosen architectural shape behavior with reference to the calculated aerodynamic coefficients, where the results from the wind tunnel test and CFD simulation are compared in the sense of reliability and accuracy of both methods.

5.1 Model Building

5.1.1 Scaling of the Model

The chosen cross-section plan was scaled down to 1:600 compared to the plan dimensions of the original tower. In addition, the height of the tower was selected to be 30 cm and then the model was fixed to a wood base, marked with degrees as shown Figure 11.

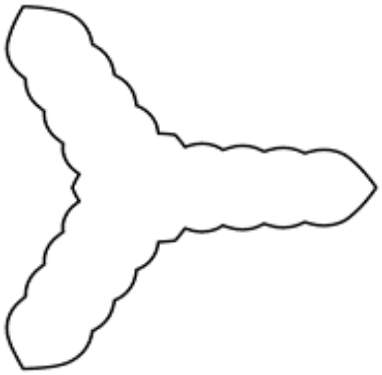

Figure 10 : Section Model of the Static Study

Figure 11 : Section Model fixed on Wood Base

5.1.2 Printing of the Model

The model was drawing using 3D-AutoCad with the following properties:

1. The model is hollow from inside to reduce the cost of printing.
2. Model wall's thickness is cm with a top base of cm
3. An opening of 1cm-diameter, is made at one side of the model to facilitate the extraction of the excess printing powder.
4. Finally, the infiltration process, where a very strong glue was used to pint all the sides of the model thus the printing powder is coherent enough and improve the strength of the model.

From 3D-AutoCad file model, an STL file is prepared to be suitable for the 3D printing as shown in Figure 12.

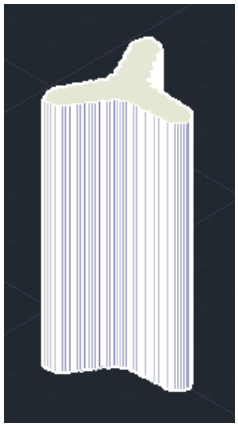

Figure 12 : 3D Model in STL format

The material used to make the 3D model was PXL with infiltration. The Modulus of Elasticity of PXL is as shown below:

$$E_m = 9450\ MPa$$

The surface of the model had to be dusted to remove the excess powder from the surface. The prepared 3D model was then fixed to a circular base with angles marked on it as mentioned previously with a total weight of the model including its base is 2.25kg, refer to Figure 13.

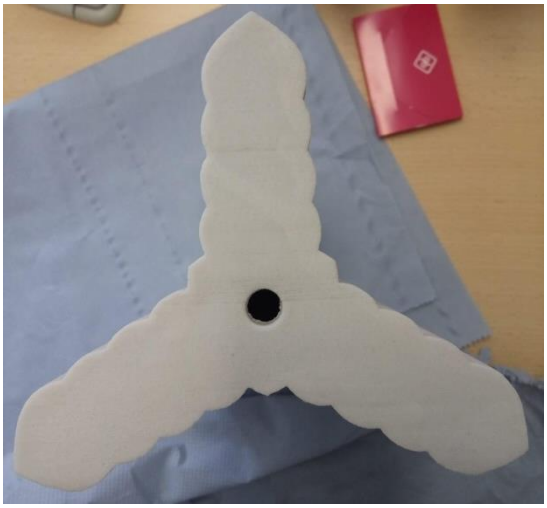	
Model's opening to remove excess powder.	3D model in the 3D printing machine.
	
Dusting the model to remove excess powder.	Infiltration process of model's surface

Figure 13 : Sectional Model Building

5.2 Wind Tunnel Test

The wind tunnel test was conducted in a closed-circuit with a wind velocity of 3m/s. The section model was tested on a 6 degree-of-freedom sensor to determine the forces as shown in Figure 14 and consequently calculate the aerodynamic coefficients.

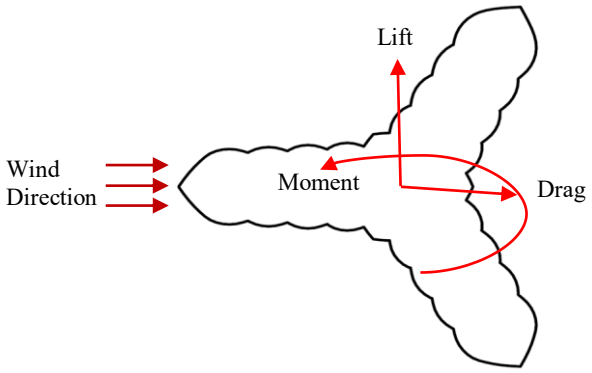

Figure 14 : Lift, Drag and Moment Directions

Thirteen different angles from -60 to +60 degrees with 10 degree increments were investigated, refer to Figure 15. The test was conducted two times to check if there were any discrepancies. The sampling rate was taken as 200 Hz which is greater than the model frequency (rigid model behavior is assumed).

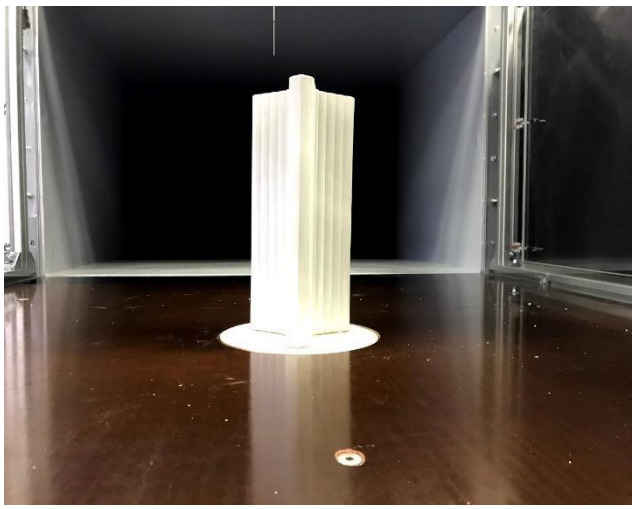

Figure 15 : 3D model in the wind tunnel

Readings for each angle were taken for five minutes. The first minute was cut from the readings as the values were lower in the beginning of the recording. The test outputs considered for the study are:

- Force in Y-direction FD (Drag force)
- Force in X-direction FL (Lift force)
- Torsion in Z-direction FM (Torsion moment)

Average of each of the three time histories were taken which were used to calculate the wind coefficients (CL, CD and CM) and the base force.

$$C_L = \frac{F_L}{\frac{1}{2}\rho B U_\infty^2}; C_D = \frac{F_D}{\frac{1}{2}\rho D U_\infty^2};\ C_M = \frac{F_M}{\frac{1}{2}\rho B^2 U_\infty^2}$$

Where,

FD: is the drag force, which is by definition the force component in the direction of the flow velocity (N),

FL: is the lift force, which is the force component in the perpendicular direction of the flow velocity (N),
FM: is the twisting moment acting (Nm),
ρ: is the mass density of the fluid,
U∞: is the flow speed of the object relative to the fluid,
D and B are projections of the cross-section perpendicular and along the wind direction as shown in Figure 16.

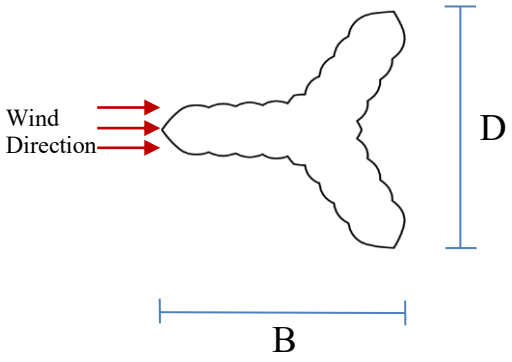

Figure 16 : B and D projections

5.2.1 Wind Tunnel Test Results

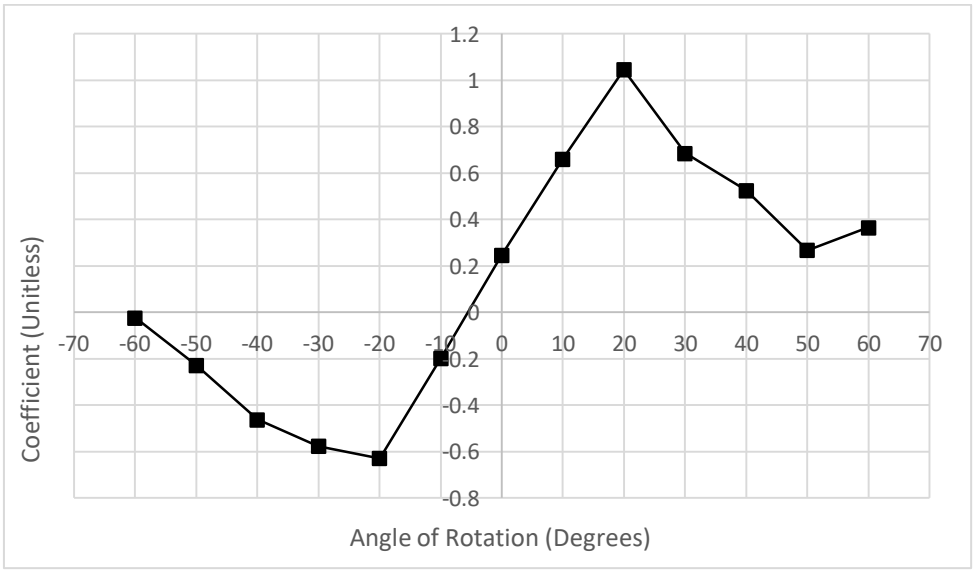

Graph 1 - Lift Coefficient for the Section Model

Lift coefficients are calculated based on forces acting on the model that are perpendicular on the wind direction. The model shows high lift forces at +20 and -20 degrees while ate 0, +60 and -60 shows minimum values.

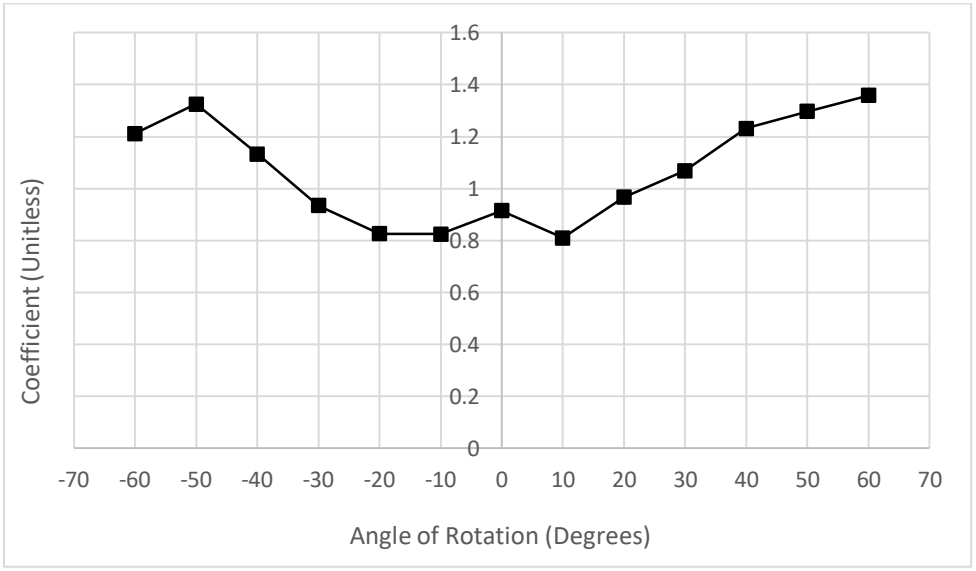

Graph 2 - Drag Coefficient for the Section Model

Drag coefficients are calculated based on forces acting on the model in the same direction of the wind load. Thee model shows high drag forces at angles between 50 and 60; and between -50 and -60 which concedes with the actual building behavior where the higher drag forces are at the tail, however at 0 degree (at the nose) the drag forces are lower than the tail of the section model.

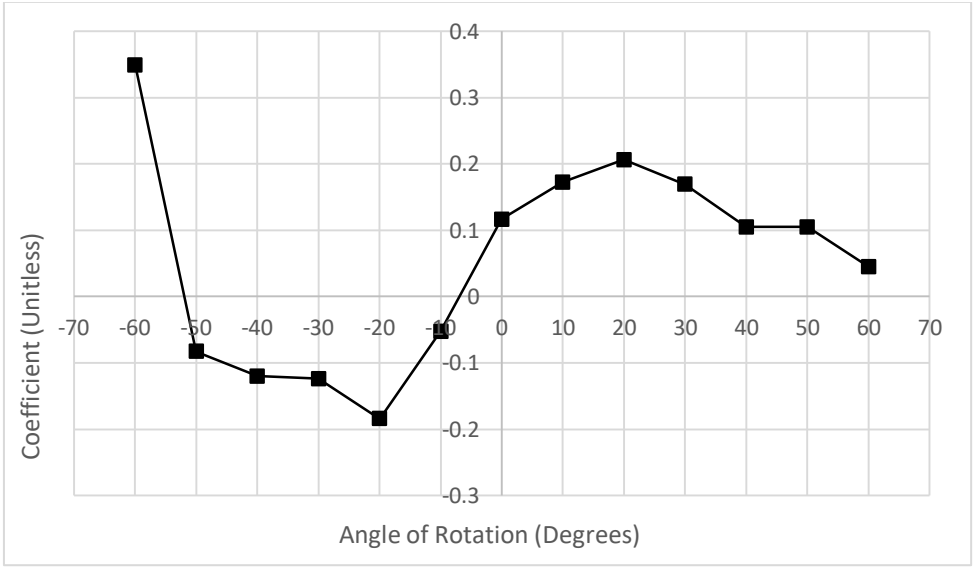

Graph 3 - Moment Coefficient for the Section Model

Moment coefficients are calculated based on the forces acting on the direction of the wind loading. The model shows high moment forces at +20 and -20 degrees, however the higher value at -60 can be considered as an outlier since it's different from the followed pattern of the forces in the positive and negative directions.

5.3 CFD Simulation

5.3.1 CFD Definition

Computational fluid dynamics (CFD)[1] is a branch of fluid mechanics that uses numerical analysis and data structures to analyze and solve problems that involve fluid flows. Computers are used to perform the calculations required to simulate the free-stream flow of the fluid, and the interaction of the fluid (wind in the present case) with surfaces defined by boundary conditions.
Initial validation of such software is typically performed using experimental apparatus such as wind tunnels, as in the case of the present project. In addition, previously performed analytical or empirical analysis of a particular problem can be used for comparison.

5.3.2 VXflow Software

VXflow is one of the software to perform CFD simulation, where it is a flow solver based on the Vortex Particle Method (the particle method is utilized to discretize the Navier-Stokes equations and to evolve the fluid flow in time).
The software will be used for both static and dynamic studies as it will be explained separately in each corresponding section. As indicated in 4.2.3, a wind speed of 55 m/s was used to perform the calculation of static wind coefficients.

5.3.3 Numerical Model Configuration

Base cross-section was modelled, based on an AutoCAD drawing of the Tower. The drawing consisted of small line elements, which were redrawn as arcs to lower the number of elements and panels in order to simplify the model and to match the requirement of modelling in VXflow, in the end 288 panels (number of panels should be between 250 and 300 panels) of approximately equal length were used. The modelled cross-section in VXflow is shown in Figure 17. The solver steps were chosen as 20000 steps to insure stability of the results.
In order to get the explore the geometry of the Section model (matching the same criterial of the wind

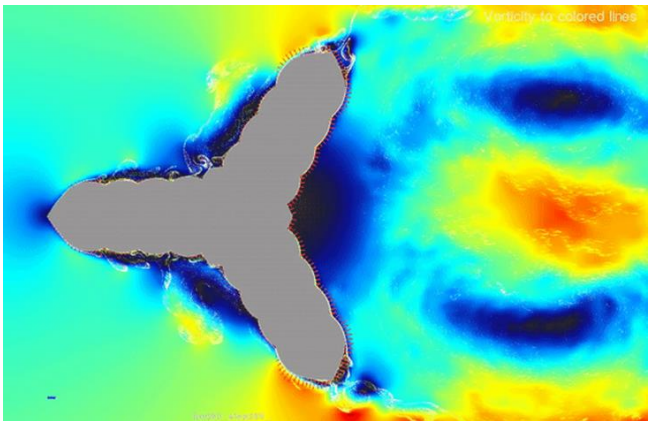

Figure 17 : Section Model in VXflow

tunnel test), 14 different attack angles were used to test the cross-section, start from -60 to +60 including 0 degrees, additionally due to the similarity of the cross-section the chosen angles are considering all possibilities of wind loading on the cross-section as shown in Figure 18.

[1] https://en.wikipedia.org/wiki/Computational_fluid_dynamics

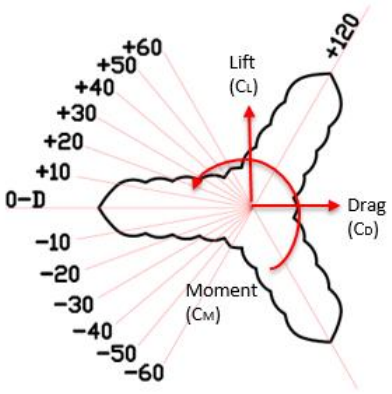

Figure 18 : Degrees of Rotations

The files were run with high processing capacity computers, the files of this study took 72 hours to get reliable results. Then another VXflow tool, VXPost, is used to process the results and calculate the wind coefficients.

5.3.4 CFD Simulation Results

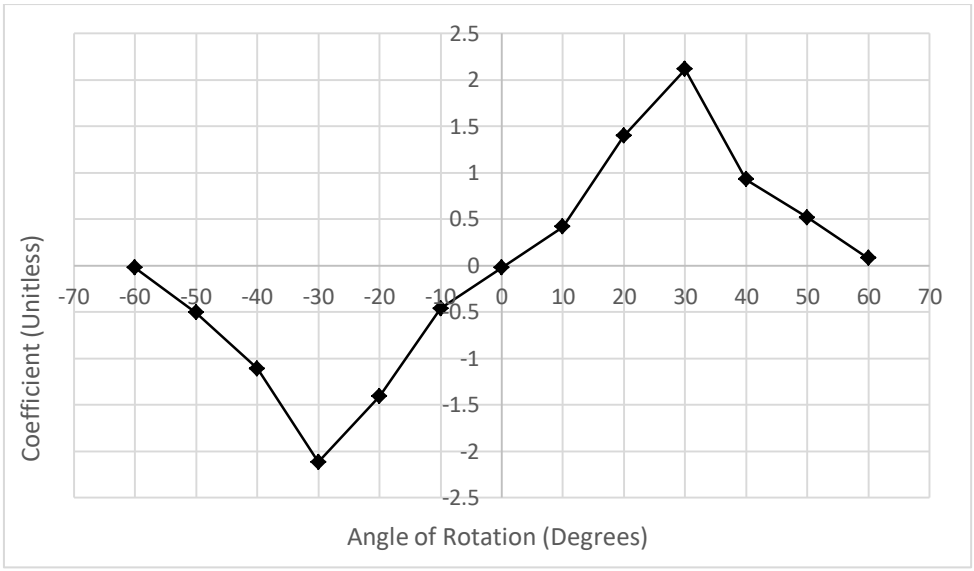

Graph 4 - Lift Coefficient for the Section Model CFD Simulation

Lift coefficients are showing higher values at angles of rotation +30 and -30 degrees while near zero values at angles of 0, -60 and +60. The result is different than the calculated values from the wind tunnel test, where it shows maximum lift coefficients at +20 and -20 degrees, as it will be explained and justified in the results comparison.

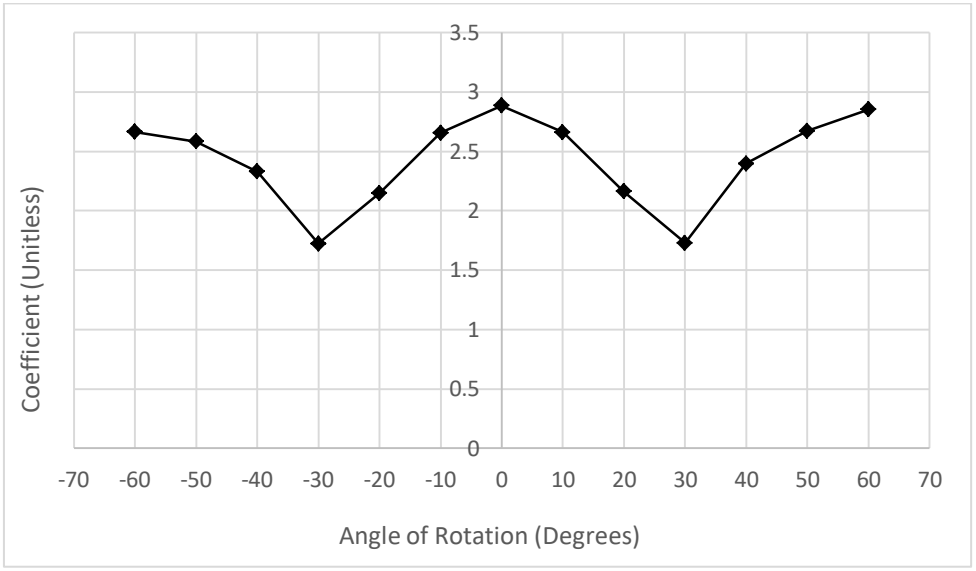

Graph 5 - Drag Coefficient for the Section Model CFD Simulation

As shown in Graph 6, the drag coefficients shows higher values at angles of rotation 0, -60 and +60 degrees while at +30 and -30 the values are minimal. It is worth to mention that the value at 0 degree is not coinciding with the results of obtained from the wind tunnel results as it will be explained in the results comparison.

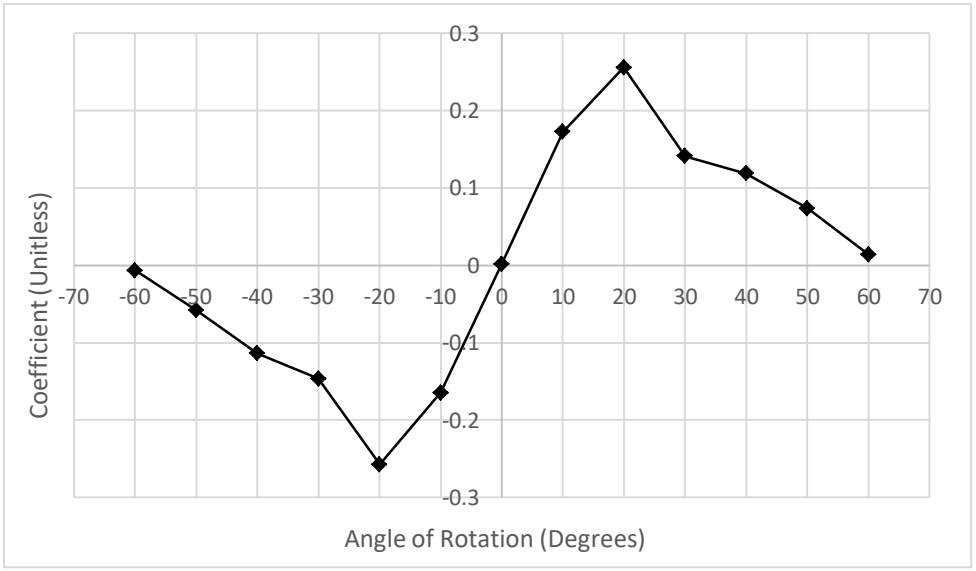

Graph 6 - Moment Coefficient for the Section Model CFD Simulation

Moment coefficients shown in Graph 7, indicated that the highest torsion forces are at angle of rotation of +20 and -20 degrees which corresponds to the results estimated from the wind tunnel test. In addition, the coefficients are near zero values in case of angle of rotation of 0, +60 and -60.

5.4 Results Comparison and Interpretation

In Graph 7, 8 and 9, results from CFD simulation and Wind Tunnel test are compared and as general observation, Coefficients' values of Wind Tunnel test are less than their corresponding values in CFD simulation. This discrepancy could be justified as due to the top effect, refer to Figure 19, where the wind flow passes over the top of the section, which results in a reduction of the forces acting body of model, thus this is considered as a setback of the wind tunnel test setting which need to be avoided in future tests.

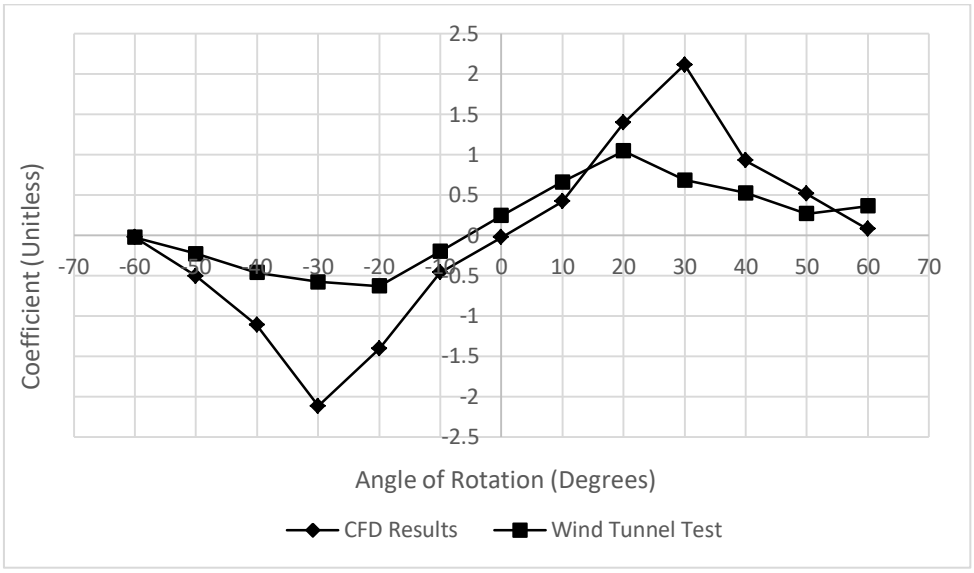

Graph 7 - Comparison between the Lift Coefficient of CFD Simulation and Wind Tunnel Test

It can be drawn from Graph 7, that the behaviour of both CFD and Wind Tunnel Test are symmetric in both negative and positive angles of attack, which is the expected due to the symmety of the cross section. However, the peak lift coefficients are at different angles 20 for the wind tunnel test and 30 for the CFD simulation which could be justified as a result of the modal building where the shape of the Section Model may have been changed due to the rubbing and infiltration process thus the outershape does not match the CFD simulation perfectly.

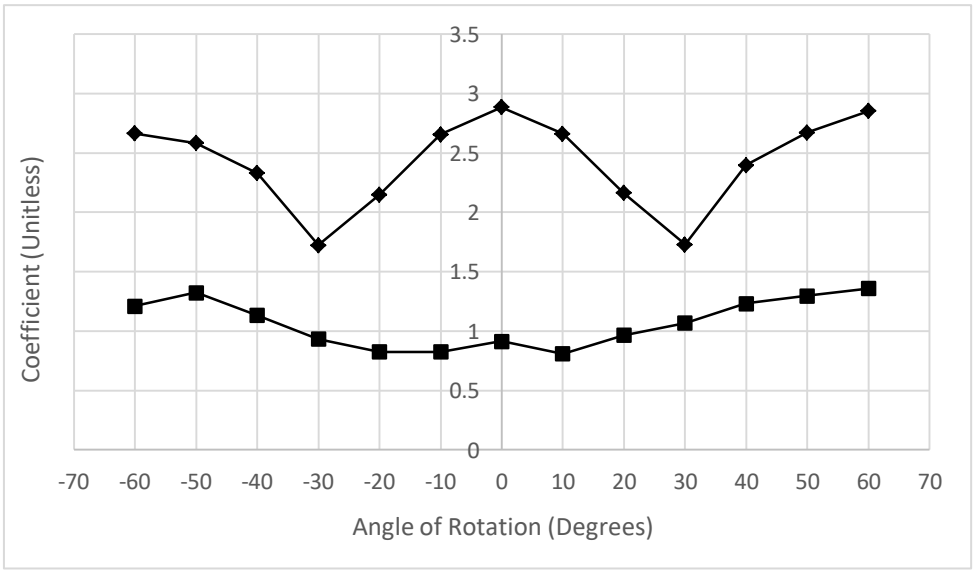

Graph 8 - Comparison between the Drag Coefficient of CFD simulation and Wind Tunnel Test

Similar to the lift coefficients are the drag coefficients, with symmetric behavior in negative and positive angles of attacks. In addition to reduction of the values, the resulted behavior of the Section model is not the same as the CFD simulation, for example the wind tunnel results at 0 degree is lower than +60 and -60 degrees, on the other hand the CFD simulation shows almost the same coefficient for 0, +60 and -60 degrees which also can be justified for the previous mentioned reasons of top effect and model building.

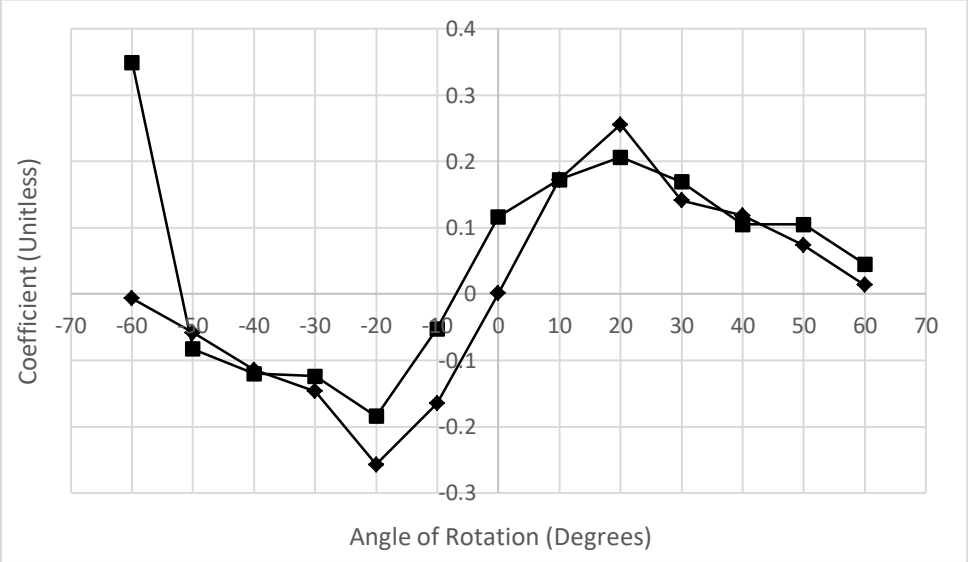

Graph 8 - Comparison between the Moment Coefficient of CFD simulation and Wind Tunnel Test

Finally, the moment coefficients results are compared, as shown in Graph 9, where the maximum coefficients are at the same angles in both the CFD simulation and Wind Tunnel Test, only the outlier in the results of wind tunnel test is exceeding all the values and does not show any correspondance to the symmetric values obtained from the negative and positive angles of atttack.

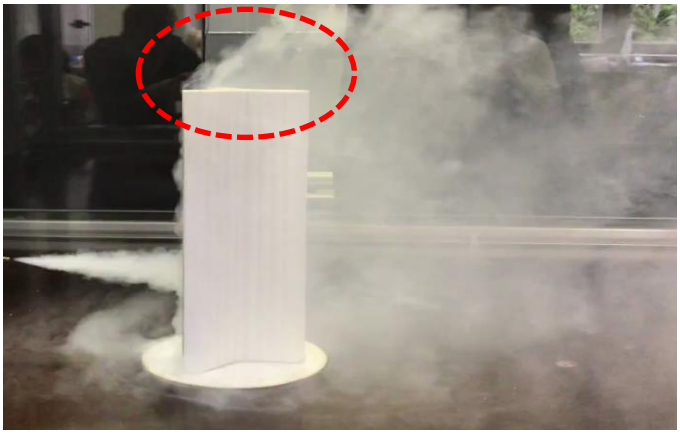

Figure 19 : Top effect of Section Model

6 Static Study of the 3D Model

In the second static study, the full tower with its cross sections is tested in the Wind Tunnel Test and Modelled in the CFD simulations. In both method assumptions and simplifications were applied to avoid the limitations of each method, however as will be explained in this section the results were not alike due to setbacks of each methodology and further refinements need to be applied in further studies.

6.1 Model Building

6.1.1 Scaling of the Model

The 3D model height was chosen to be 60cm to fit inside the wind tunnel chamber, which had an allowance of 70 cm height. All the 27 different cross-sections, shown in Figure 20, were taken for this 3D model, hence resembles the exact aerodynamic shape of the Burj Khalifa. The model was scaled down to 1:1380 compared to the real height of Burj Khalifa. The 3D model was prepared in AutoCAD software and then converted into an STL format to match the requirement format of the printing machine.

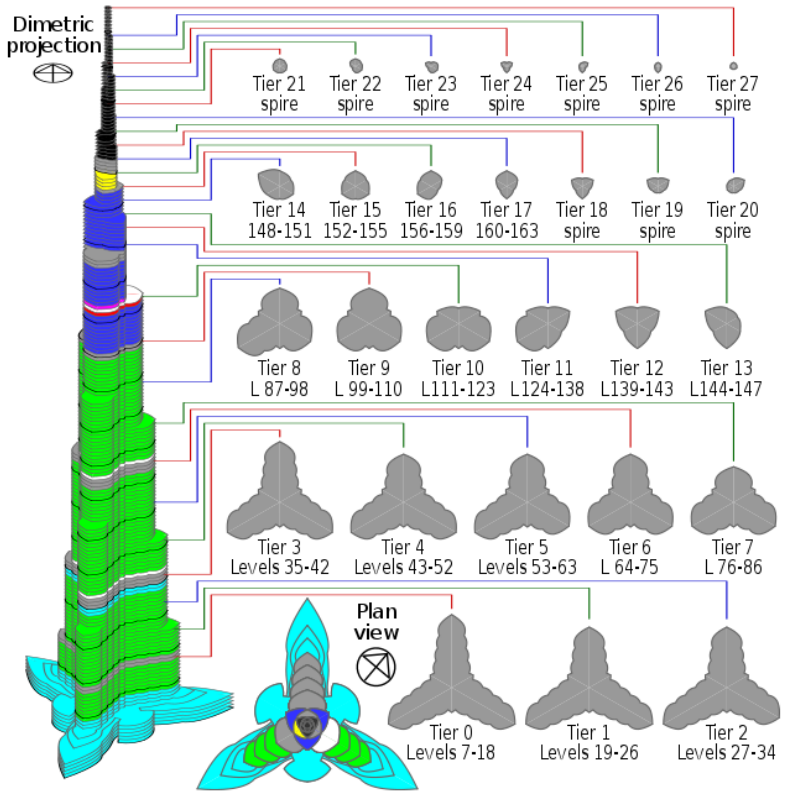

Figure 20 : Different Cross Sections (Slices) used for the 3D model

[Source: wikipedia.org/wiki/Burj_Khalifa]

6.1.2 Printing of the Model

The model was divided into two equal parts, 30 cm each since the maximum printing height of the machine is only 30 cm. The lower part of the model was made hollow to reduce the printing cost of the model and the top part is made fully solid to increase its strength as the tower cross-section becomes very slender with increase of the height. To attach both parts together and to ensure good contact, a 4cm tip was extruded from the top part with the same dimensions of the opening in the lower part, in addition to using strong glue in the connection location. After that the model was fitted on a circular base plate with angles inscribed on it. The material used to make the 3D model was PXL with infiltration (same as used before in the Section Model) with a modulus of elasticity of 9450 MPa. Infiltration then was done to improve the strength of the model as shown in Figure 21.

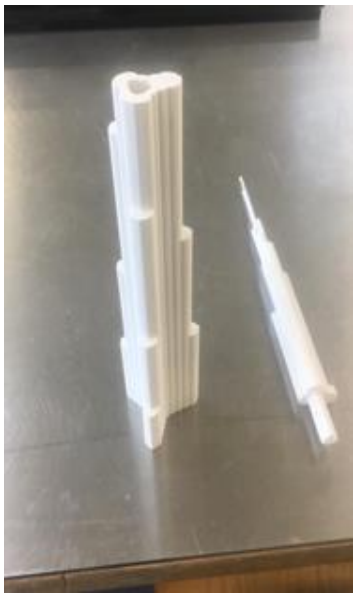

Two parts of the model before infiltration

Lower part of the model during infiltration

Lower part after infiltration

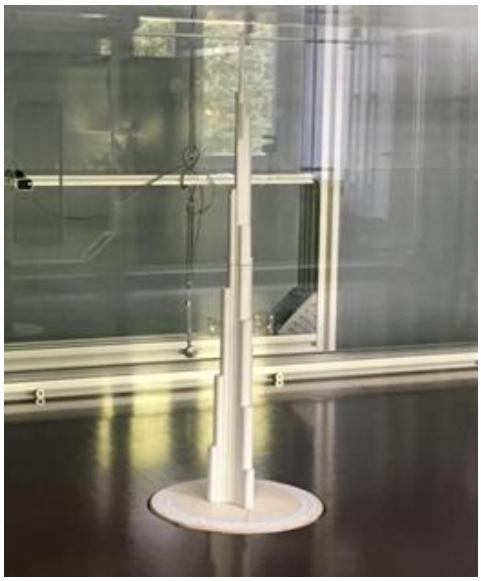

Both parts are attached and fixed on the base

Figure 21 : 3D Model Building

6.2 Wind Tunnel Test

Six different angles of attack were considered as essential wind directions to identify the wind effect on the 3D model which concedes with the literature of the real tower. Three angles where the wind blows the nose of the model (the wing) while the other three blow the tail (between two wings) as illustrated in Figure 22.

From the literature, the chosen tower orientation was based on many wind tunnel tests where it was concluded that on the blowing wind on one of the tower noses produce the minimal forces at the base of the structure while one of the structure tails produce the maximum base forces consequently the tower tail was oriented to the minimum wind speed direction while the nose to the maximum wind speed direction as shown in Figure 23.

The tests were conducted twice to increase the precision and avoid effects that could results from tests' setup. The test wind velocity was 3m/s.

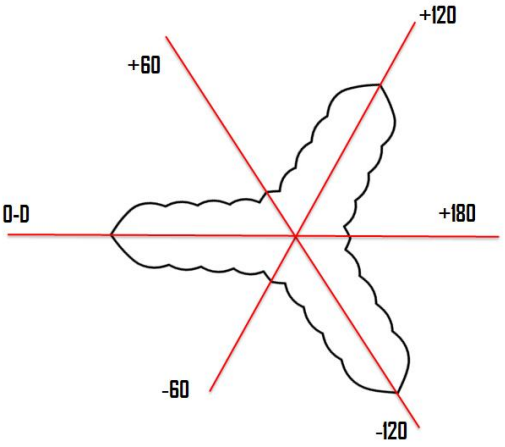

Figure 22 : Tested wind directions

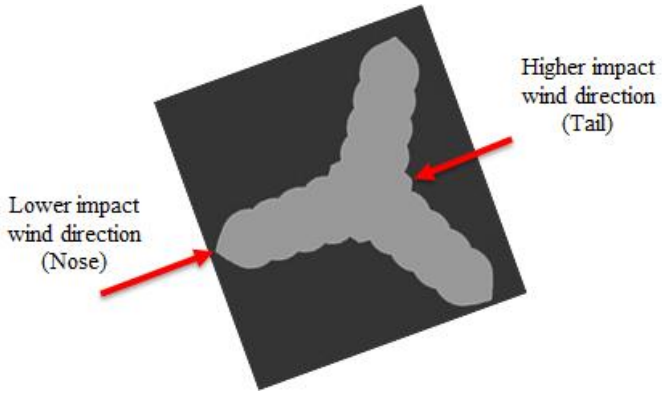

Figure 23 : The Predominant Wind Directions acting on Burj Khalifa

Figure 24 : 3D Model in the Wind Tunnel Chamber

Readings from each angle were taken for four minutes. The first minute was removed from the readings as the values were lower in the beginning of the recording. The test outputs considered for the study are:

- Force in Y-direction FD (Drag force)
- Force in X-direction FL (Lift force)
- Torsion in Z-direction FM (Torsion moment)
- Moment around X-direction (Overturning moment)

It should be mentioned that bases forces are directly compared with the results from CFD simulation without calculation of aerodynamic coefficients since the model consist of 27 section each have a different aerodynamic coefficients. However, in order to calculate such coefficient for each of the cross section the procedures of the section model test is to be used while varying the used cross section.

6.2.1 Wind Tunnel Test Results

In general the below shown forces in this section are multiplied by 10^4 for the purpose of presenting the results only since the wind tunnel test results are quite small due to the small configuration of the test: scaling the model to be 1:1380 and low wind speed of 3m/s.

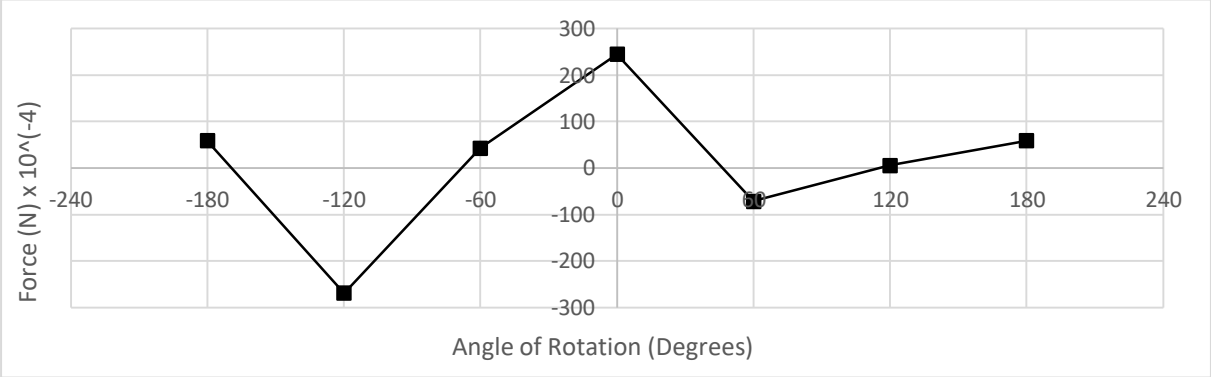

Graph 10 - Lift Force of 3D Model Wind Tunnel Test

By observing the result of the lift force in Graph 10, forces values at the tails (+60, -60 and -180 degrees) are almost equal and less than some values at tails (0 and -120 degrees). In like manner, the maximum lift force are captured at angles of 0 and -120 degrees.

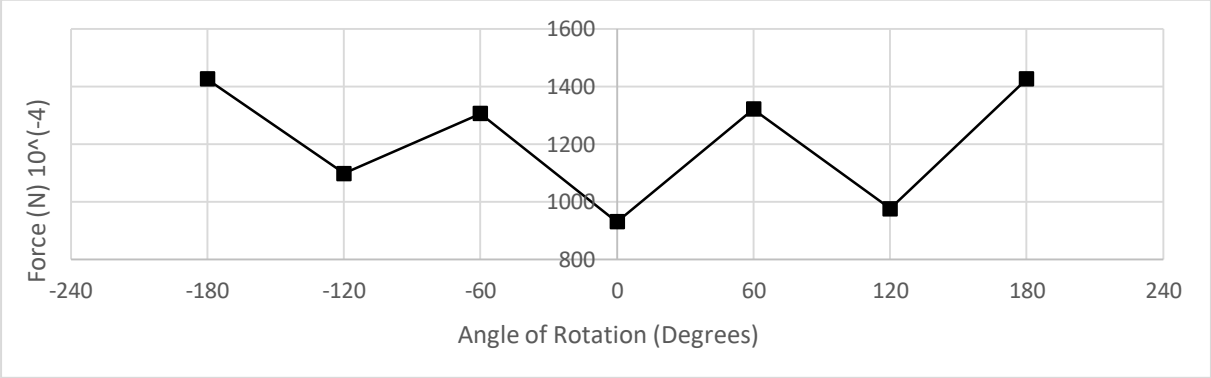

Graph 11 - Drag Force of 3D Model Wind Tunnel Test

For the drag forces shown in Graph , forces' values at the noses (, + and -120 degrees) are less than all the values at tails (+60, -60 and +180 degrees). This result concedes perfectly with the literature of the tower about the tail and nose results.

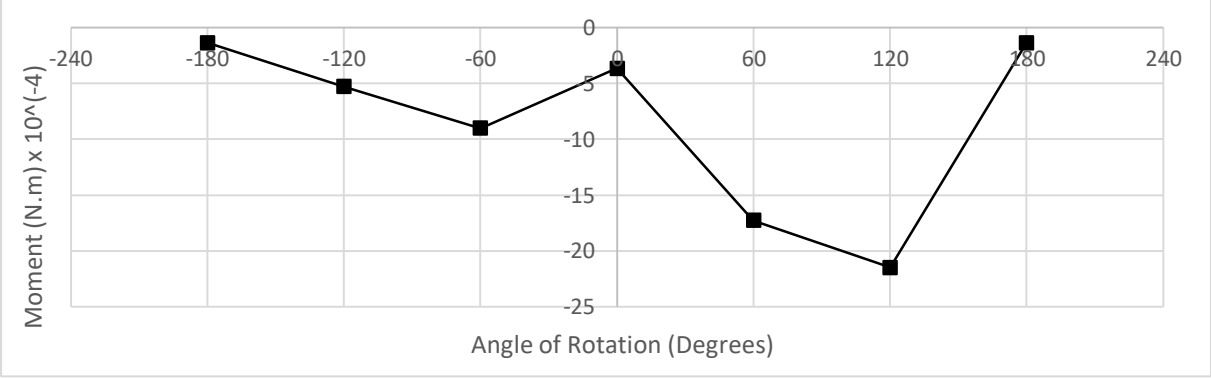

Graph 12 - Torsional Moment of 3D Model Wind Tunnel Test

In Graph 12, torsional moment is illustrated with a maximum value at one nose (+120 degree) while values at the noses show high values at -60 and +60, however the +180 degree nose shows minimum value of torsional moment.

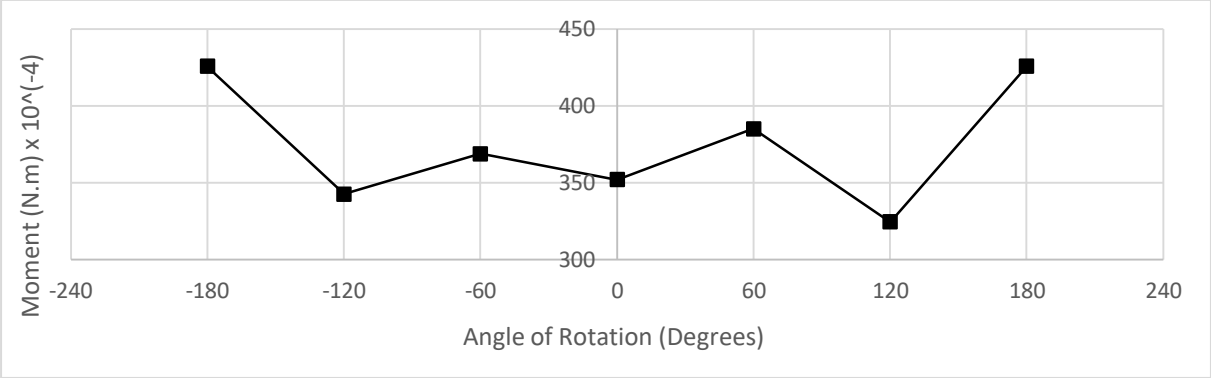

Graph 13 - Overturning Moment of 3D Model Wind Tunnel Test

Similarly, shown in Graph 13, Overturning moment is captured with maximum value at +180 degree (tail) and shows lower values at 0, -120 and +120 degrees (noses) which matchs the expected peaks as the drag forces.

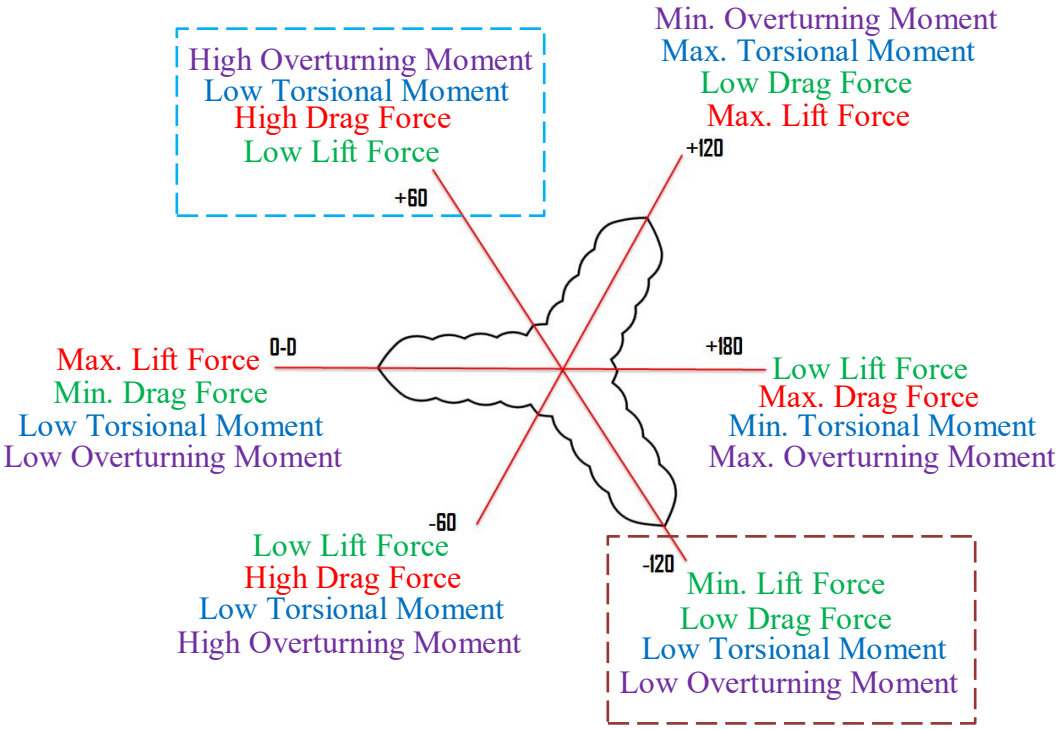

Figure 25 : Overall Acting Forces on the 3D Model

Finally, as shown in Figure 25, -120 direction of the 3D model gives low values for the 4 components of forces thus similar to the real tower, the model can be rotated so that the maximum wind speed is to act in that direction to have minimal base forces.

6.3 CFD Simulation

For the purpose of creating a model that represent the geometry of the structure, each cross section of the tower should be modelled as a slice (name that represent the cross section in VXflow) and the number of the total cross sections is 27. Thus, due to the high computational time that is required to obtain the solution for each slice, only 7 sections where chosen as an approximation of the given geometry of the tower as shown in Figure 28 and Figure 27. With the same 6 angles of wind attack that were used in the wind tunnel test, -120, -60, 0, 60, 120 and 180 as shown in Figure 26.

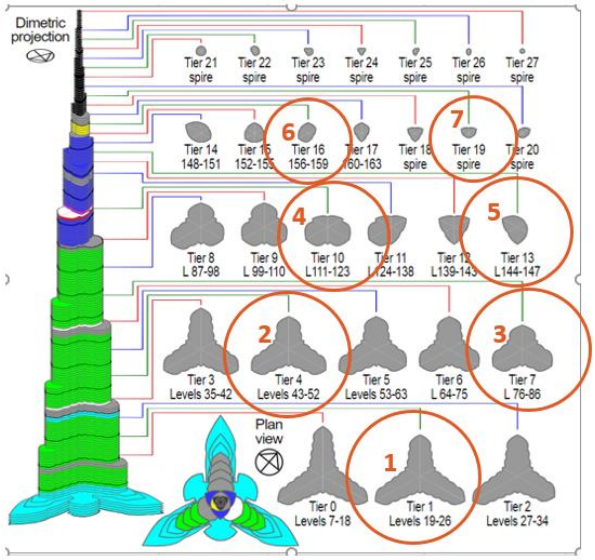

Figure 28 : Chosen Cross Sections (Slices)

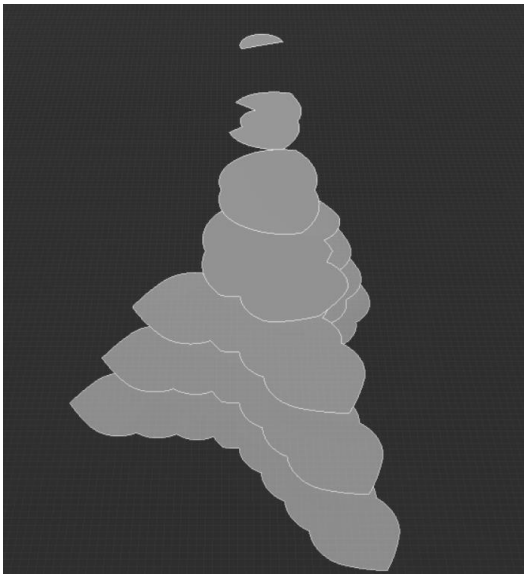

Figure 27 : Slices in VXflow

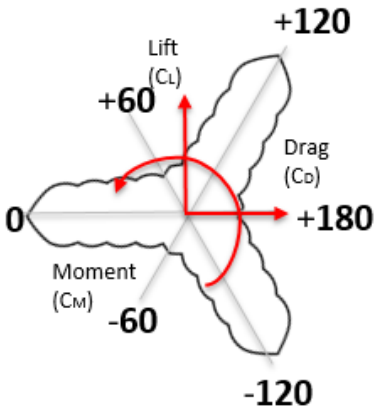

Figure 26 : Angles of Attack

For this Multi-slice mode, the static wind coefficients were not calculated due to the fact each section/slice of the 3D model has a different coefficient which calculation of a single coefficient for the tower is not relevant however it makes sense to calculate the base forces and compare them to the Wind Tunnel Test results.

6.3.1 CFD Simulation Results

The results are multiplied by factor in this section for the purpose of presenting the results since the results are quite high since the model is fully scaled with the exact dimensions of the real tower and the wind speed used is 55m/s. With the same concept presented before, the base forces are calculated and compared with the wind tunnel test results.

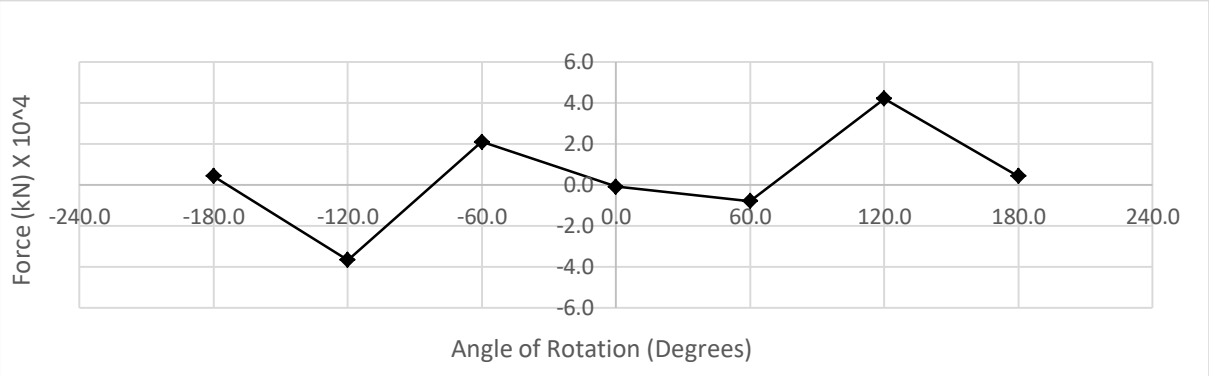

Graph 10 - Lift Forces of Multi-Slice Model

In Graph 11, shown lift force where the maximum lift force is at +120 degree angle of rotation while at the other angles of rotations low lift forces are captured. In addition, the lift forces are almost symmetrical but reversed pattern if the negative angles with the positive angles results are compared.

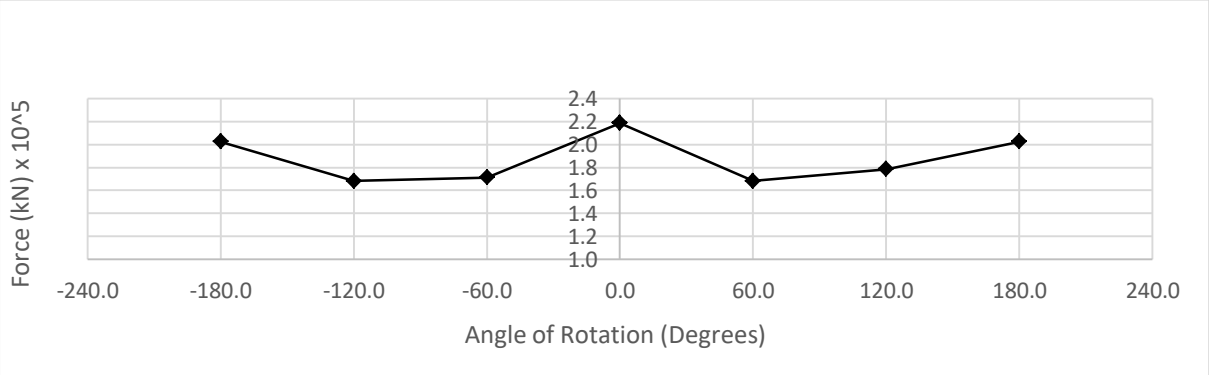

Graph 12 - Drag Forces of Multi-Slice Model

For the Drag Forces, shown in Graph 13, the pattern of the results is symmetrical for both negative and positive angles of rotation results. High drag forces are observed at 0 and 180 angles of rotation where the maximum drag is at 0 degree.

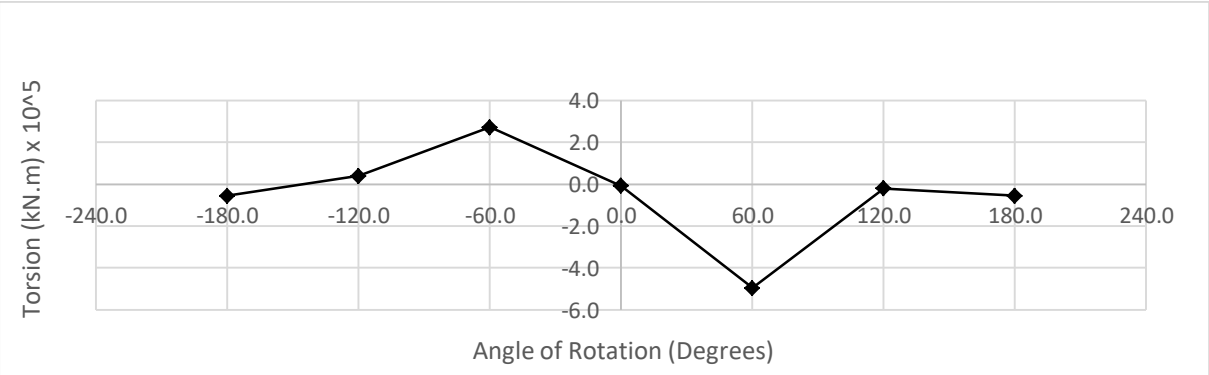

Graph 14 - Torsional Moment of Multi-Slice Model

Torsional Moment values as shown in Graph 15, show symmetric and reversed pattern between negative and positive rotation angles. 60 degree of rotation is the maximum torsional moment angle of rotation then -60 degree is the next high value while the rest of the angles are minimal in comparison to +60 and -60 degrees.

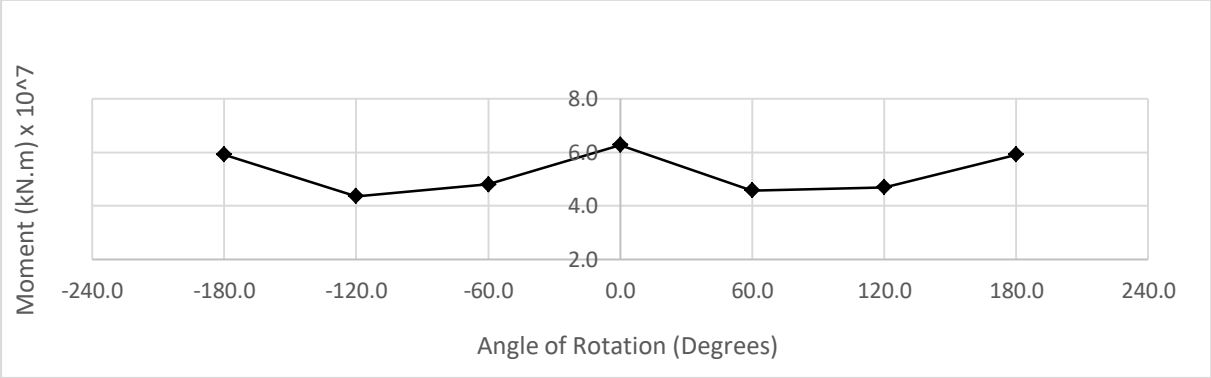

Graph 16 - Overturning Moment of Multi-Slice Model

Finally, the overturning moment values are maximum at 0 degree and then the next high value is at +180 degree while the minimum value is at -120 degree.

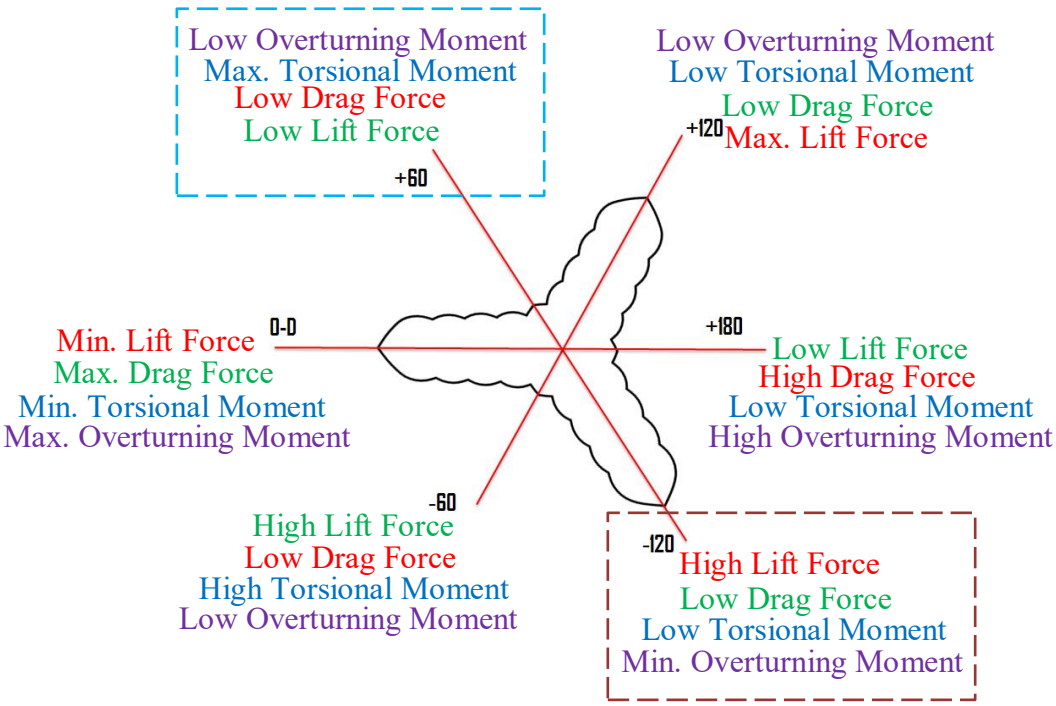

Figure 29 : Overall Forces Acting on the Multi-Slice Model

Similar to the wind tunnel test results, the critical direction of the multi-slice model, as shown in Figure 29, -120 degree and +60 degree of rotation gives low values for the 3 components of forces but with a high lift force and maximum torsional moment at the corresponding direction, however, -120 degree direction is much preferable due to the minimum overturning moment. Thus similar to the real tower, the model can be rotated so that the maximum wind speed is to act in that direction to have minimal base forces.

6.4 Results Comparison and Interpretation

The following is the comparison between the results of CFD simulations and the Wind Tunnel Test, however it should be noted that the results of **the wind tunnel test is multiplied by a factor of 10000,** to compare the behavior of the structure against wind in both CFD and the Wind Tunnel Test. It's concluded that there must be an error in the in the results in both wind tunnel and CFD as they are both diverging from the actual building forces where CFD show a higher forces by factor of 8, and this might be explained as a limitation of the multi-slice mode since it's only considering 7 slices, and the model cannot capture the breaking of wind forces along its height (the spiral phenomena). Further, the deviation of the wind tunnel test results could result from the produced model since the roughness of the material could not be controlled during the process of the model building.

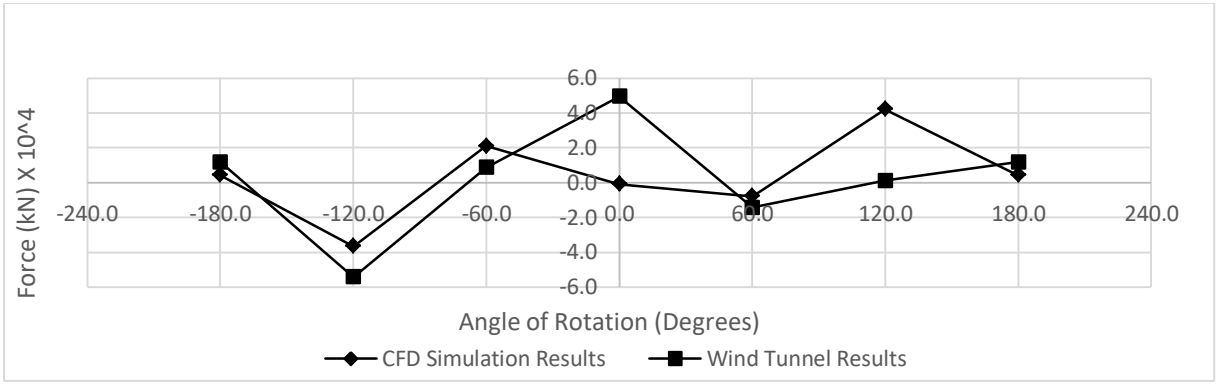

Figure 30 : Lift Force Comparison

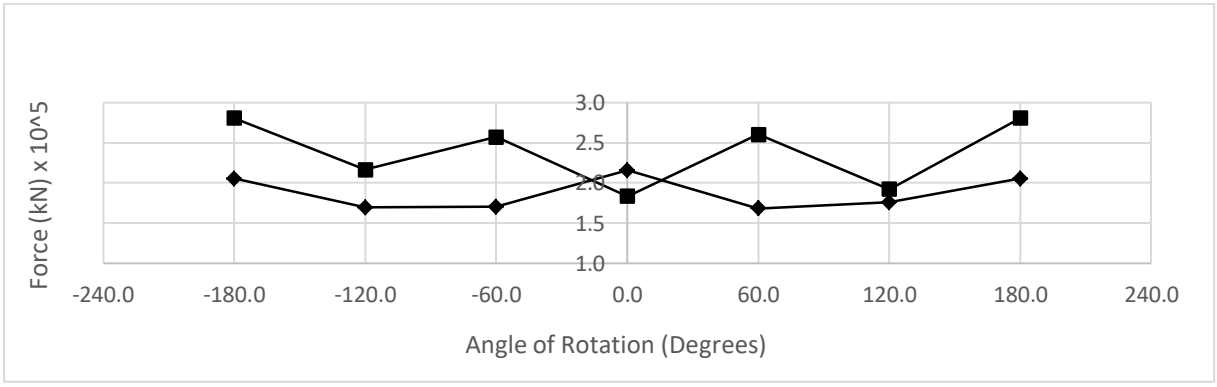

Figure 31: Drag Force Comparison

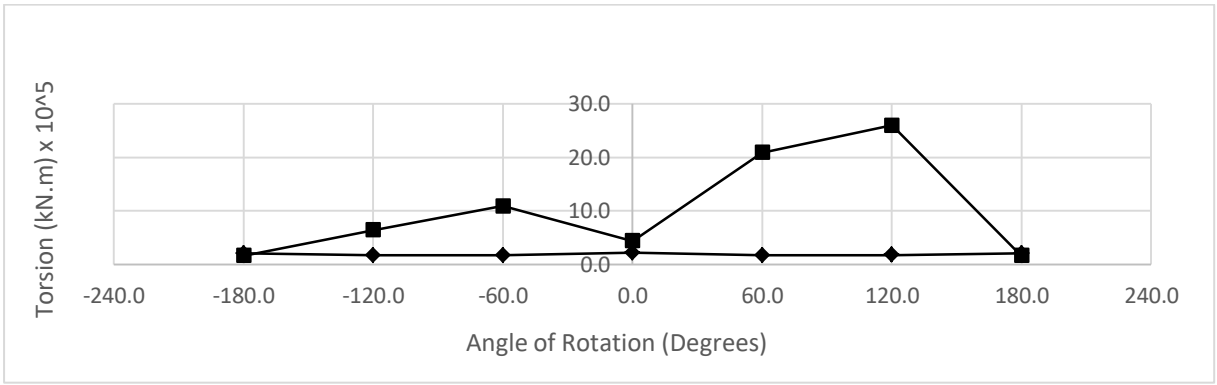

Figure 32 : Torsional Moment Comparison

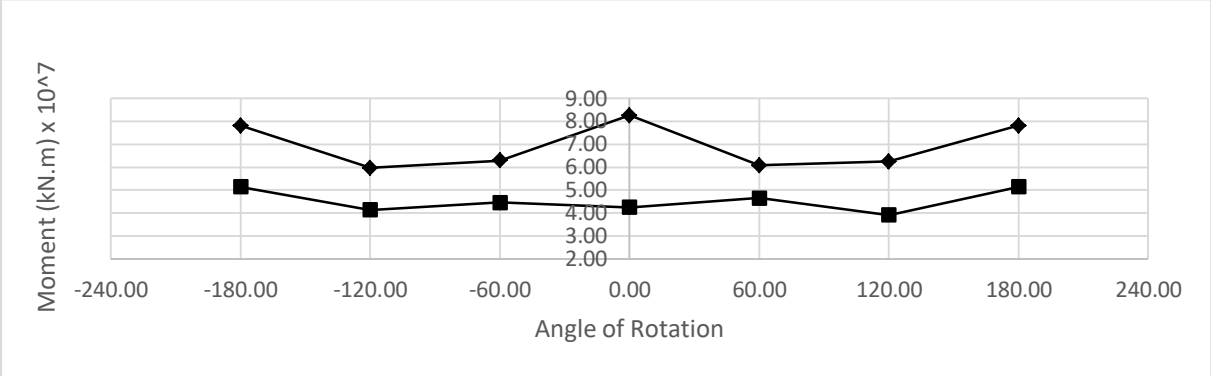

Figure 33 : Overturning Moment Comparison

7 Dynamic Study of the 3D Model (Vortex Induced Vibrations)

Using CFD simulations, a dynamic study was performed to capture the effect of Vortex-Induced Vibrations on the 3D model of the tower, where the model interacts with the wind perpendicular to the wind direction.

The following parameters are needed for the CFD simulations:

1. Modal mass of the structure corresponding to the first mode of vibration.
2. Stiffness of the structure
3. First Mode shape of the structure
4. Resonant wind speed for each slice

Further below, it is explained how each parameter is calculated and the assumptions taken into consideration.

7.1 Finite Element Model

For the mass (m) calculation, 20% of the live load is assumed to be effective in mass to be considered in modal analysis as shown in the following equation:

$$m=DL+0.2\times LL,$$

Where, DL represents dead load of construction given by literature and LL represents live load assumed from usage of each floor founded in literature and values determined by design codes. Uniform Building Code 97 and Euro-code standard were used for the study. The total height of the tower was divided into seven parts and each part was represented with its own cross section. The cross sections of each part are shown Figure 34.

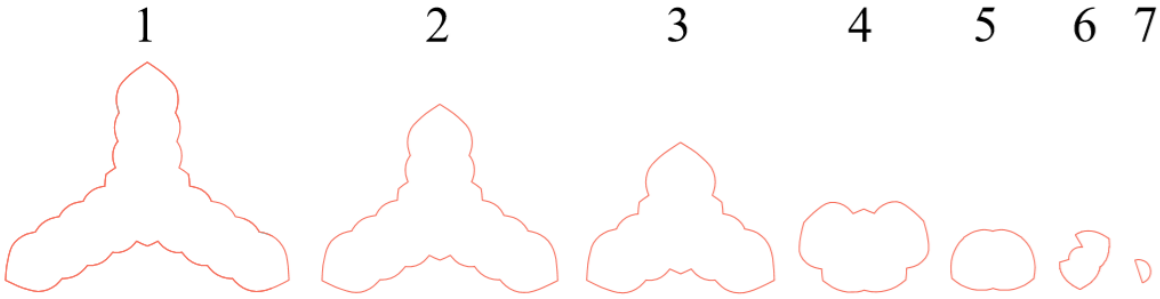

Figure 34 : Seven Cross Sections, from the Base to the Top of the Tower

7.1.1 Dead Load Calculation

The area for each cross section was calculated separately and multiplied with the corresponding number of floors and that is how the total area of the construction was determined. Further the total dead load (which is 500 000 tons) was divided with the total area calculated. Finally the mass for each of the seven parts were calculated with the following equations:

$$A\ [t/m2] = \frac{\text{total dead load}}{\text{total area}}$$

$$\text{Mass of each part [t]} = A \times \text{total area for each part}$$

7.1.2 Live Load Calculation

For each floor the usability had to be checked from the literature (Burj Khalifa as a Technical Object: Re-visualizing the Technological Innovation of the World's Tallest Building through Simondon's Philosophy Osama Al-Sehail School of Architecture, McGill University, Montreal August 2014). The usability is shown in the Table 1:

Section	Number of floors	Usability of floors
1	34	Hotel
	2	Mechanical equipment
2	31	Hotel
	2	Mechanical equipment
3	32	Hotel
	3	Mechanical equipment
4	31	Hotel
	2	Mechanical equipment
5	10	Hotel
	2	Mechanical equipment
6	13	Hotel
	1	Mechanical equipment
	-	Spire
7	-	Spire

Table 1 : Usability taken from Literature

From the Uniform Building Code 97 the live load for the tower is 2.4 kN/m² and a value for mechanical equipment were considered from the Euro-code standard. The floors were assumed to be light manufacturing floors and the value of 6 kN/m² were used. For the spire part, the weight was assumed to be 4000 tons as suggested in the literature ("Vanity height: how much space in skyscrapers is unoccupied?" The Guardian. Retrieved 20 February 2018.) With the value of live loads, the total live load for each section were calculated by multiplying the value of live load with the total area of each cross section.

7.1.3 Stiffness Calculation

Stiffness (k) was calculated with the following equation:

$$k=3\times E\times I_p/h^3$$

Where, E is the elastic modulus, I_p is the polar moment of inertia and h is the height of each section.
For the first three sections the concrete used was C80/95, for the fourth and fifth section C60/75 and for the sixth section a part was C60/75 concrete and the other part was a steel spire. The last section was also the steel spire.

Material	E [MPa]
C60/75	39100
C80/95	42244
Steel	210000

Table 2 : Elastic Modulus of Concrete and Steel

For simplification the structural system of the tower, shown in Figure 35, was assumed and consequently the relative structural system was interpreted in the different 7 cross sections to calculate the global stiffness of the tower as illustrated in Figure 36.

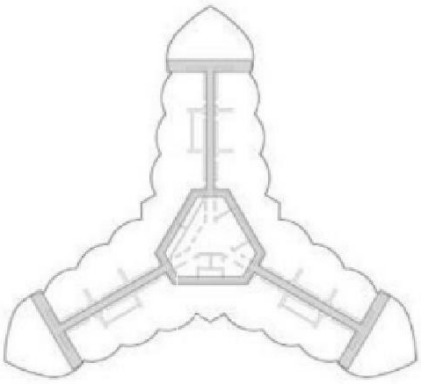

Figure 35: Burj Khalifa Structural System

[Source: https://eyeforengineering.wordpress.com]

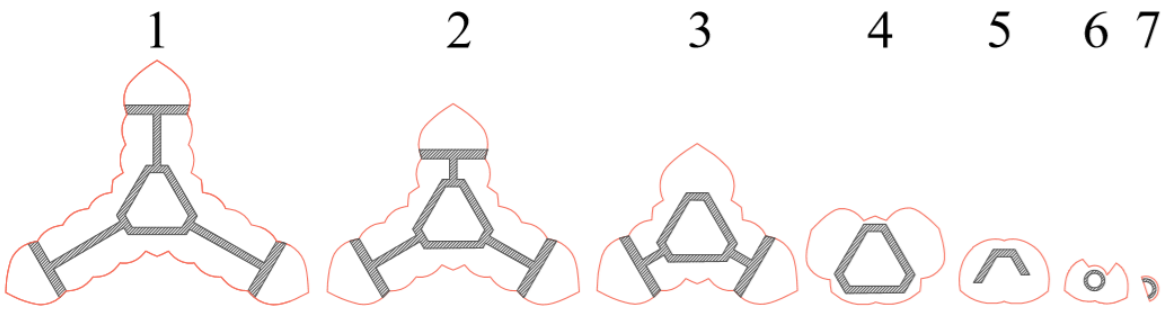

Figure 36 : Cross Sections for Different Slices

The polar moments of inertia were calculated as shown in the Table 3, which then used in then the calculation of the stiffness. The relevant height of each section is also shown in Table 3.

Section	h [m]	I_p $[m^4]$
1	220,5	81372,15
2	152,9	41771,74
3	158,8	10682,97
4	101,4	4449,04
5	59,7	217,88
6	88,9	54,32
7	45,8	27,16

Table 3 : Polar Moments of Inertia

7.1.4 The First Sofistik Model

From the literature modes one, two and five were obtained as illustrated in Figure 37. These values were used as a guidance to get the right frequency from Sofistik model. In Table 4, it is shown the calculated stiffness in the first column and then these stiffness were multiplied by a factor of 1400 to get the right frequency.

k [kN/m]	Multiply k by factor of 1400
961914,2	1346679905,5
1480970,8	2073359118,0
338085,9	473320287,2
500553,7	700775205,5
120117,3	168164289,1
48710,7	68195017,4
178115,9	249362244,4

Table 4 : Stiffness Calculation

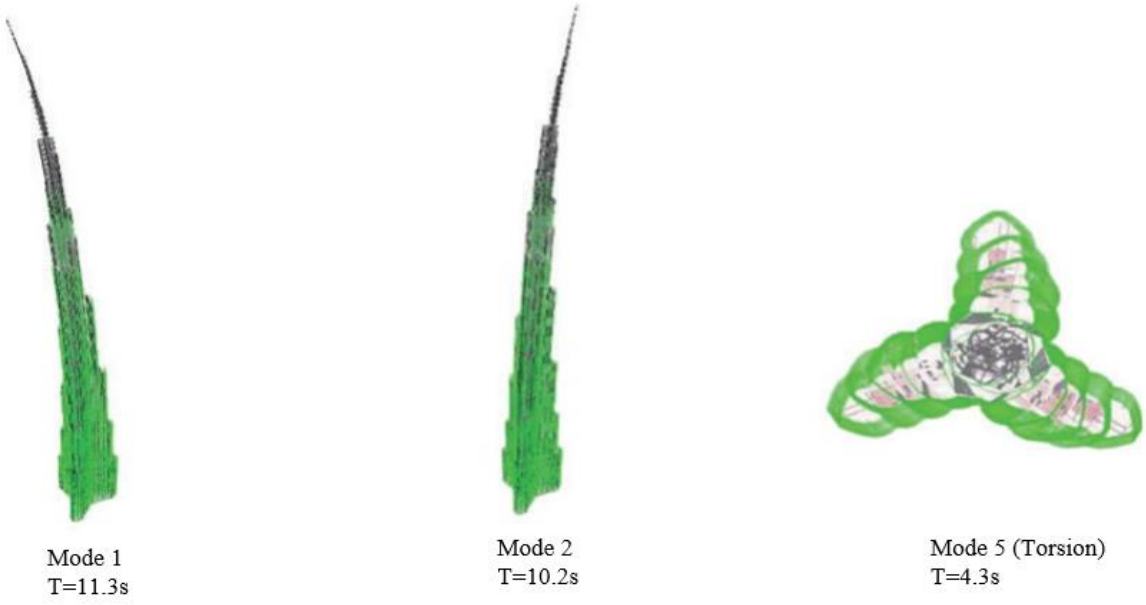

Figure 37 : Three Modes from Literature, BURJ DUBAI

[Source: Engineering the World's tallest building]

In Table 5, shown the calculated frequencies by Sofistik and Figure 38 shown the assumed static model, where the masses are connected with springs and each spring represent the relevant part of the tower where 7 springs represent 7 different stiffness.

Loadcases	Load Distribution Area	
System		
1 Eigenform	1 f=	0.080 Hz
2 Eigenform	2 f=	0.152 Hz
3 Eigenform	3 f=	0.316 Hz
4 Eigenform	4 f=	0.354 Hz
5 Eigenform	5 f=	0.730 Hz

Table 5 : Calculated Frequencies with Sofistik Model

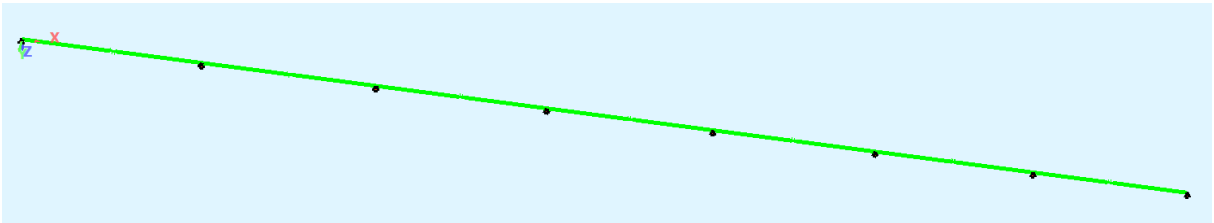

Figure 38 : First Sofistik model

7.1.5 The Second Sofistik Model

Another Sofistik model were made to visualize the different model shapes of the structure and compare them with output of the literature. In this model the cross section of the tower was assumed as an equivalent rectangular cross section the entire height of the tower.

Using stiffness calculated from the first model, modulus of elasticity to reach the same from frequency from the literature.

Elastic modulus was calculated with the following equation:

$$E = \frac{3 \times E \times I_P}{h^3}$$

In Table 6, calculation of Elastic modulus is shown. And to match the first mode from literature elastic module was multiply by 0.08.

E [kPa]	Multiply E by factor 0,08
3341999,8	267360,0
1715589,0	137247,1
438755,8	35100,5
169125,4	13530,0
8282,7	662,6
11091,1	887,3
5545,5	443,6

Table 6 : Calculated Elastic Models

Shown in Table 7, the obtained frequencies using the second Sofistik Model.

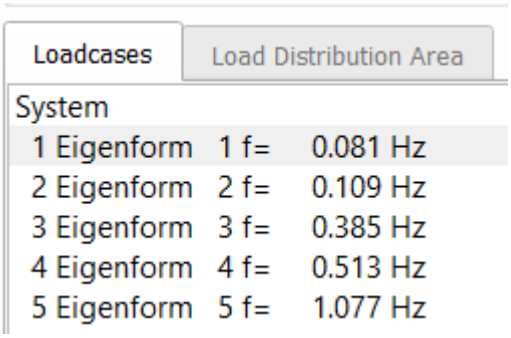

Table 7 : Calculated Frequencies with Sofistik Model

In the picture below the first and the second mode are represented.

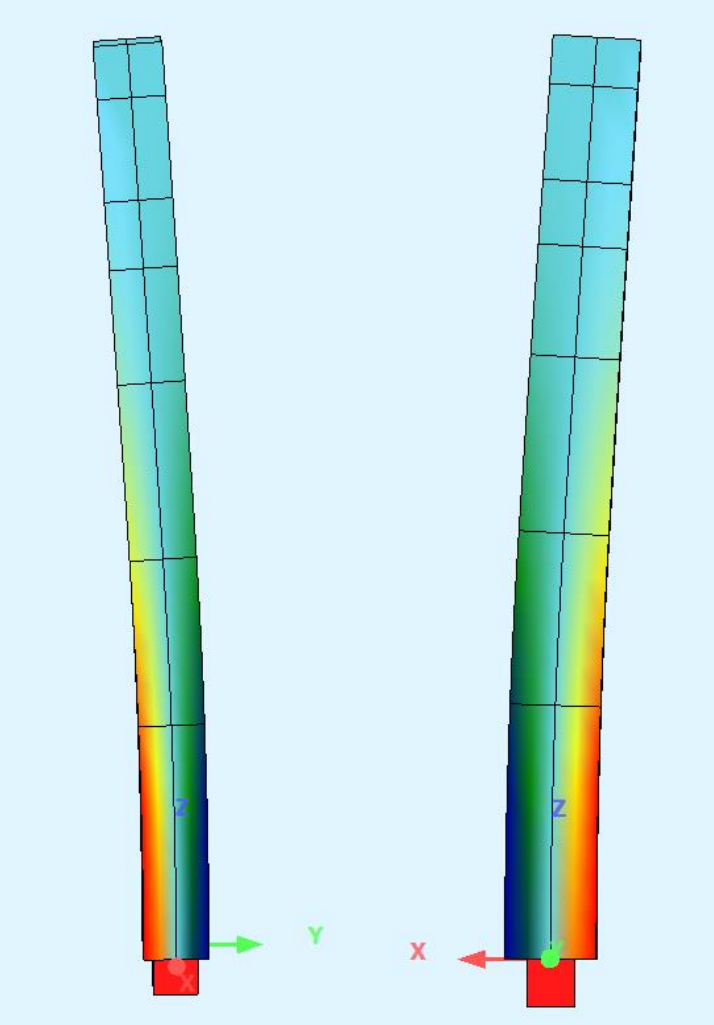

Figure 39 : First and Second Modes

7.1.6 Eigenvalues Comparison

In Table 8 and Figure 40, shown the comparison of frequencies from Sofistik model and the values obtained from literature. The first mode matches perfectly with the literature and the second mode is near to the right value with a small percentage of error.

Mode Number	Results from the literature	Results from Sofistik model
Mode 1 [Hz]	0,088	0,081
Mode 2 [Hz]	0,098	0,109
Mode 3 [Hz]	-	0,385
Mode 4 [Hz]	-	0,513
Mode 5 [Hz]	0,233	1,077

Table 8 : Comparison of Frequencies from Sofistik and the Literature

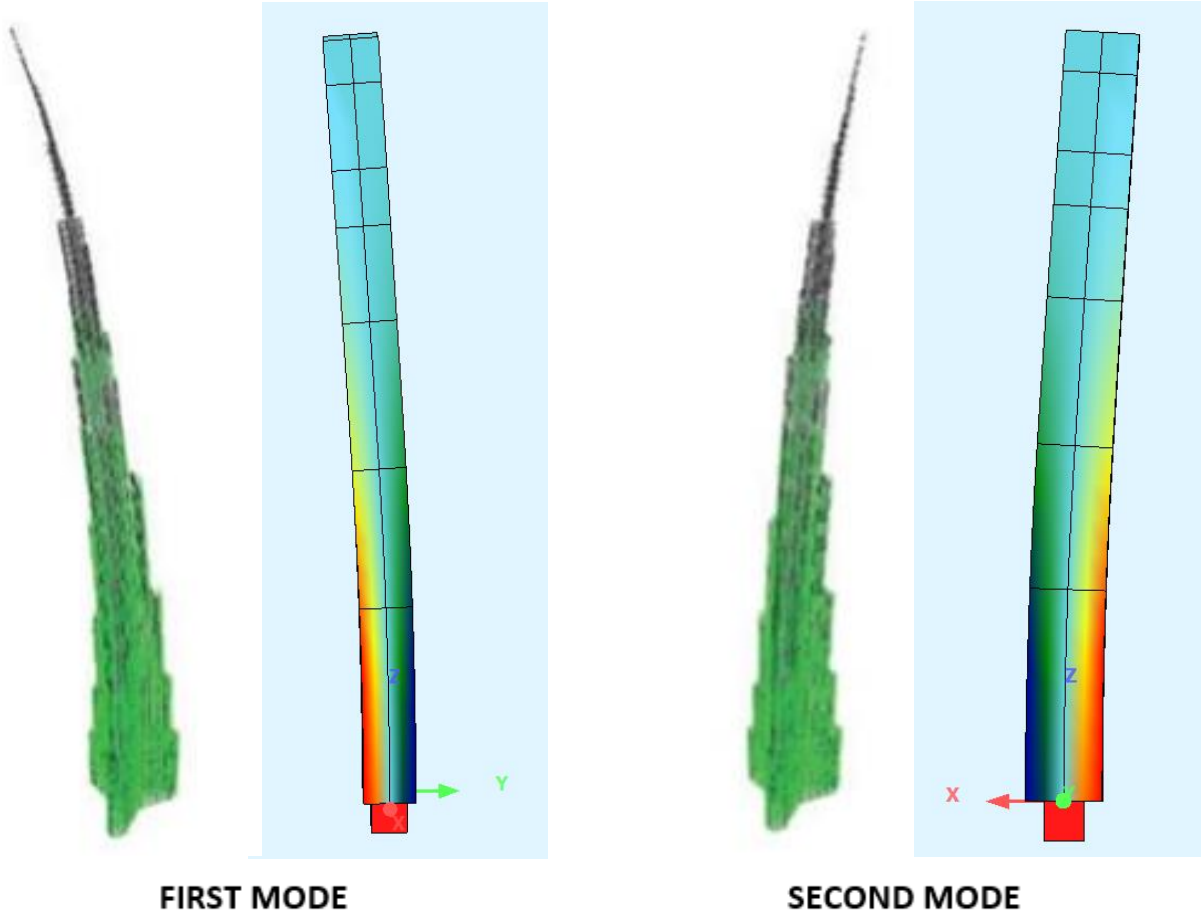

Figure 40 : Comparison of the First Two Modes

7.1.8 Modal Mass Calculation

When the frequency of the Sofistik model fairly corresponded the first mode from literature, the eigenvectors were extracted, as shown in Table 9, and from this matrix the maximum value was taken as given in Table 10. This maximum value used to normalize the eigenvectors as illustrated in Table 11. The normalized eigenvector was required for the calculation of the modal mass which was then squared, as in Table 12, and multiplied by the mass matrix, given in Table 14. The modal mass is the sum of modal mass matrix, calculated in Tons in Table 15. The following equations are used to perform the previous explained procedure.

$$Eigenvector\ from\ Sofistik \rightarrow maximum\ value$$

$$\rightarrow normalized\ eigenvector = \frac{eigenvector}{maximum\ value}$$

$$Modal\ mass\ matrix = normalized\ eigenvector^2 \times Mass\ matrix$$

$$Modal\ mass = sum\ of\ Modal\ mass\ matrix$$

	u-X [m]	u-Y [m]	u-Z [m]	phi-X [rad]	phi-Y [rad]	phi-Z [rad]
Eigenvector	0,00E+00	0,00E+00	0,00E+00	0,00E+00	0,00E+00	0,00E+00
	-5,24E-16	3,86E-02	-4,09E-20	-3,19E-01	-5,72E-15	-8,60E-16
	-2,28E-15	1,07E-01	-8,38E-20	-5,49E-01	-1,71E-14	-1,89E-15
	-5,38E-15	1,99E-01	-9,55E-20	-6,04E-01	-2,15E-14	-2,31E-15
	-7,63E-15	2,61E-01	-9,83E-20	-6,16E-01	-2,28E-14	-2,49E-15
	-9,00E-15	2,98E-01	-9,92E-20	-6,19E-01	-2,31E-14	-2,57E-15
	-1,11E-14	3,53E-01	-9,98E-20	-6,20E-01	-2,33E-14	-2,63E-15
	-1,21E-14	3,81E-01	-9,99E-20	-6,20E-01	-2,33E-14	-2,64E-15

Table 9 : Eigenvector

Maximum [m]	0,3813

Table 10 : Maximum Value of Eigenvector

Normalized Eigenvector	0,0E+00	0,0E+00	0,0E+00	0,0E+00	0,0E+00	0,0E+00
	-1,4E-15	1,0E-01	-1,1E-19	-8,4E-01	-1,5E-14	-2,3E-15
	-6,0E-15	2,8E-01	-2,2E-19	-1,4E+00	-4,5E-14	-5,0E-15
	-1,4E-14	5,2E-01	-2,5E-19	-1,6E+00	-5,6E-14	-6,1E-15
	-2,0E-14	6,8E-01	-2,6E-19	-1,6E+00	-6,0E-14	-6,5E-15
	-2,4E-14	7,8E-01	-2,6E-19	-1,6E+00	-6,1E-14	-6,7E-15
	-2,9E-14	9,3E-01	-2,6E-19	-1,6E+00	-6,1E-14	-6,9E-15
	-3,2E-14	1,0E+00	-2,6E-19	-1,6E+00	-6,1E-14	-6,9E-15

Table 11 : Normalized Eigenvector

Eigenvector Square	0	0	0	0	0	0
	1,89144E-30	0,010221512	1,15282E-38	0,69904159	2,25275E-28	5,09057E-30
	3,56296E-29	0,078452881	4,82547E-38	2,072301069	2,01122E-27	2,45432E-29
	1,98934E-28	0,272652139	6,26903E-38	2,506736826	3,16757E-27	3,66703E-29
	4,0021E-28	0,468540789	6,63944E-38	2,607382202	3,55983E-27	4,27132E-29
	5,56876E-28	0,609980254	6,763E-38	2,632853059	3,67021E-27	4,52876E-29
	8,4135E-28	0,856583503	6,84921E-38	2,645634914	3,73083E-27	4,74664E-29
	1,01202E-27	1	6,85882E-38	2,645634914	3,73403E-27	4,7756E-29

Table 12 : Eigenvector Square

Mass Matrix	0	0	0	0	0	0	0
	184821,694	0	0	0	0	0	0
	0	137264,6	0	0	0	0	0
	0	0	111409,6	0	0	0	0
	0	0	0	60685,7	0	0	0
	0	0	0	0	10376,25	0	0
	0	0	0	0	0	5149,675	0
	0	0	0	0	0	0	2468,765

Table 13 : Mass Matrix

Modal Mass Matrix	0	0	0	0	0	0
	3,49578E-25	1889,157209	2,13066E-33	129198,0505	4,16358E-23	9,40847E-25
	4,89068E-24	10768,79964	6,62366E-33	284453,4809	2,76069E-22	3,3689E-24
	2,21631E-23	30376,06514	6,9843E-33	279274,5413	3,52897E-22	4,08542E-24
	2,4287E-23	28433,72712	4,02919E-33	158230,8218	2,16031E-22	2,59208E-24
	5,77828E-24	6329,305369	7,01746E-34	27319,13189	3,8083E-23	4,69916E-25
	4,33268E-24	4411,126657	3,52712E-34	13624,15999	1,92126E-23	2,44437E-25
	2,49843E-24	2468,764637	1,69328E-34	6531,449918	9,21845E-24	1,17898E-25

Table 14 : Modal Mass Matrix

Modal Mass [t]	983308,58

Table 15 : Modal Mass Considered

7.1.9 Resonant Speed Calculation

In order to estimate the critical speed of the tower, where the structure is prone to Vortex Induced Vibration, procedures shown in Figure 41, where as a first step using the results of the static 3D model, the lift force was extracted using Fast Fourier Transform (FFT) the flutter frequency was determined then Strouhal number is obtained using the following equation:

$$Strouhal\ Number = \frac{f_v \times D}{U}$$

Where,
f_v: flutter frequency
D: depth of the each slice
U: wind speed equal 55m/s.

The pervious calculation was done for each slice from the 7 slices and then finally, using Strouhal number, the resonant speed for each slice was estimated using the following formula:

$$Resonant\ Speed\ (U_{res}) = \frac{f \times D}{Strouhal\ Number}$$

Where,
f: frequency of the first mode of vibration.

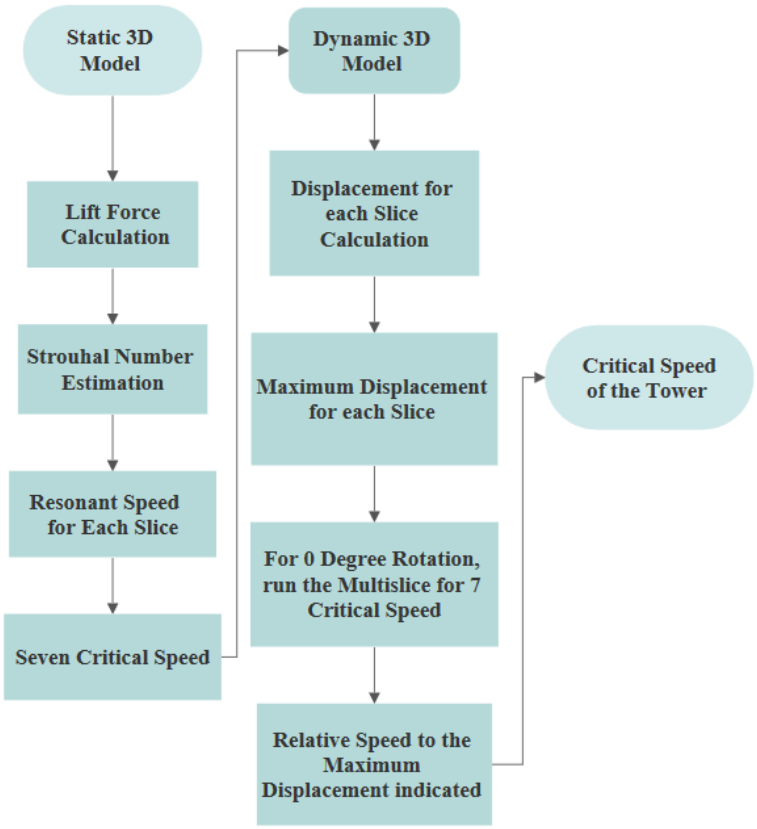

Figure 41 : Critical Speed Calculation Procedures

In Table 16 *: Resonant Speed Values*, shown the corresponding calculation of slice with its relevant depth (D), flutter frequency (f_v) and Strouhal number. And as shown that 7 different speeds were obtained at which the relevant slice is prone to flutter effect.

No. of slice	f_v [Hz]	D[m]	U[m]	St. Number	U_{res} [m]
1	0,152	83,17	55	0,230	31,95
2	0,160	69,17	55	0,202	30,27
3	0,248	55,08	55	0,248	19,61
4	0,287	38,02	55	0,198	16,91
5	0,476	24,79	55	0,214	10,21
6	0,643	17	55	0,203	7,56
7	1,841	4,60	55	0,154	2,64

Table 16 : Resonant Speed Values

As a last step, 7 different Multi-slice files where set to run at the obtained speeds at the 0 degree rotation angle. The results are presented in 7.2.

7.2 Vortex Induced Vibrations Results

After the 7 multi-slice files were run at different speeds, the maximum peak displacement for each slice at each speed were obtained, as shown in Graph 17, and it's concluded that the resonant speed for the slices in this direction is around 20m/s, since all the slices shows maximum displacement at this speed.

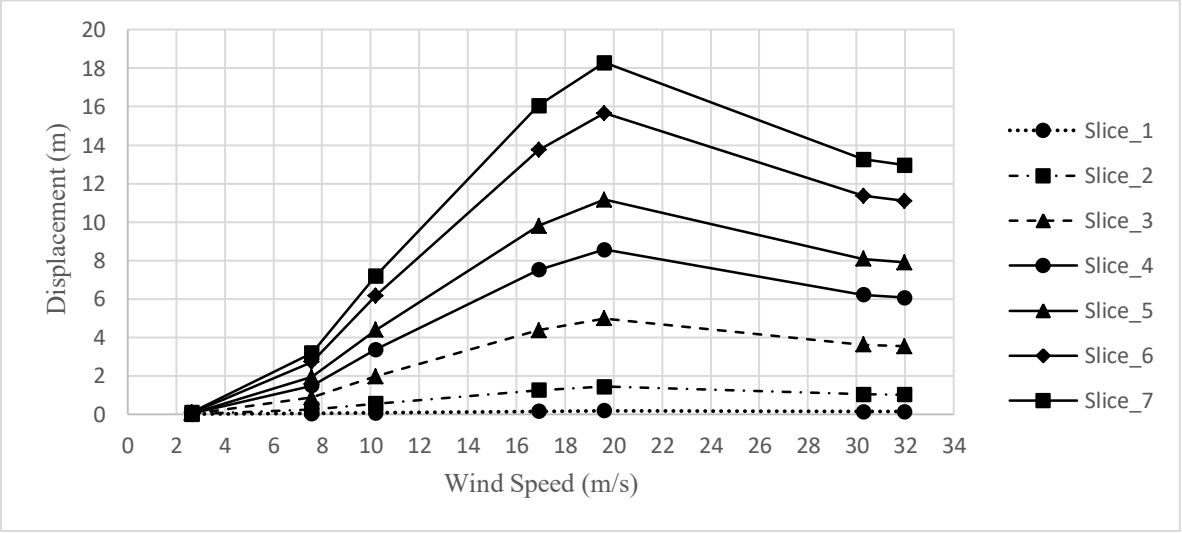

Graph 18 - VIV displacements for the corresponding Slices

8 Conclusion and Future Recommendations

The experimental and numerical models could capture the main features of the tower:

- It was observed that the drag coefficients are lower at the nose and higher at the tail, which coincides with the literature of the interaction of the tower shape with the wind loads.
- The aerodynamic of the shape of the tower broke the correlation of the wind forces, where cross-section shape of the tower breaks the vortices.

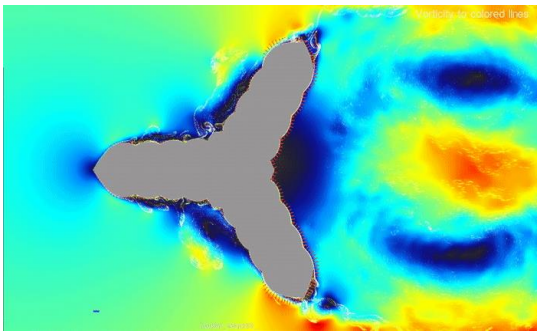

Figure 42 : Aerodynamic Shape of the Tower

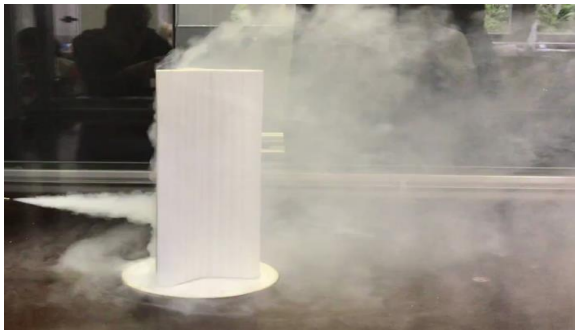

Figure 43 : Top Effect of the Constant Cross-Section Model

- The structural behavior of the tower could be identified from the experimental models in the wind tunnel and numerical CFD simulations.

- However, there are discrepancies between the experimental and the numerical models (CFD), hence the following recommendations can be implemented to improve the accuracy of the results

- Wind Tunnel Test (Section Model): A top plate could be attached on the 3D model and the model should be lifted to the middle of the Tunnel. This could allow the wind to pass around the 3D model and not over it. By lifting the model, the boundary layer effect could be eliminated.

- Wind Tunnel Test (Section Model): It's recommended that the model is tested in an inverted position, not vertically but horizontally with a sensor at one end and another sensor in the far end and to be lifted in the middle of the wind tunnel chamber. The enhancement expected from this procedure is not to depend on one sensor to take the measurements and in addition to eliminate the boundary layer effect on the model.

- Wind Tunnel Test (3D Model): Modelling the terrain around the tower would resemble more the real structure.

- CFD Simulations (Dynamic Study): Addition of more slices to represent the exact shape of the tower. Also by studying more directions in increment of 10 degrees could give a better understanding.

List of Figures

List of Tables

9 References

[1] W F Baker, D S Korista and C Novak, "Engineering the World's Tallest Building : Burj Dubai," *CTBUH 8th World Congress,* p. 10, March 2008.

[2] A. Abdelrazaq, "Validating the Structural Behavior and Response of Burj Khalifa: Synopsis of the Full Scale Structural Health Monitoring Programs," *International Journal of High-Rise Buildings ,* pp. Vol 1, No 1, 37-51, March 2012 .

[3] J. Aldred, "Burj Khalifa-a new high for high-performance concrete," *ICE,* pp. 66-73, May 2010.

[4] J Weigand, "Bringing to ife the World's Tallest Structure," *The Journal of Undergraduate Research at the University of Tennessee ,* pp. 83-89, March 2013 .

[5] W F Baker, J J Pawlikowski and B S Young, "The Challenges in Designing the World's Tallest Structure: The Burj Dubai Tower," *Research Gate ,* pp. 1471-1480, April 2009.

[6] P. A. Irwin and W. F. Baker, "The Burj Dubai Tower : Wind Engineering," *Structure magazine ,* pp. 29-31, June 2006.

[7] O. Al-Sehail, "Burj Khalifa as a Technical Object: Re-visualizing the Technological Innovation of the World's Tallest Building through Simondon's Philosophy," School of Architecture, McGill University, Montreal , August 2014.

[8] A. Abdelrazaq, "Design and Construction Planning of the Burj Khalifa, Dubai, UAE," *Structures Congress, ASCE,* pp. 2993-3005, 2010.

[9] B Baker and J Pawlikowski, "The Design and Construction of the World's Tallest Building: The Burj Khalifa, Dubai," Structural Engineering International , April 2015.

[10] P. A. Irwin, "Votices and tall buildings: A recipe for resonance," *American Institute of Physics,* pp. 68-69, September 2010.

[11] Uniform Building Code (UBC-97), 1997.

[12] EN 1991-1-1: Eurocode 1: Actions on Structures, 2004.

[13] *SOFiSTiK AG Software,* Version 2018.

IV. PROJECT ASSIGNMENT 2

Optimization of wind barrier for bridge deck cross-section under wind loading

(a) Study and literature review about behaviour of different cross sections under wind. Study and literature review about multi objective optimization.
(b) Modelling and simulation of the reference bridge cross-section (basic cross section) using CFD tool VXflow at steady flow and determining the static wind coefficients.
(c) Study on different wind barriers and their effects on the static force coefficients when included to the bridge section; analyses for Vortex Induced Vibration (VIV)
(d) Use the FEM model of the bridge analysis, with wind barriers.
(e) Analyzing the statistical wind profiles along the bridge cross-section for different wind barriers.
(f) Compare the wind coefficients and the overturning forces to identify the optimized wind barriers for the bridge cross section.
(g) Draw different set-ups of wind barriers in .STL format and print them in 3D (workshop building) for experimental tests.
(h) Submission of the reports and presentation of the results.

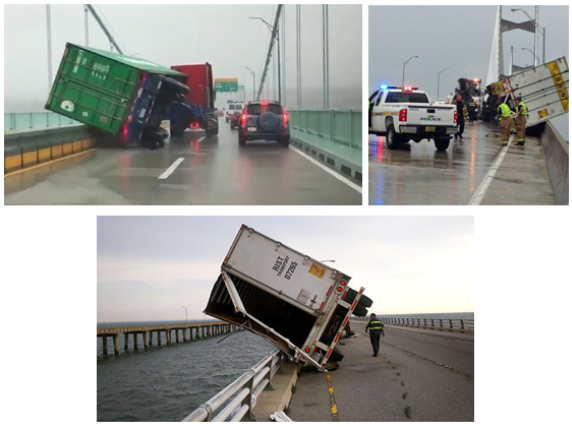

Overturning of vehicles on bridges (Google Images sources, i.e. https://www.dailymail.co.uk/news/)

Following report with the pages from 1 to 32 correspond to pages 68 to 99 of the report at hand

Erasmus+ Wind Project in
Forecast Engineering: From Past Design to Future Decisions
August 2019, Weimar, Germany

Wind Project 2

Optimization of Wind Barrier for Great Belt Bridge under Wind Loading

Submitted by

Abdelghany Sherif
Abdou Islam
Gortnar Jernej
Markasović Dorotea
Suarez Afonso
Vaz Leonor

BAUHAUS-UNIVERSITÄT WEIMAR

Faculty of Civil Engineering

Structural Engineering Department

Table of Contents

List of Figures

List of Tables

1 Introduction

With our project, we are analyzing the influence of the wind on the bridge deck section with added wind barriers. With adding barriers, our goal is to reduce wind influence on overpassing vehicles but also not to increase the wind influence on the bridge deck. As we can predict, side wind is causing forces on the bridge deck (drag, lift and moment), this forces also occurs on vehicles on the bridge and may causes them to overturn as you can see in Figure 1.1. With adding the wind barriers, there would increase in forces on the bridge and reduce the influence on the vehicles.

Figure 1.1 Example of the overturning.

What is important to know is, that wind induced accidence, such as overturning, can cause life and property loss. To prevent the overturning on plain sections this usually means closing the bridge for trucks. Closing the bridge also cause an economic and time loss for transporting. This is the main reason why responsible engineers, for designing the bridge deck, wants to improve ride comfort and safety of overpassing.

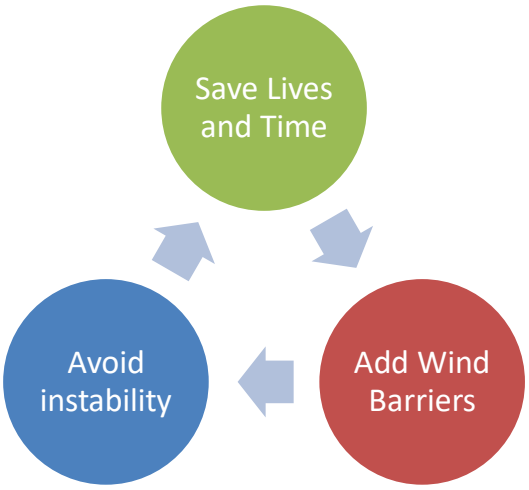

Figure 1.2 Project target circle

With this project, our target is to save lives and time, when crossing the bridge, with adding wind barriers on the deck and to avoid any unsafety, like instability, because of changing the bridge shape. As you can see in Figure 1.1, all of the targets are connected so we need an optimization study to get the best shape out of.

2 Project objective

Our main project objective is to reduce wind influence on vehicles that are crossing the Great Belt bridge. As we mentioned in the introduction, wind can cause closure of the bridge or even overturning of the vehicles. With literature review, we saw that wind barriers reduces the wind effect most efficiently and we confirmed that with preliminary testing in wind tunnel. As we will describe in the section 3, we did the study procedure as our project tasks demanded it, found a way of reducing the overturning moment, and minimize the effect on the great belt bridge.

3 Study procedure

We started our study with identifying the types of the barriers that we analyzed. We chose three different types of the barriers: (1) Solid barrier with a height of three, 0 m, (2) perforated barrier with a height of 3, 0 m and 33% perforation and (3) curved perforated barrier with height 3, 0 m and perforation around 30%. We divided our work on two parts (1) Experimental and (2) Numerical and study the same phenomena with both of the study procedures. If we refer on Figure 3.1, we completed our tasks gradually, which we will explain them later in the report, and at the end we did the comparison study of both results.

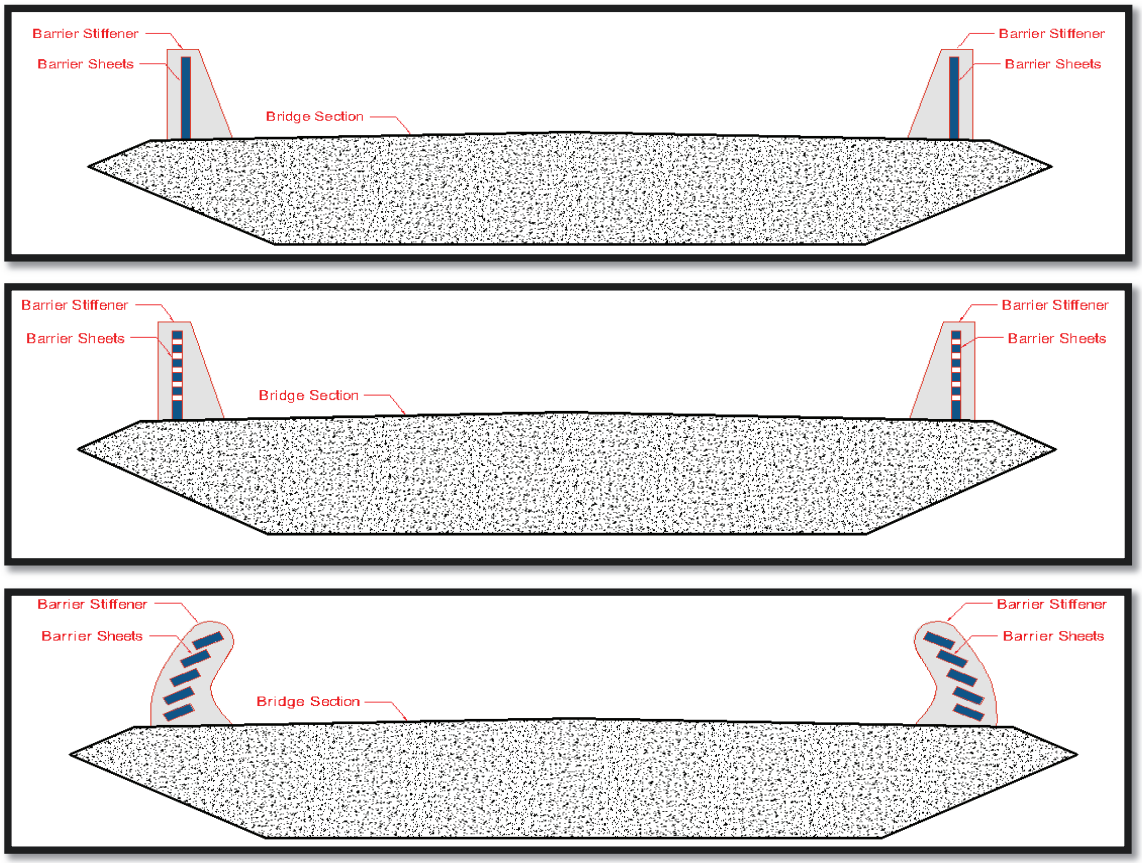

Figure 3.1 Barriers cross-sections

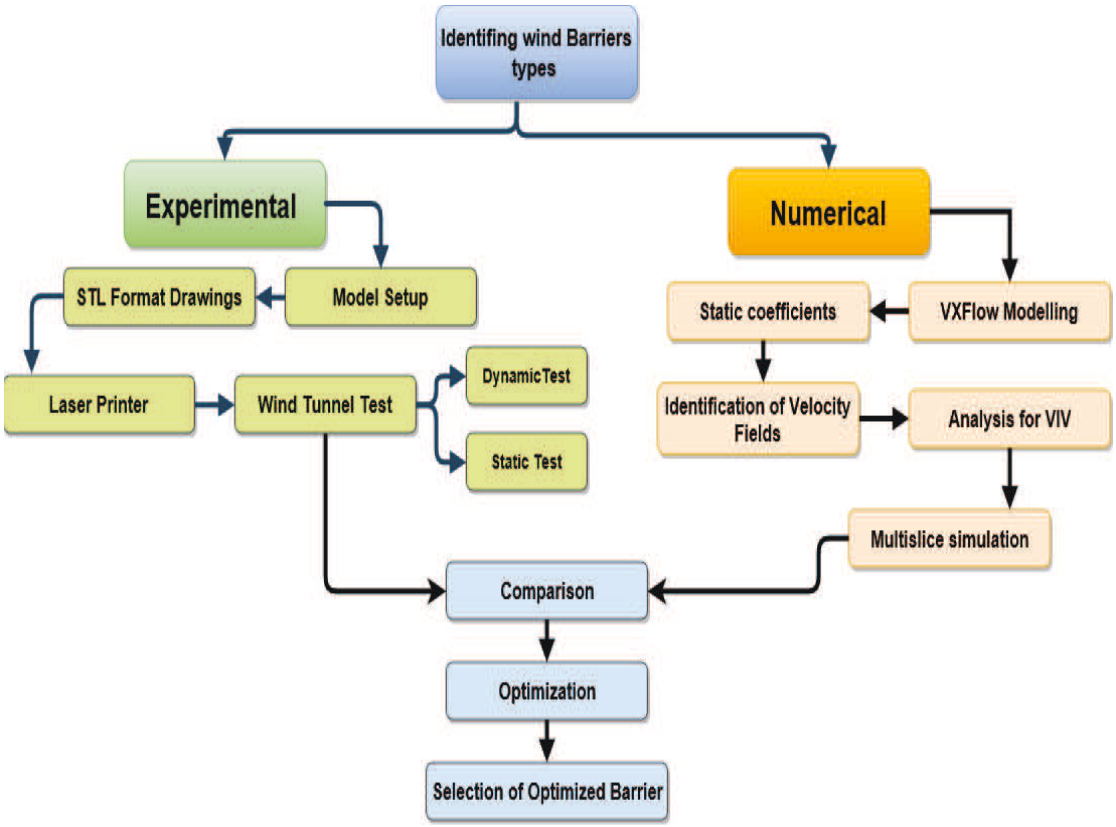

Figure 3.2 Path of Study procedure

4 Wind tunnel test

4.1 Model setup

4.1.1 Scaling

Our model was scaled from the real measurements of the Great Belt Bridge to fit it in the wind tunnel. We also scaled the data and parameters which were needed to analyze the model in the wind tunnel. We were searching the frequency of the bridge and stiffness of the bridge to run the dynamic simulation in the wind tunnel. We used next ratios of the scaling the bridge as shown in table 4.1.

$$\mathbf{f} = \frac{1}{2\pi}\sqrt{\frac{k}{m}} = \frac{w}{2\pi} \qquad (1)$$

$$k = (2\pi f)^2 m \qquad (2)$$

K = (2 x 3.14 x 2.78)^2 x 2.587
So, K = 788.5 KN/m

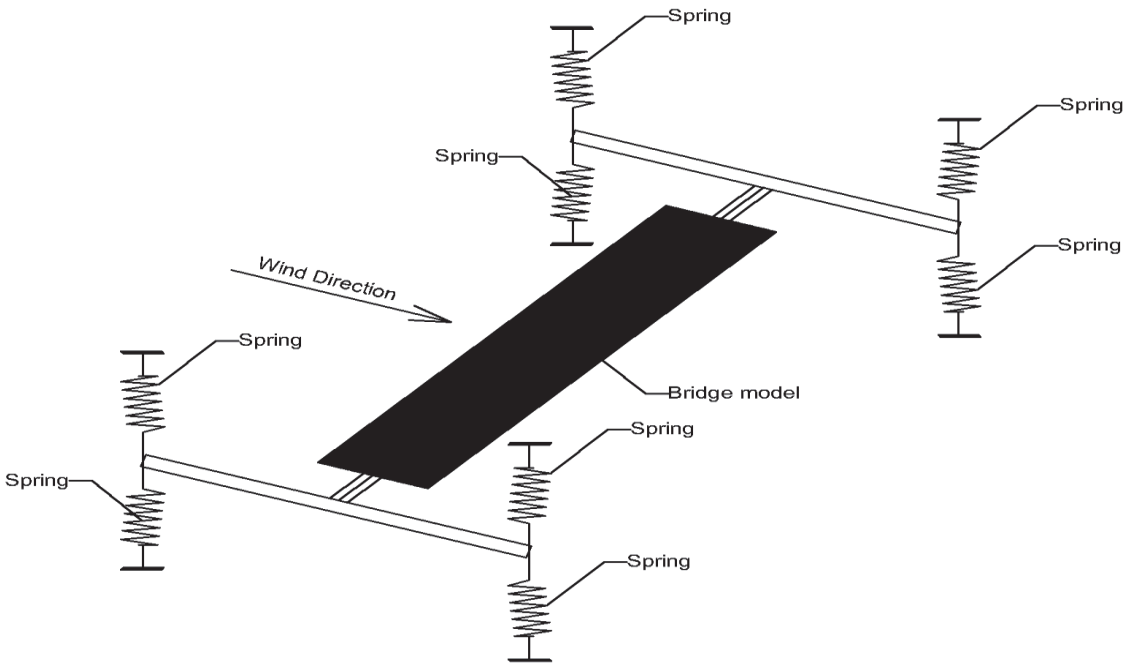

Figure 4.1 Dynamic test methodology

Table 4.1 Scaling rules.

Parameters	Scale ratio
Length	$1/\boldsymbol{\lambda}_L$
Wind velocity	$1/\boldsymbol{\lambda}_U$
Mass per unit length	$1/\boldsymbol{\lambda}_L^2$
Mass inertial per unit length	$1/\boldsymbol{\lambda}_L^4$
Structural frequency	$\boldsymbol{\lambda}_L/\ \boldsymbol{\lambda}_U$
Damping ratio	1

Table 4.2 Scaling of the model.

Property	Full scale	Scale Ratio	Scale Down
Length	-	1:100	1.2 m
Wind Velocity	40.0 m/s	1:10	4 m/s
Mass per Unit Length	21.56 t/m	$1:(100)^2$	2.156 kg/m

4.1.2 Building the model

To create a model for wind tunnel test, we tried to make it close enough to our VXflow models in terms of dimensions, fixation and behavior. On the other hand, the model should be economical and easy to be installed and executed. We first used the model of bridge cross section without barrier and then installed barriers to it, using four fixation points along with the bridge in addition to two fixed points at ends. At fixation points, we used stiffeners to ensure that during test the whole model acted as one unit.

After searching for the suitable material to use in building our model, we chose two different type of material, which is available and compatible with the aim of our project. For the main body of the bridge we used (Styrofoam) and for stiffeners and barriers we used (MDF) with thickness 2 to 3 mm.

We drew our model and barriers in the STL format drawings in AutoCAD, which were needed for laser cutting machine. We cut out the barriers from MDF board of thickness 2 mm and our stiffeners from board of thickness 3 mm. We built our model in the way that barriers can be changed and prepared for the analysis.

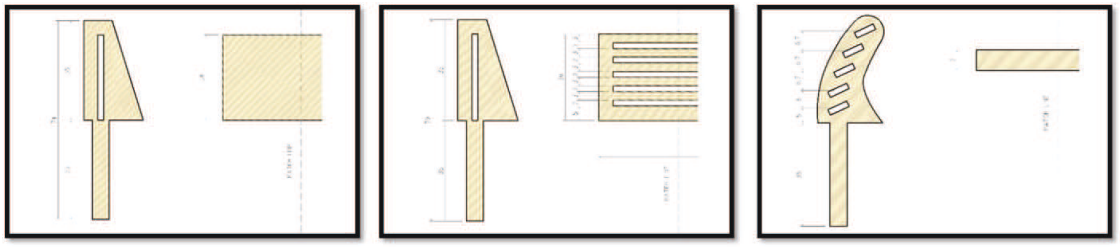

Figure 4.2 Stiffeners of barriers in model

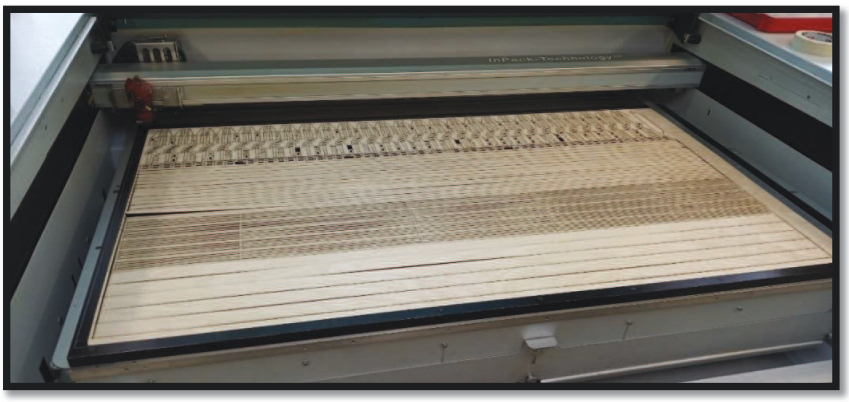

Figure 4.3 Laser cutter

The following photos show the wind tunnel laboratory at "Bauhaus-University Weimar" and installation of our bridge model.

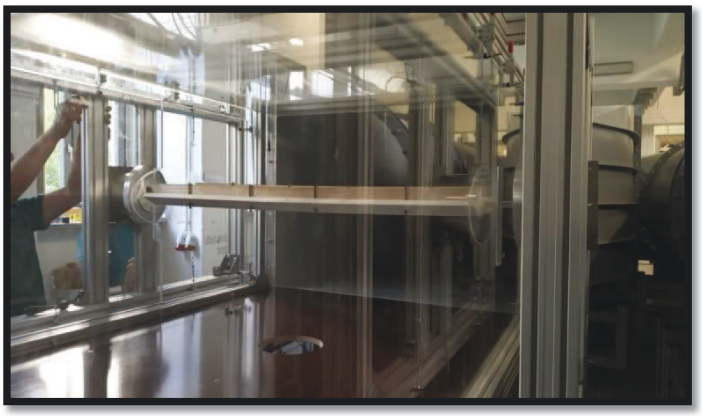

Figure 4.4 Static test

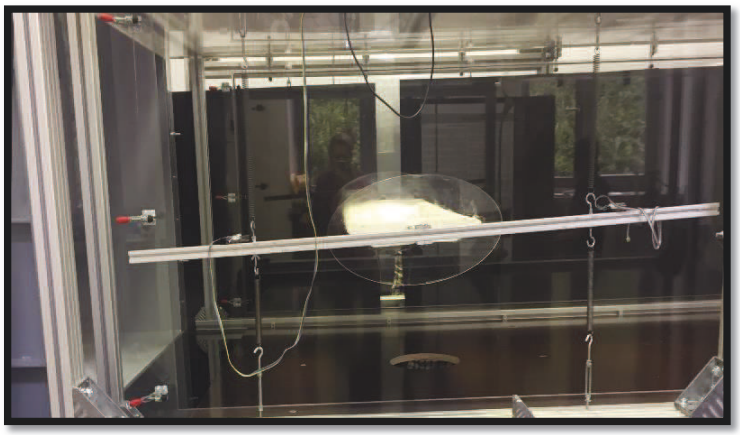

Figure 4.5 Dynamic test

4.2 Wind tunnel test

Wind tunnel tests has been done for static and dynamic approaches to calculate coefficients and compare them with numerical calculations.

4.2.1 Static Analysis

With static analysis, we measured static coefficients, which are relevant for further study in the wind tunnel. Static analysis means that the bridge deck is stable during the analysis and that the wind speed is constant. With this analysis, we can process static coefficients for the drag (C_D), lift (C_L) and moment (C_M) and later recalculate them into the forces. This coefficient are unitless and are normalized regarding to the width (31 m) and height of the bridge (4.33 m). Our study included five different position of bridge deck section. We tested our section at the angels of
-10º, -5º, 0º, 5º and 10º.

After the tests, we post-processed our data with software MATLAB and got static coefficients for the different attack angles. In next few tables and figures we will show you our results of the static experiment.

Table 4.3 Experimental data for basic section, static coefficients.

Exp. Basic Section					
Angle	-10.00	-5.00	0.00	5.00	10.00
C_L	-0.8682	-0.5061	0.0048	0.4804	0.9526
C_D	0.1757	-0.0162	-0.0599	0.0867	0.1148
C_M	-0.1996	-0.1517	-0.0586	0.1007	0.2067

Shown in table 4.3 we can see the behavior of the coefficient regarding the different attack angel for basic cross section. We can see that inclination of the bridge gives us negative results. Reason for that is that with changing the angel we are changing the area of the wind influence. This means that coefficients are increasing.

Table 4.4 Experimental data for solid barrier, static coefficients.

Exp. Solid Barrier					
Angle	-10.00	-5.00	0.00	5.00	10.00
C_L	-1.0941	-0.2612	0.0779	0.1086	0.1035
C_D	0.269	0.1936	0.2194	0.265	0.3417
C_M	-0.3327	-0.1236	-0.0709	-0.0272	0.0105

Shown in table 4.4 we can see response of the bridge deck section with solid barriers. We can see that comparing to basic section all of the coefficients have increased and that with adding wind barriers we increase the forces in the bridge. We predicted that behavior already in introduction and we are now confirming it with experimental analysis.

Table 4.5 Experimental data for perforated barrier, static coefficients.

Exp. Perforated Barrier					
Angle	-10.00	-5.00	0.00	5.00	10.00
C_L	-1.1347	-0.6151	-0.1421	0.1087	0.27
C_D	0.2528	0.1823	0.191	0.2351	0.3064
C_M	-0.1987	-0.098	-0.0238	0.0043	0.0621

Table 4.5 gives us the values of static analysis for deck section with perforated barriers. As expected, the results comparing to basic cross section are higher and this gives us the felling that with adding any kind of barriers, even perforated and curved barrier the influence of wind will increase. We can see that in the experiment perforated barrier gives us better results and more reasonable then for the section with solid barriers.

Table 4.6 Experimental data for curved barrier, static coefficients.

Exp. Curved Barrier					
Angle	-10.00	-5.00	0.00	5.00	10.00
C_L	-0.0046	-0.1126	0.0348	-0.0298	-0.012
C_D	0.0152	-0.0589	0.0193	-0.0079	0.001
C_M	0.0057	0.003	0.0069	-0.0016	0.0063

Table 4.6 is showing the behavior of the bridge deck during static analysis for the deck section with curved barriers. As for the basic section, also this section is not giving us very reasonable results. We can see that lift and moment are behaving in the same way that perforated and solid section but drag coefficients is behaving in the different way. We can explain that in a way, that curved barriers causes more vortices than perforated one. In addition, those results differ to the perforated barrier.

In figures below, we are showing the values of the experimental analysis in way that is more representative. We can see that the shapes of the curves are showing that in all of the experiments the response of the bridge deck section is the same for lift (Figure 4.1) and moment (Figure 4.3) coefficient. On the other hand, we can see in Figure 4.2 that drag is very different for each kind of barrier. The most satisfying results we got for solid barrier and perforated barrier. In addition, as the figure shows, if the decision would be made only on experimental analysis of the drag force, we would choose perforated one.

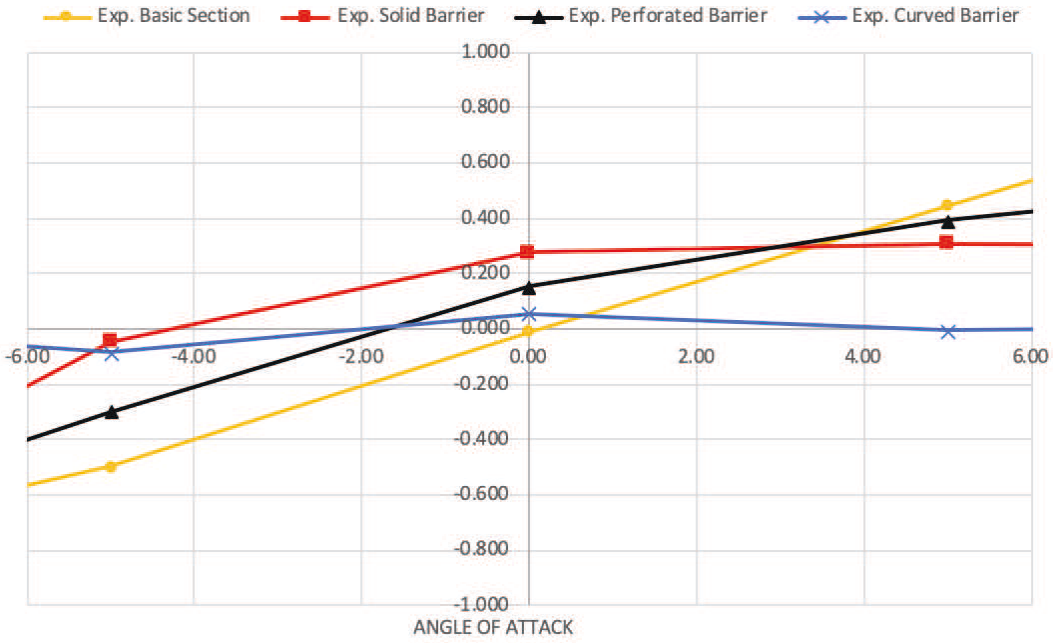

Figure 4.6 Results for lift coefficient of the experimental analysis

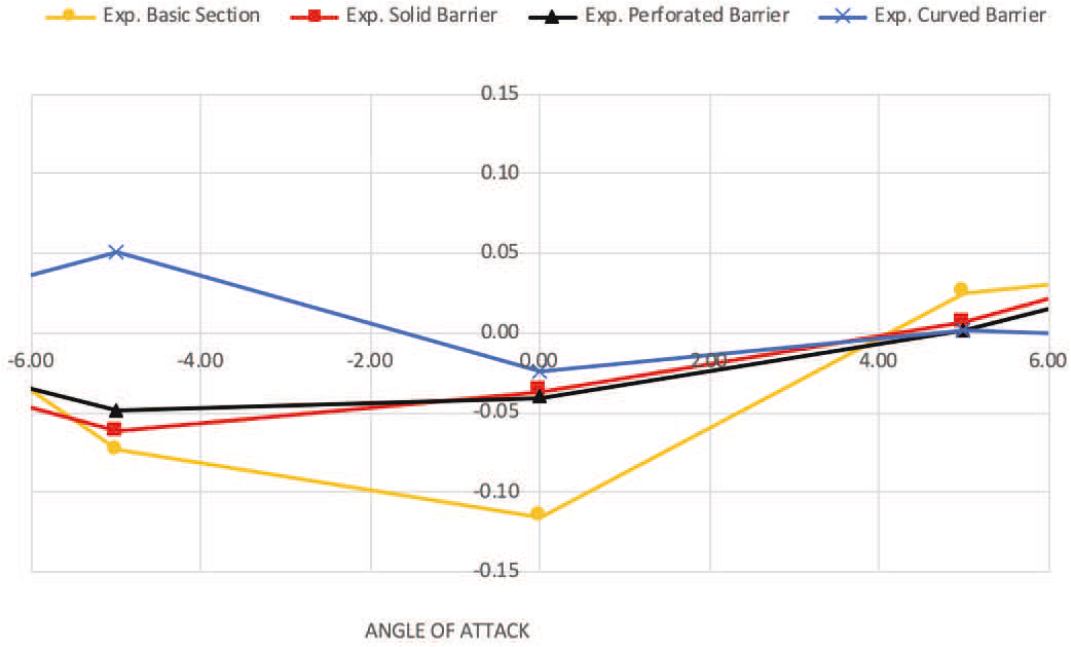

Figure 4.7 Results for drag coefficient of the experimental analysis

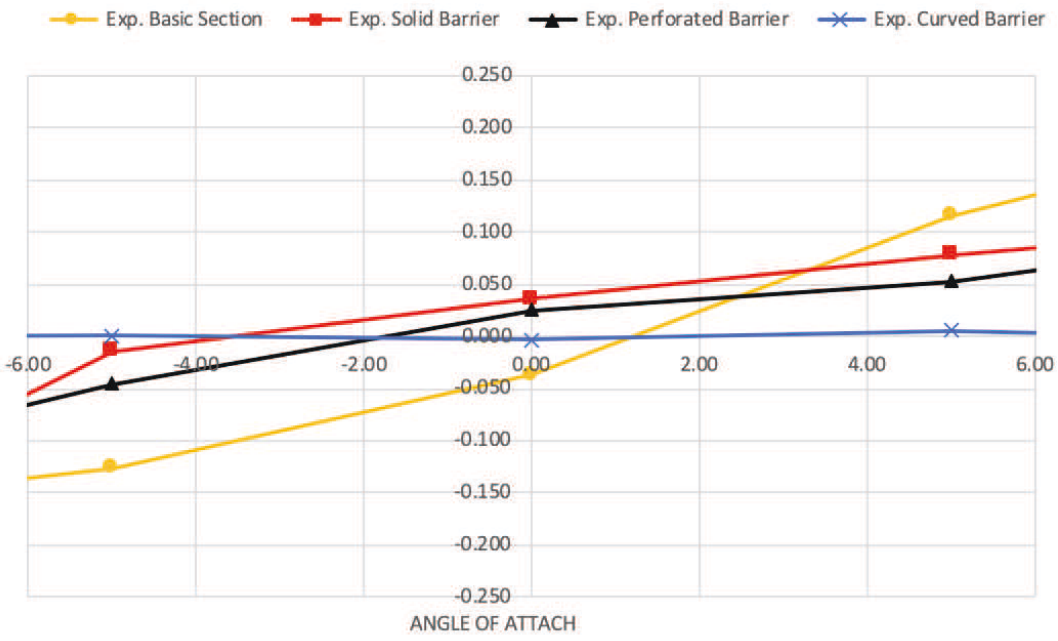

Figure 4.8 Results for moment coefficient of the experimental analysis

4.2.2 Dynamic Analysis

With the dynamic analysis, we measure the time histories of acceleration at one wind speed. We want to approach to the resonance wind speed and measure the peak acceleration of the bridge deck. The deck is fixed with four springs on each side, which allows him to move free in any direction. We measure the response of the bridge deck with one sensor, which measures acceleration in direction X, Y and Z. After we do the analysis, we gadder data and do the post-processing using MATLAB. We need to filter our data before post process them and integrate them twice around mean area. After that, we can show the displacement over time as shown in the figures below.

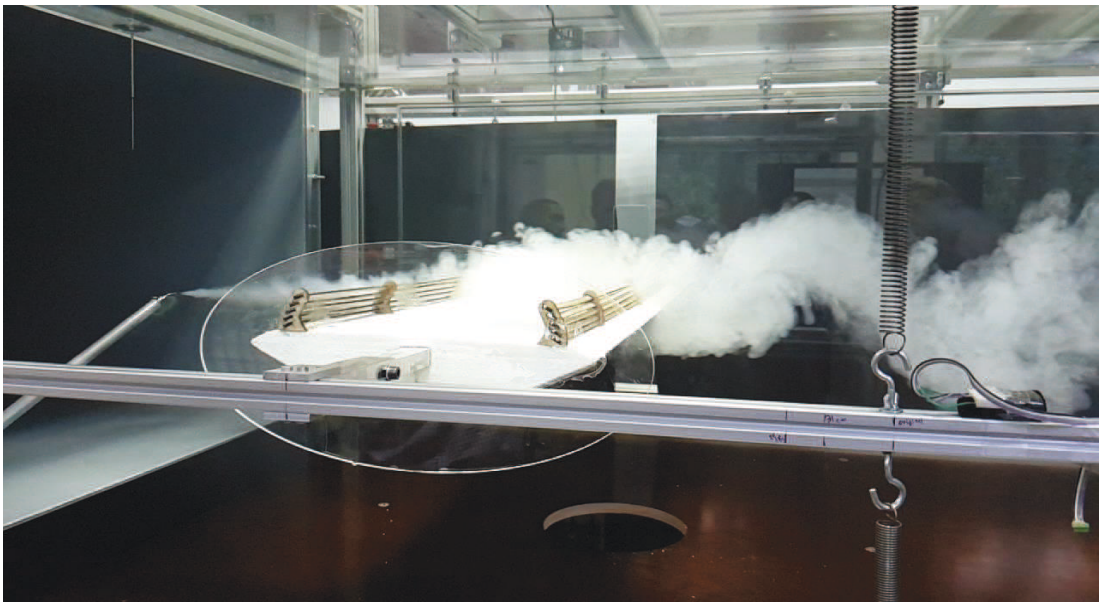

Figure 4.9 Dynamic wind tunnel test

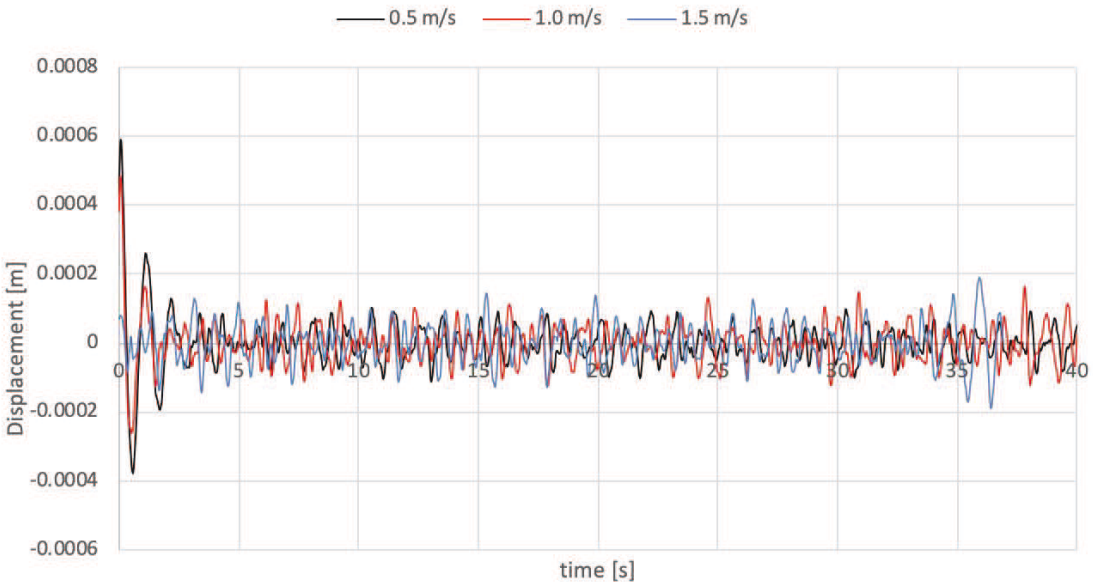

Figure 4.10 Response in the dynamic analysis for the basic cross section.

We can see in Figure 4.10 the movement of the bridge deck section at wind speed 0.5 m/s, 1.0 m/s and 1.5 m/s. These velocities are scaled to the model that is in the wind tunnel. We expected the resonance wind speed to be around 0.5 m/s for scaled model. Because we were using our springs with different stiffness as calculated, we tried our model also at scaled wind speed of 1 m/s and 1.5 m/s. Our prediction of the resonance wind speed was not that good because we did not get the movement of the bridge deck section as we expected. We can correlate this to an aerodynamic shape of the bridge deck, and that critical wind speed needs to be precise. For our study, the movement of the basic section was not that important because we wanted to focus on the sections with barriers.

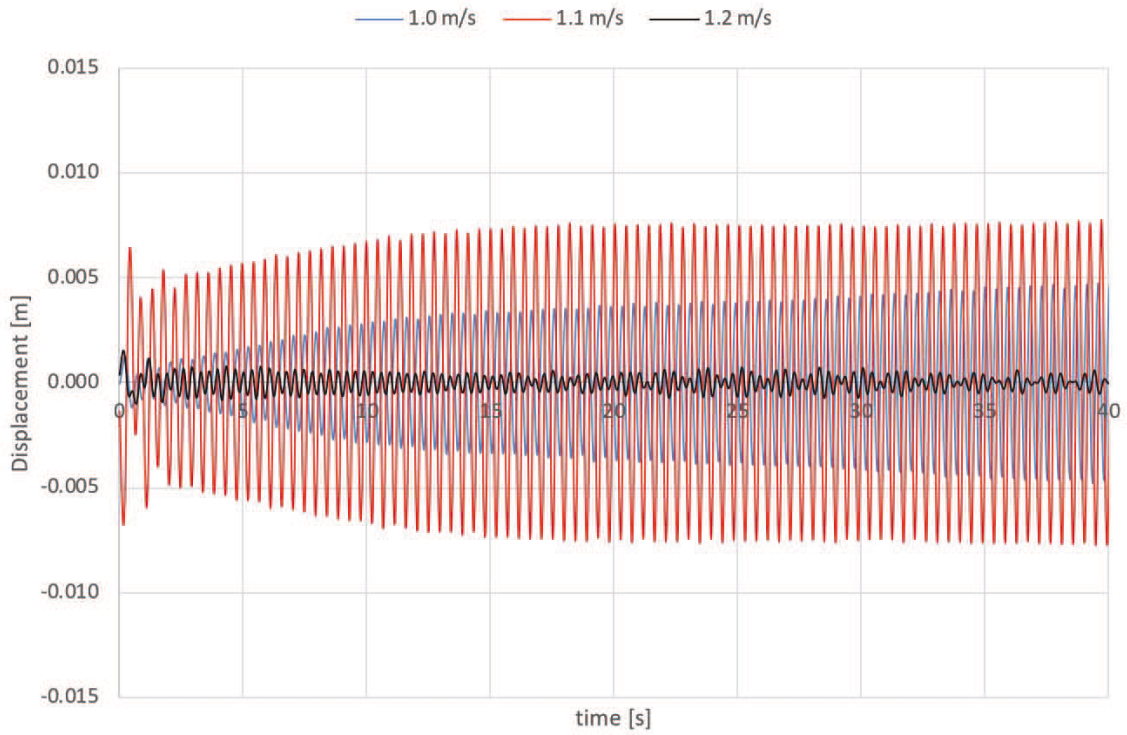

Figure 4.11 Response in the dynamic analysis for the solid barrier.

In Figure 4.11, we can see the response of the bridge deck section with attached solid barriers at three different wind speed. We tested our deck section with three different types of wind speed that were scaled for the wind tunnel section. We predicted, that resonance wind speed should be around 1.0 m/s scaled for the modal and regarding to numerical simulations. We started our study from 0.5 m/s and increased the wind speed every minute. At the wind speed 1.0 m /s, we got a response from the bridge deck and got a resonance mode. After we increased the sped to one, 1 m/s we got a bigger response to a new wind speed and got the highest amplitude of the movement. For the highest amplitude, the displacement was 0.0076 m for scaled model.

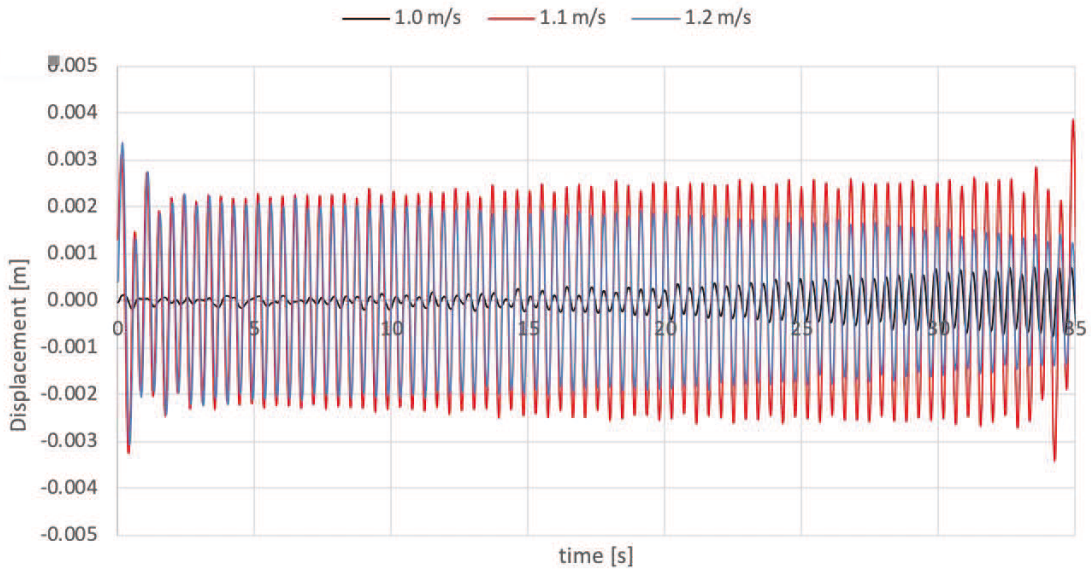

Figure 4.12 Response in the dynamic analysis for perforated barrier.

Our goal was to get the response of all different types of wind barriers. In the Figure 4.12, we can see the response of the section with perforated wind barriers. From the calculation in the numerical analysis, we got the resonance wind speed for scaled model also around 1.0 m/s. We started the analysis with the same starting wind speed as for solid section and increased the wind speed by step 0.1 m/s. We got the response of the bridge section at 1.0 m/s as shown in Figure 4.3 and the maximum response for the wind speed 1.1 m/s for scaled section. For wind speed 1.1 m/s, our section is in resonance mode.

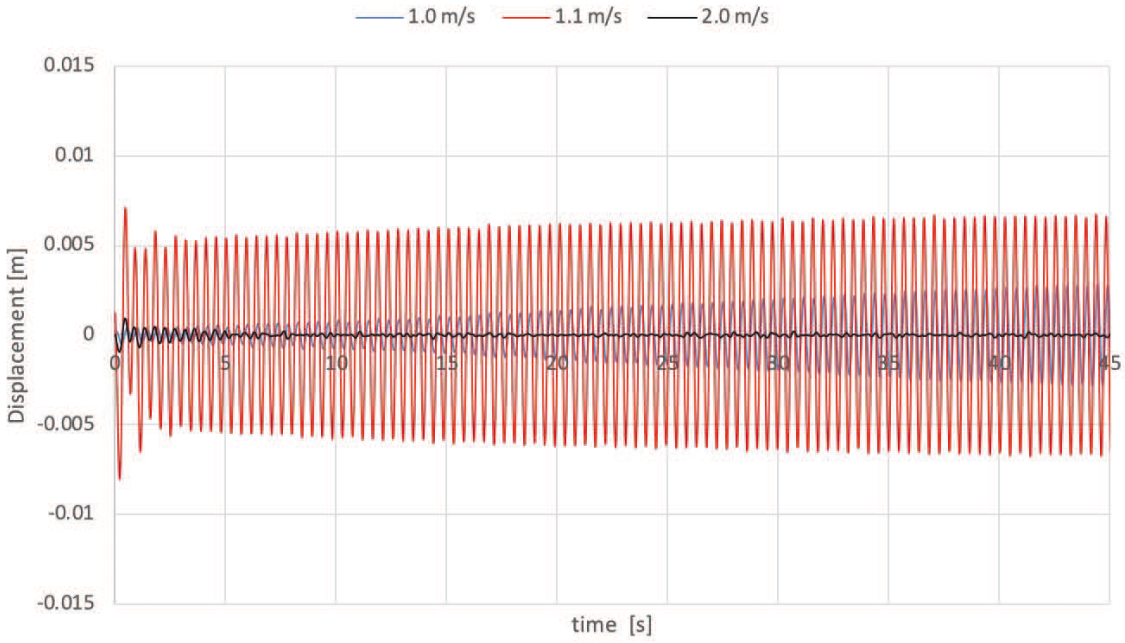

Figure 4.13 Response in dynamic analysis for curved barrier.

The dynamic test was for curved barrier. As shown in Figure 4.13, we can see that also for this type of barriers the resonance wind speed is 1.1 m/s. We got the highest amplitude with this wind speed and the highest displacement of 0.00649 m.

With the dynamic study, we confirmed our prediction of resonance wind speed for bridge section and barriers and got the response of the bridge section to compare it with the numerical part.

5 Numerical Simulations

5.1 VXflow Modelling

For starting a numerical study, we needed to create the models for numerical study using VXflow software. We prepared the codes describing the input files including: the geometry of section, wind velocity, number of panels, etc. We prepared input files for all of the different types of wind barriers and made the analysis on all of them. In figures below (from 5.1 to 5.4), you can see the visualization of the input files for static analysis. Our input files are in appendix to this submission.

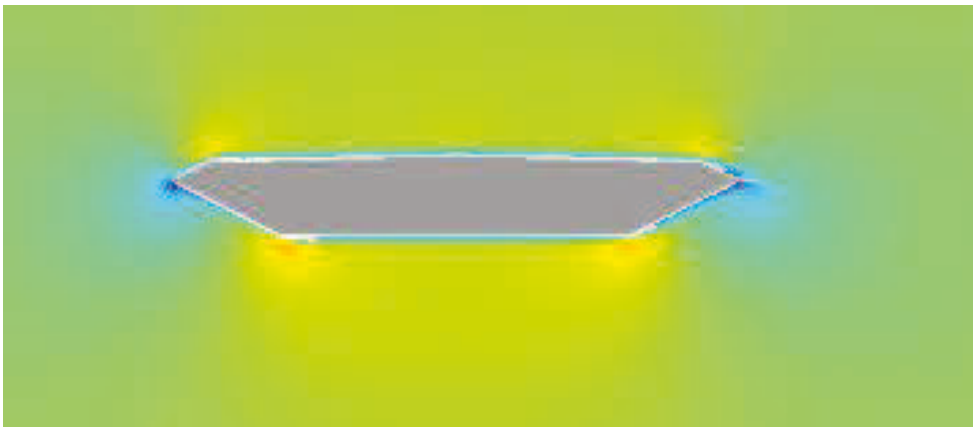

Figure 5.1 Vxflow model of the basic section

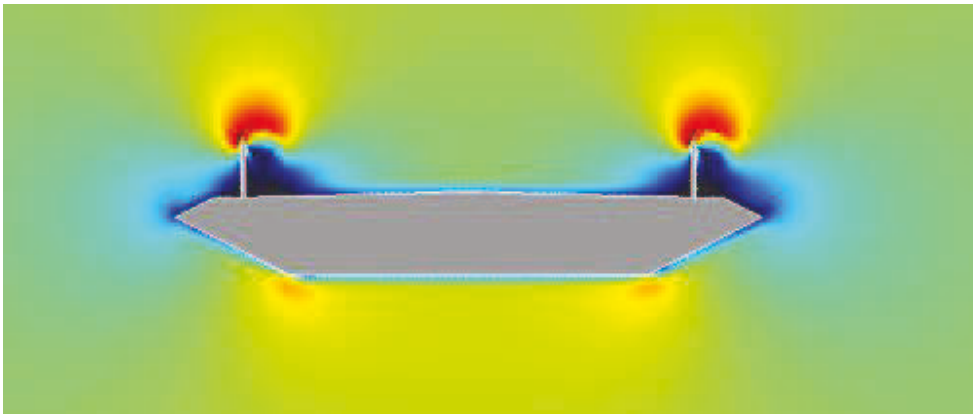

Figure 5.2 Vxflow model of the solid barrier section

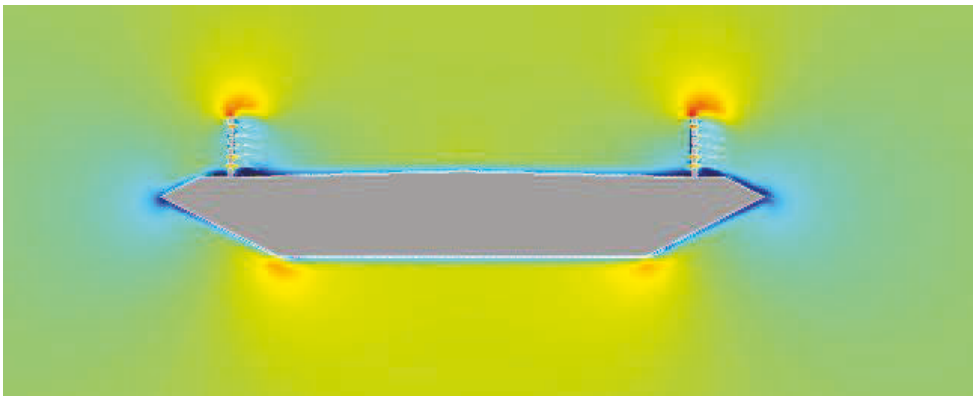

Figure 5.3 Vxflow model of the perforated barrier section

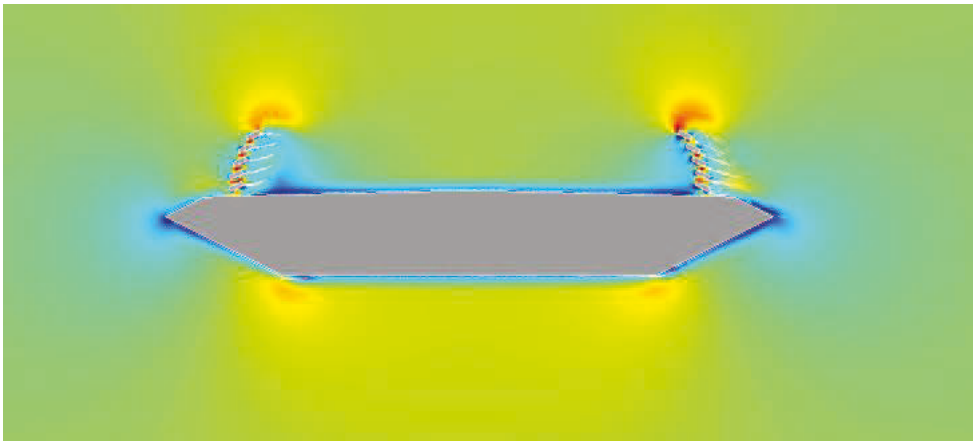

Figure 5.4 Vxflow model of the curved barrier section

5.2 Static analysis

As already mentioned in experimental part, the static analysis is to determine the coefficients for further analysis. Therefore, we also need to mention that with static coefficients we can assess influence of the wind barrier on the bridge section. If static coefficients are small, the wind barrier influence on the bridge is small, which means that forces in the bridge will not drastically. If these coefficients are larger, this brings us to conclusion that the influence of the wind barrier on bridge section is bigger and so are forces. We also mentioned that with adding barriers to the bridge section we are increasing the wind influence on the bridge deck section and decreasing the influence on the vehicle. Because of the increase of the influence on the bridge, we need to get the static coefficients for different angels of the attack for all kind off barriers and compare them at the end. In the tables and figures below, we will show you, what kind of influence the barriers have on bridge section and what kind of barrier is the best regarding to numerical part of the project.

Table 5.1 Static coefficients for basic section.

Basic section							
Angle	-6.00	-4.00	-2.00	0.00	2.00	4.00	6.00
CL	-0.354	-0.239	-0.105	0.0452	0.021	0.096	0.205
CD	0.452	0.342	0.297	0.293	0.312	0.373	0.647
CM	-0.099	-0.062	-0.021	0.020	0.0653	0.106	0.101
Strouhal No.				0.055			
Vcr [m/s]				7.87			

Table 5.1 is showing us the results of the static analysis for basic section without barriers. As we can see, the coefficients in this table are small, which means that influence of the wind is not that high. The values can be explained because of the aerodynamic shape of the section. If section is designed in aerodynamic shape, it means that the flow is streamlined. If the flow is streamlined, the influence of the wind is less noticeable because of the less vortices.

Table 5.2 Static coefficients for section with solid barriers.

Solid Barrier							
C_L	0.014	0.129	0.121	0.078	0.053	-0.026	0.056
C_D	1.052	0.753	0.806	0.974	1.052	1.235	1.422
C_M	-0.069	-0.081	-0.070	-0.060	-0.044	-0.023	-0.006
Strouhal No.				0.080			
Vcr [m/s]				5.41			

Table 5.2 gives us the values after adding the solid barriers to the bridge deck section. We can see that with adding the barriers all of the coefficients rise and the wind influence on the bridge deck increases. We can see that drag force CD increases drastically. The reason of increase is that area of the wind influence has increased. The same problem is with lift coefficient and moment. Another thing that the wind barrier has an effect on is Strouhal number. With adding wind barrier, we got lower values of Strouhal number, which means that resonance wind speed, occurs earlier than for the basic section.

Table 5.3 Static coefficients for section with perforated barriers.

Perforated barrier							
Angle	-6.00	-4.00	-2.00	0.00	2.00	4.00	6.00
CL	-0.664	-0.551	-0.501	-0.435	-0.345	-0.312	-0.248
CD	1.559	1.202	1.097	1.118	1.189	1.236	1.340
CM	-0.064	-0.077	-0.061	-0.035	-0.011	0.012	0.036
Strouhal No.				0.115			
Vcr [m/s]				3.77			

Table 5.3 show us the response of the bridge deck if we put on the perforated barriers. Surprisingly we can see that drag force here is bigger than shown in table 5.2. We can correlate this with the idea, that solid section creates more vortices around the bridge section that can influence in the positive way

with reducing the drag. In addition, we can see that lift coefficient is always negative. This means that wind always influence on the bridge deck in the way that it pushes him down.
This can increase the displacement because of the static forces that are on the bridge (such as self-weight). We can see that it is also important that moment coefficient is smaller for the perforated barrier than for the solid barrier. This can be easily explained with the area if the wind influence. Because the solid barrier has bigger area where wind can influence, the overturning moment is slightly bigger than for the perforated one.

Table 5.4 Static coefficients for section with curved barriers.

Curved barrier							
Angle	-6.00	-4.00	-2.00	0.00	2.00	4.00	6.00
CL	-0.602	-0.549	-0.481	-0.445	-0.371	-0.338	-0.271
CD	1.533	1.321	1.271	1.252	1.259	1.264	1.323
CM	-0.078	-0.074	-0.052	-0.025	-0.003	0.029	0.053
Strouhal No.				0.100			
Vcr [m/s]				4.33			

Table 5.4 show us the results for curved perforated barrier. Here we can see that with adding curves to the perforated barriers we do not improve much the response of the section. We will show the comparison of the tables in figures below, but we can say that curved and perforated barrier is giving us the same results and we did not improve anything with adding curves.

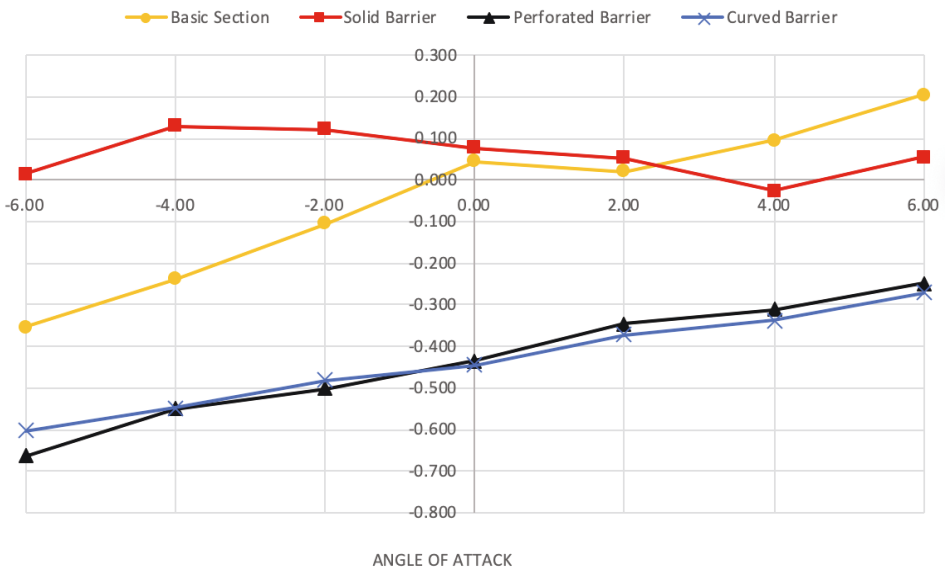

Figure 5.5 Lift coefficient from static analysis for all of the sections.

In Figure 5.5, we are showing all of the numerical data for static simulation. With this figure, we can compare the influence of adding different barriers to cross section. As we already mentioned before, we can now clearly see, that perforated and curved one have similar response on lift coefficient. We can see that solid one is the closest to basic cross section, but it increases the coefficients at some angles.

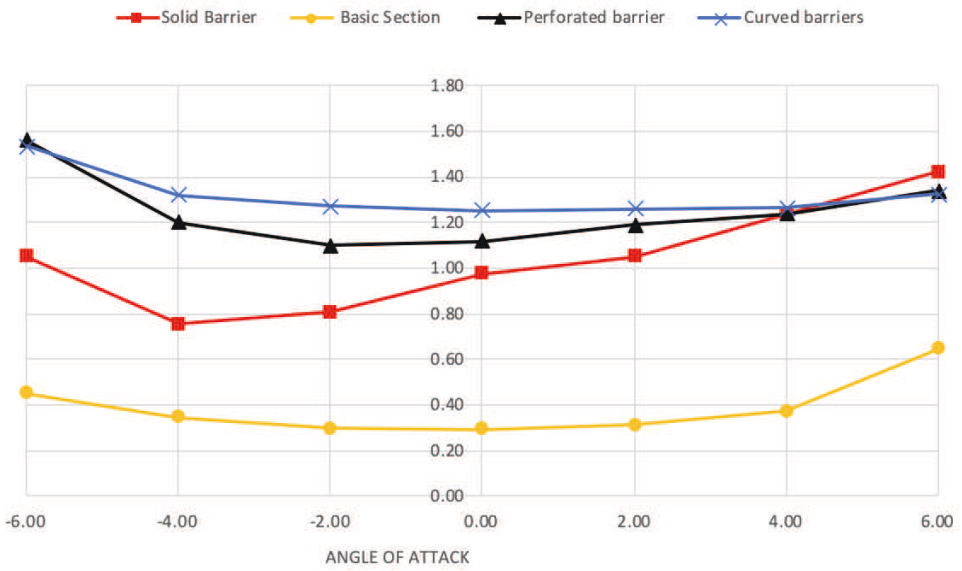

Figure 5.6 Drag coefficients from static analysis for all of sections.

In this Figure 5.6 we can see, that the drag force has increased with adding any kind of the barrier to the cross section. Interesting part is that perforated and curved barrier gave us bigger drag than solid one. Although they are close, the solid barrier gave us the best results if we would choose the barriers just assessing the drag coefficient.

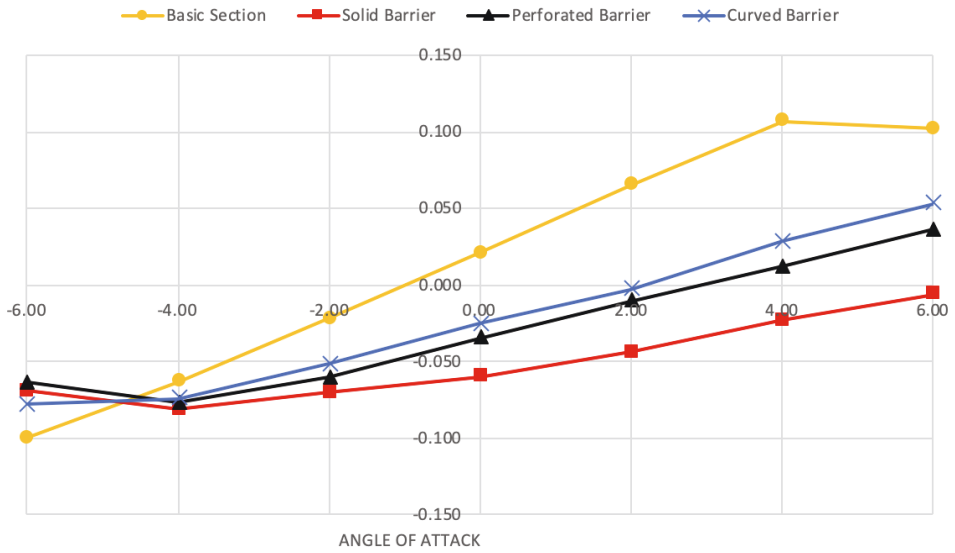

Figure 5.7 Moment coefficient from static analysis for all sections.

With looking in the Figure 5.7, we can see that with adding barriers we cause the reduction in the moment in positive angles and increasing in the negative angles. This can be explained that additional area where wind can influence causes the response of the section in the counter clockwise direction. This means that in negative angles, the cross section with barriers will have bigger moment coefficients and in the positive angles, the values would be smaller. If we compere the different types

of barriers regarding to this table we can see, that perforated and curved barriers give the closest response to the basic section.

In the figures below (from 5.8 to 5.11), we are showing the response spectrum of Strouhal number for different types of barriers. The interesting part is that the response of some section is not clear. With not clear response, we have multiplied peaks of the Strouhal number and in this case, we have more cases of resonance speed. The most important part of the response spectrum are the highest peaks of Strukal number. With these peaks, we can calculate the resonance wind speed and later do the dynamic analysis.

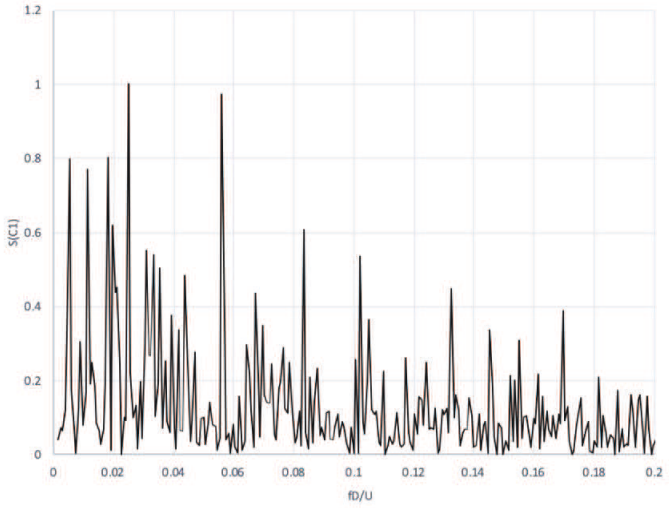

Figure 5.8 Response spectrum of Strouhal number for basic section.

For the basic section, the interesting part is that there is multiply peaks. We expected that the results would show us one peak from which we would get the critical wind speed. As we will show later, in the table, the peak of the Strouhal number is 0.055 and the critical velocity is 7.87 m/s.

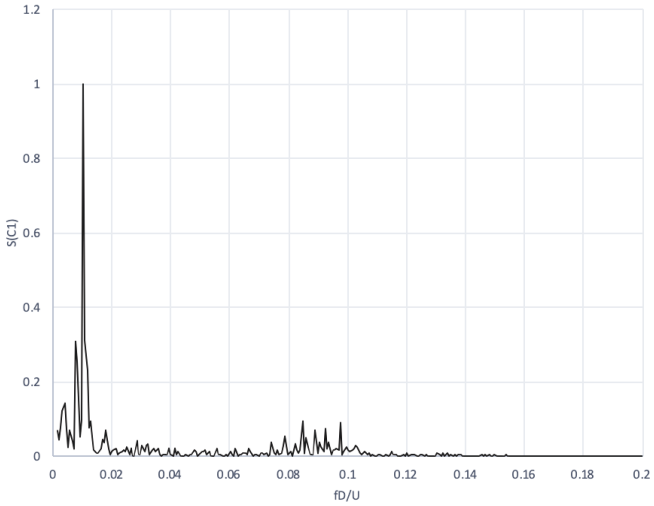

Figure 5.9 Response spectrum of Strouhal number for section with solid barriers.

The clearest response is for the solid section. We can explain this that with only one peak the resonance speed is at maximum Strouhal number. We can refer to Figure 5.9 and see that the value of Strouhal number of 0.08 and critical wind speed of 5.41 m/s.

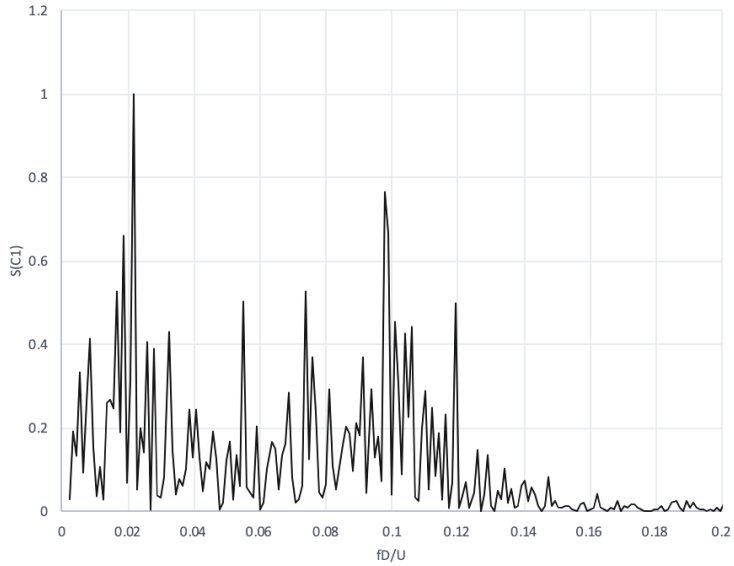

Figure 5.10 Response spectrum of Strouhal number for section with perforated barriers.

Section with the perforated barrier, as shown in Figure 5.10, gives bur blurry results. Here we cannot say that we have a resonance speed at first peak because we have a multiply peaks at this response. We took out the highest value of the Strouhal number, which is 0.12 and calculated the critical wind speed of 3.76 m/s.

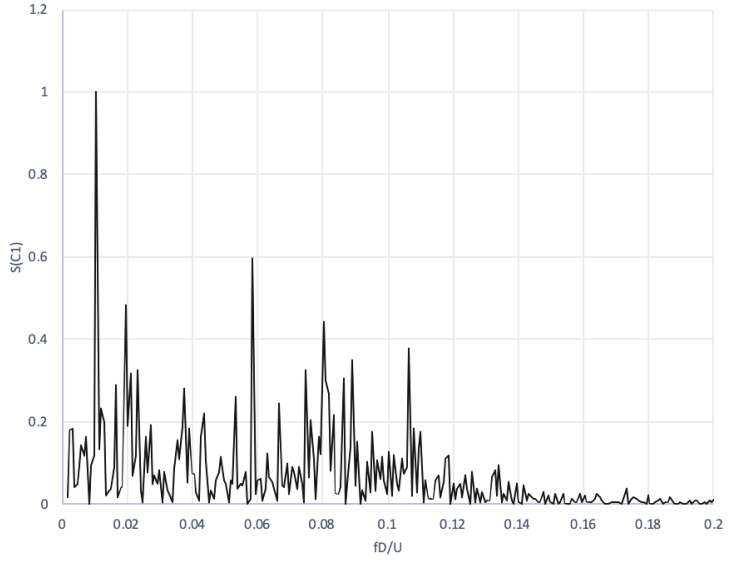

Figure 5.11 Response spectrum of Strouhal number for section with curved barriers.

Similar as before in Figure 5.10 we can see also in Figure 5.11. The response spectrum has multiple peaks, and this means that we cannot refer on only one resonance speed. We took the highest value of the response spectrum, which is 0.1 and calculated the resonance wind speed 4.33 m/s.

Table 5.5 Resonance wind speed from static analysis for all sections.

Section type	Basic	Solid Barrier	Perforated Barrier	Curved Barrier
Strouhal No.	0.055	0.08	0.12	0.10
V_{res} [m/s]	7.87	5.41	3.76	4.33

In this table 5.5, we are showing all of the resonance wind speed for all kind of barriers. These numbers were determined from the equation for Strouhal number.

5.3 Dynamic analysis

We also did the dynamic analysis with numerical approach. We calculated the resonance wind speed, as we can see in section 5.2, and ran the analysis for speeds that are lover and higher of the resonance speed. If we calculate the dynamic response for multiple wind speed, we can be sure that the resonance speed is the one that gave us the higher displacement. With dynamic analysis, we calculate the movement of the bridge deck section. We look time histories of all of the dynamic response for the displacement and ca lculate the maximum absolute value.

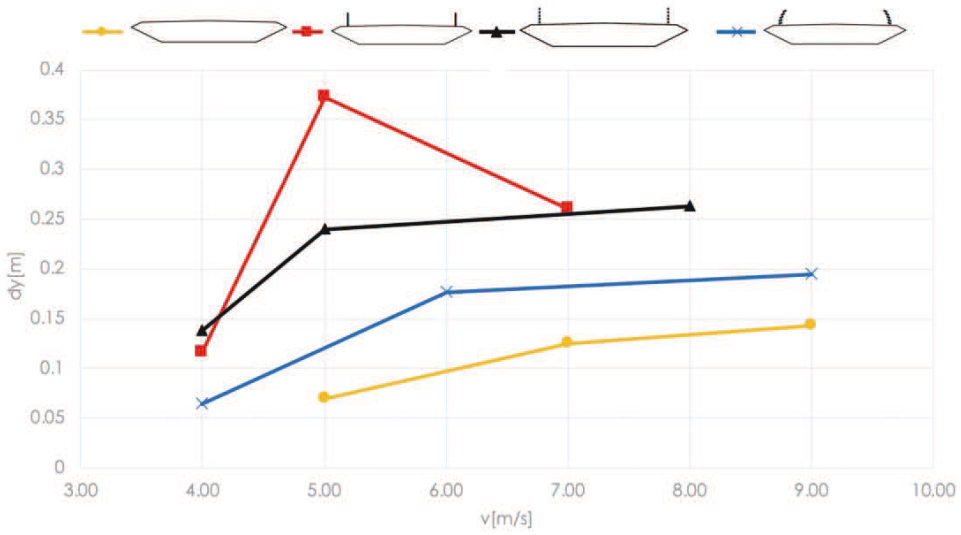

Figure 5.12 Displacement values around the resonance velocity

In the Figure 5.12, we are showing the response of the bridge deck section on the multiple wind speed analysis. We can see that solid barrier gave us the largest displacement and that the resonance speed was calculated correct. We can see that for all other barriers and section the displacement is rising regarding to velocity. This can be explained with the multiple peaks in Strouhal number. Because we did not have just one peak, we could not be sure in picking the right Strouhal number. If we would like to get the resonance speed, we would have to calculate the dynamic response for even higher velocities.

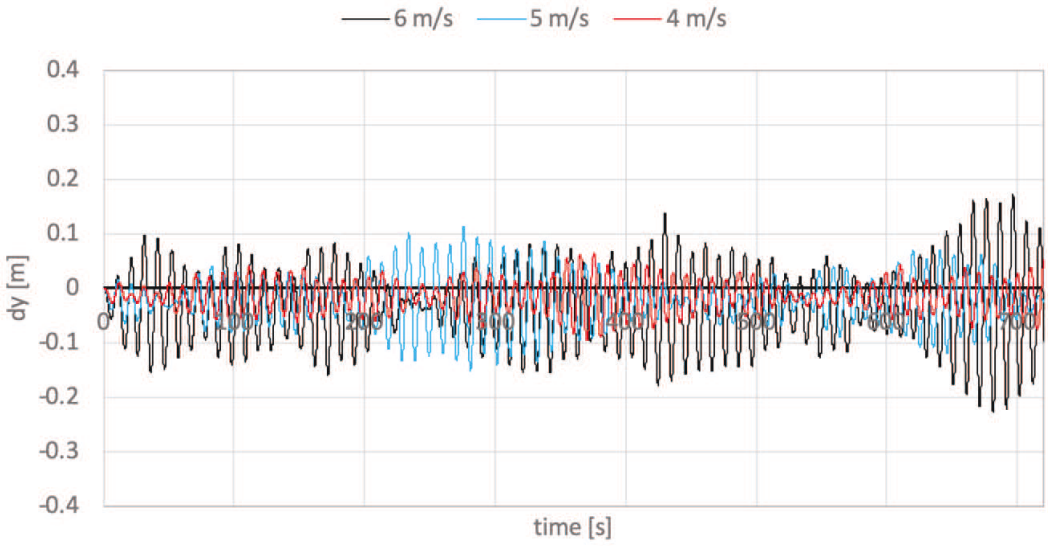

Figure 5.13 Dynamic response of cross section with solid barrier

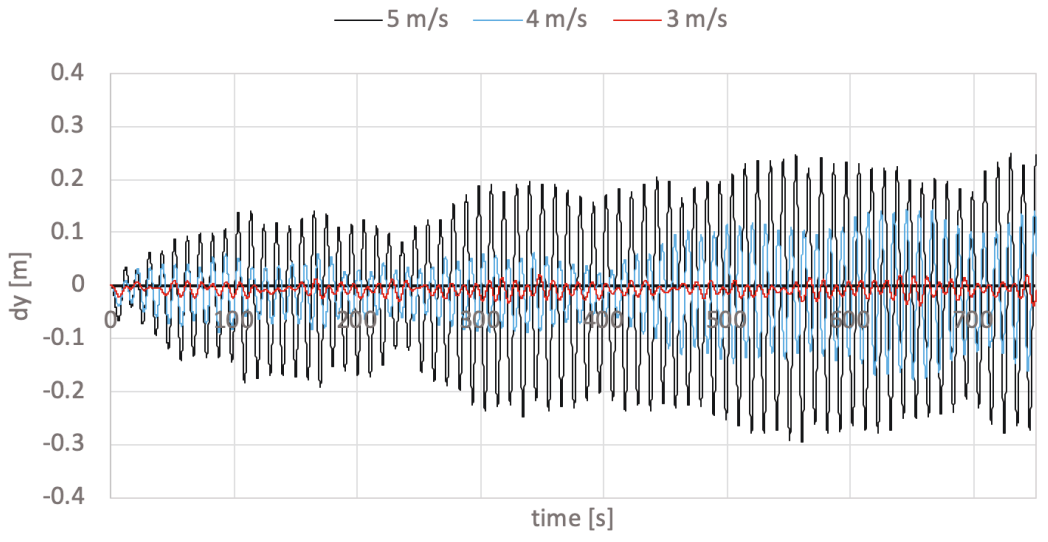

Figure 5.14 Dynamic response of cross section with perforated barrier

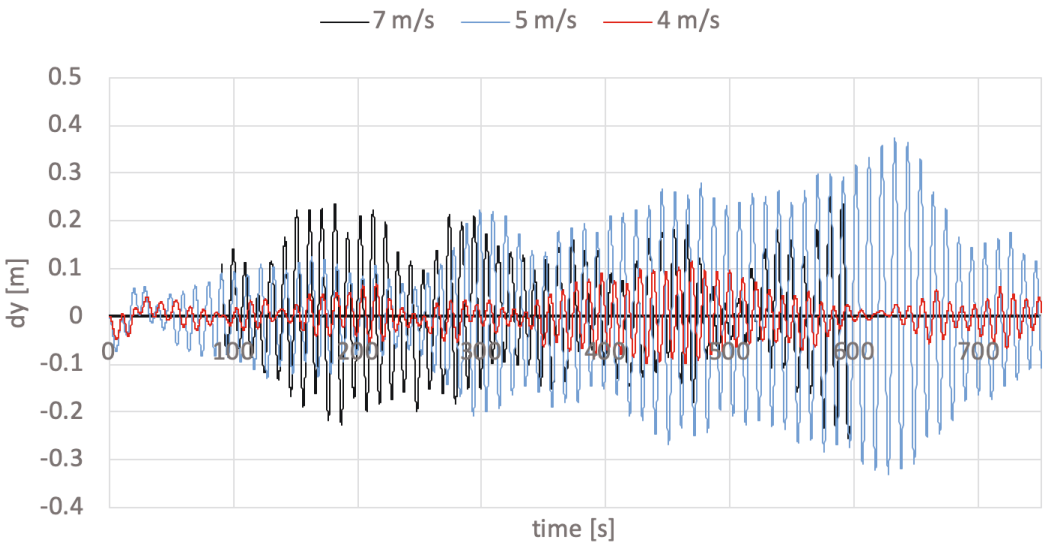

Figure 5.15 Dynamic response of the bridge section with curved barriers

In Figures 5.13 to 5.15, we can see the response of the bridge section with different barriers. We can see that all of the sections have a resonance response between the four and 6 m/s. In addition, we need to take in to account is the response or maximum displacement of the dynamic response. We can see that Solid section gives us the maximum response and maximum displacement, and this can be one of the criterion why it is better to choose perforated over curved.

5.4 Velocity profiles and overturning moment

Our study also included the study of velocity fields across the bridge deck. With this study, we can see the influence of the wind barriers on the bridge velocity fields across the bridge deck. We can predict that the higher the velocity fields are, the higher the overturning moments are. We can also say that bridge deck which is completely open is giving us the highest results of overturning moment and velocity fields.

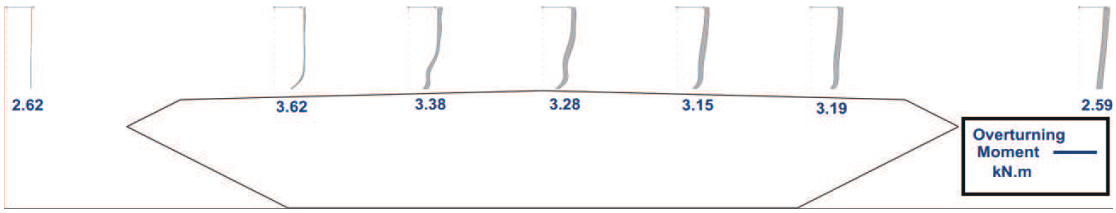

Figure 5.16 Velocity fields across the basic cross section

As we were expecting about basic cross section, we can confirm with the Figure 5.16. In a figure we can see, that velocity field on the bridge deck is almost constant and that it is not reducing across the bridge deck. We can corelate that, that vehicles are most exposed on the bridge deck without barriers. Here we have the highest velocity profiles and the highest values of the overturning moment which is 3.63 kNm for the vehicle of height 4 m.

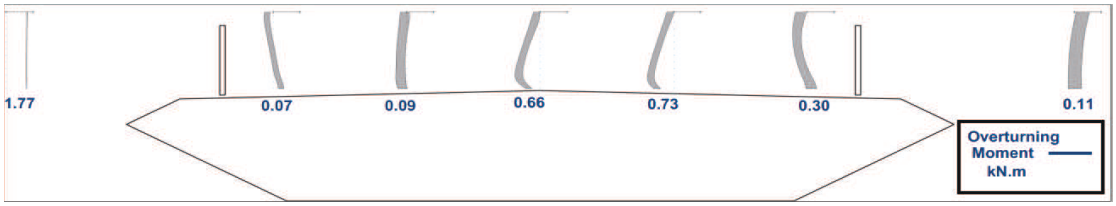

Figure 5.17 Velocity profiles across the bridge deck with solid barriers

Figure 5.17 is giving us a very good look in the behavior of the section. We can see that because of the increased vortices the velocity profile switches from positive to negative and this is causing negative overturning moment. For the vehicles traveling on the first lane the reduction is the biggest and they are probably safe form overturning. But if we take a look of the velocity profile at the last lane, we can see that overturning moment increases and this gives us an idea, that trucks and vehicles can overturn on the inside of the bridge deck.

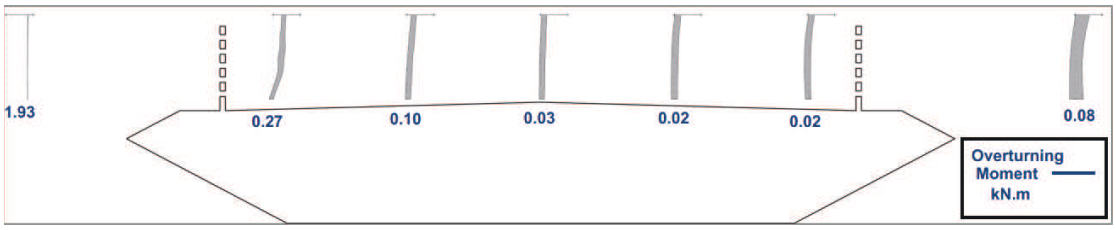

Figure 5.18 Velocity profiles across the bridge deck with perforated barriers

We can see in Figure 5.18 that perforated barrier is giving us very satisfying results. If we take a look across bridge deck, we can see that overturning moment is drastically reducing in each lane from left to right. This gives us an idea, that even though the vehicle here is more exposed the effect of wind barriers on the wind is in the right way to reduce the moment and keep the velocity profile as stream lined as possible. These results are very good, because the reduction of the overturning moment is the most (from 1.93 kNm to 0.02 kNm).

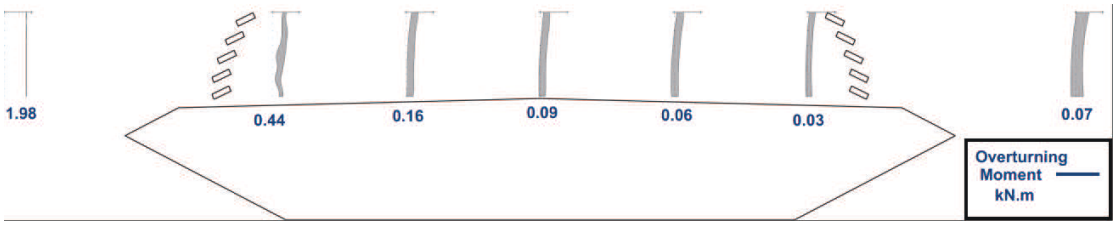

Figure 5.19 Velocity profiles across the bridge deck with curved perforated barriers

The last Figure 5.19 in this section is showing us the behavior of the velocity profile for curved barrier. We can see that the effect on the velocity profile is similar to the one with perforated barrier. Because the barriers are slightly curved the wind gets more vortices than with perforated barriers. We can see that this is why the reduction of the overturning moment for this section is not as high as for the perforated barrier. The reduction in this case goes from 1.98 kN.m to 0.06 kN.m.

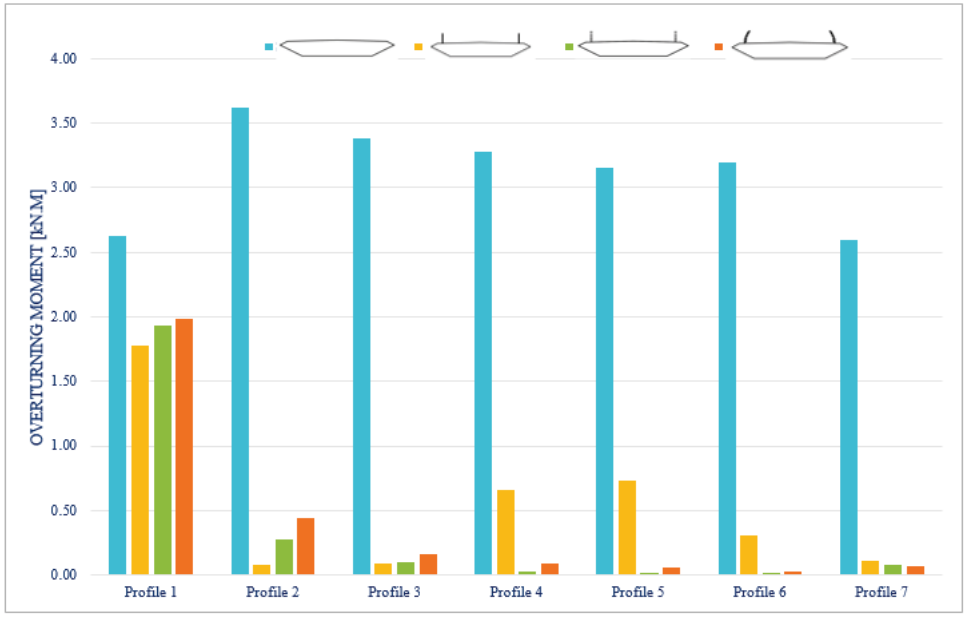

Figure 5.20 Comparison of the reduction of overturning moment.

6 Comparison between Experimental and Numerical Results

In Figures 6.1 to 6.2 we are showing the results we got from numerical and experimental study for solid section. We can see in Figure 6.4 that declinations are slightly bigger for lift coefficients than for basic section. Still the shape of the results is looking good and we got a complete match at the angel 0º. In Figure 6.5 the drag is declined more than lift and moment, but still the shape regarding to the numerical part is looking good.

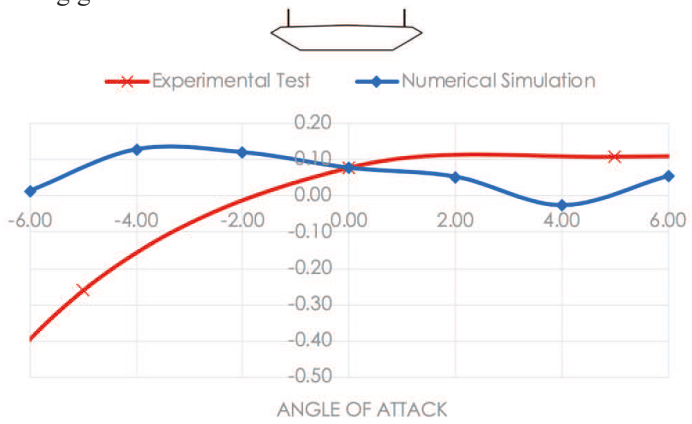

Figure 6.1 Comparison of lift coefficient between experimental and numerical study.

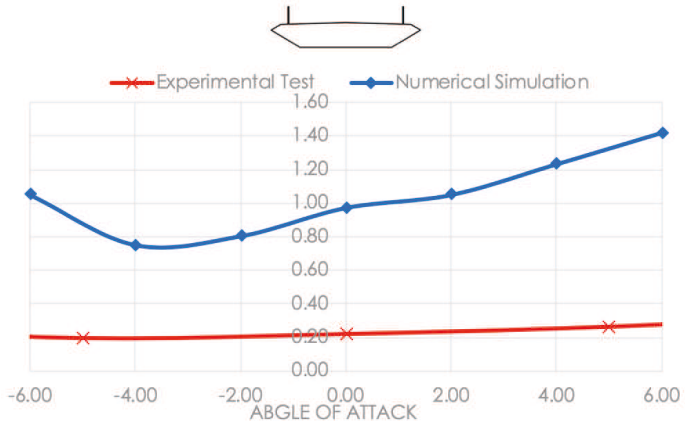

Figure 6.2 Comparison of drag coefficient between experimental and numerical study.

In Figures 6.3 to 6.4 we are presenting the comparison between experimental and numerical part for the perforated barrier. As it is for solid barriers and basic section there is slight declination of the graphs, but both of the studies are giving us the same behavior of the section with added perforated barriers. With this comparison we can confirm that the scaled model and numerical model are behaving the same and that results can be confirmed.

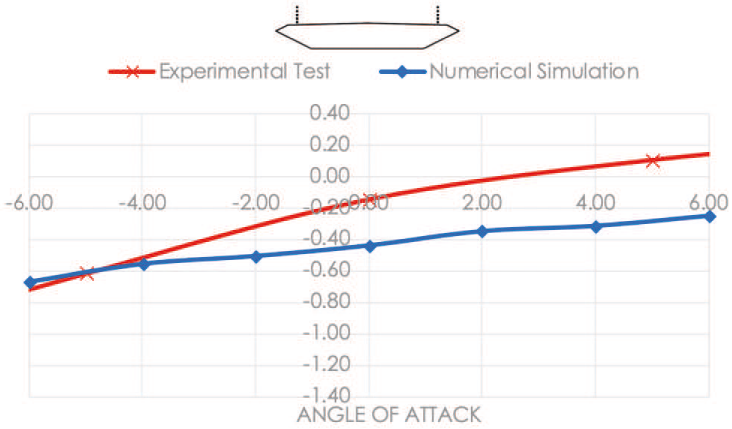

Figure 6.3 Comparison of lift coefficient between experimental and numerical study.

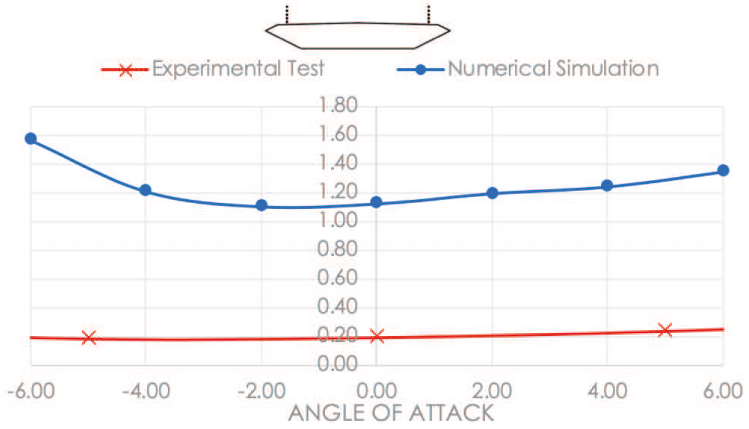

Figure 6.4 Comparison of drag coefficient between experimental and numerical study.

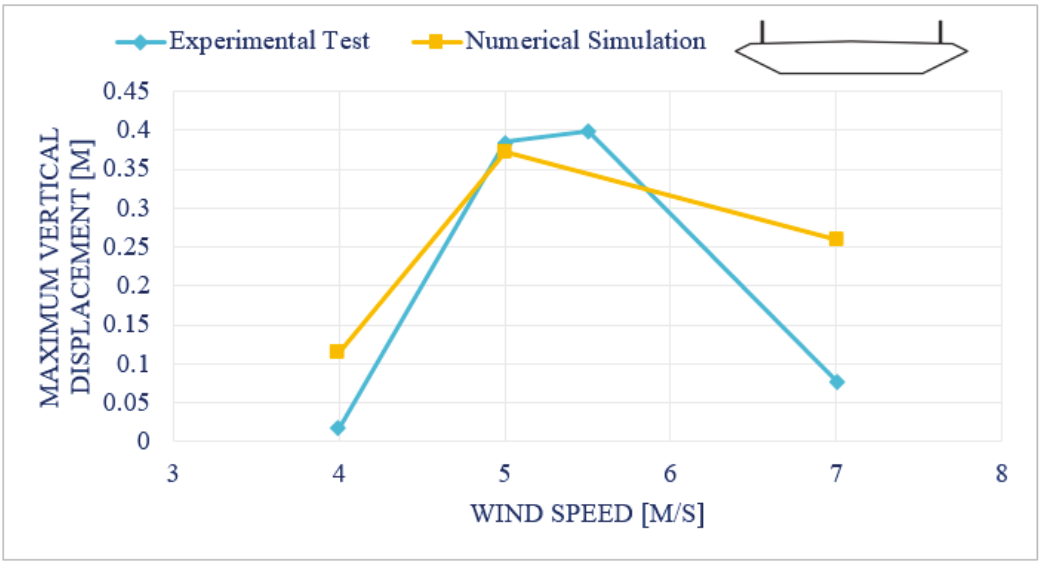

Figure 6.5 Comparison of the dynamic response for solid barrier.

In Figure 6.5, we are showing you the comparison of the response on dynamic analysis for cross section with solid barrier. We can see that experimental result are giving us the same response as numerical result, which confirms our prediction for resonance wind speed.

7 Conclusion and Selection

The most suitable barrier was the perforated one. There were some reasons at the beginning why it would be good to select solid barrier, but at the end, if we look at the velocity profiles and response of the bridge with perforated or curved barriers, it can be noticed that the velocity profiles across the deck are much better than the solid barrier. In addition, the overturning moment at perforated barriers reduces drastically when wind enters through the barrier. There is an option to optimize the shape of a solid barrier and make it more streamline. In that case, the vortices would not be that big and the reduction of the wind influence on the vehicle would be, regarding to our study, drastically smaller. In the Figure 5.2, it can be observed how the overturning moment reduces across the lanes of the bridge. In the first lane, the reduction for solid barrier is bigger, but if we look at other lanes, the overturning moment increases in negative direction. This means that the overturning of the truck would happen on the inside of two lanes.

References

[1] Aerodynamic and aeroelastic characteristics of typical bridge decks equipped with wind barriers at the windward bridge-deck edge ; Andrija Buljac a,b, Hrvoje Kozmar, Stanislav Pospíšil b, Michael Machác˘ek b.

[2] Experimental Investigation of Effect of Windshield Barriers on the Aerodynamic Properties of the Multi box Bridge Decks ; Xi Chen.

[3] Viscous Flow Modeling Using the Vortex Particles Method; Henryk Kudela and Ziemowit Miłosz Malecha.

[4] Morgenthal, G. Aerodynamic Analysis of Structures Using High resolution Vortex Particle Methods. PhD thesis, University of Cambridge, 2002.

V. PROJECT ASSIGNMENT 3

Flutter stability analysis of the Bosphorus bridge

(a) Study and literature review about the flutter phenomenon.
(b) Modelling and simulation of the reference bridge cross-section (basic cross section) using CFD tool, VXflow at steady flow.
(c) Performing the modal analysis of the reference bridge in a finite element software (SOFiSTiK).
(d) Using the obtained modes perform fully-coupled simulation (wind-structure interaction) for the bridge cross section using CFD tool VXflow in order to determine the critical flutter wind speed.
(e) Build the section model and test it in the Wind Tunnel (Laser Cut technique for creating the model).
(f) Static wind coefficients and flutter limit should be determined from the measurements.
(g) Perform forced vibration simulations and compute the aerodynamic derivatives for the given cross section. Then calculate the critical wind speed based on the eigenvalue analysis and using the aerodynamic derivatives of the real cross section.
(h) Comparison of the results from the two different approaches.
(i) Submission of the reports and presentation of the results.

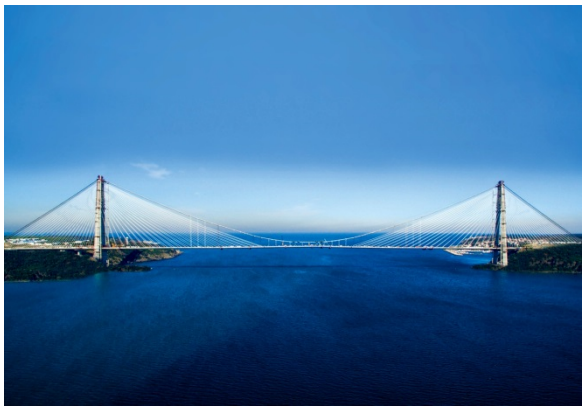

Bosphorus Bridge, Turkey (Source image: https://www.heidelbergcement.com/en/bosphorus-bridge)

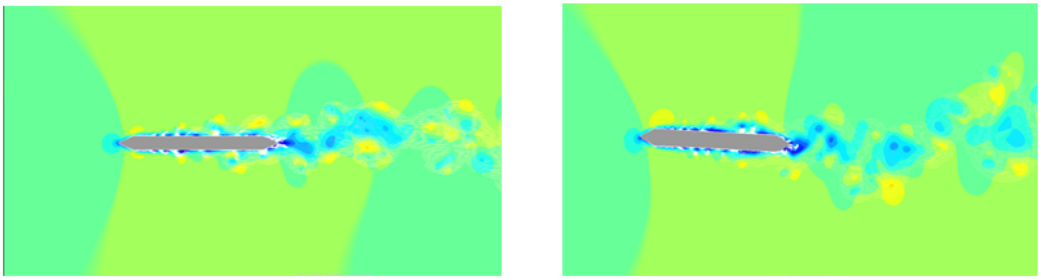

Presentation of forced CFD analysis of a bridge section, heave(left) and pitch(right)

Following report with the pages from 1 to 32 correspond to pages 102 to 133 of the report at hand

Flutter analysis of 3rd Bosphorus Bridge

Erasmus+ M.Sc. Course

Pervan Benjamin
Emkić Amel
Caetano de Almeida Rafaela
Almeida Ribeiro Heliodoro Daniel
Lino Wilde Hermann Mauricio
Adel Ismael Elsayed Ali Ahmed

Bauhaus-University Weimar

Table of Contents

Declaration

Hereby, we declare that we worked on this Report independently and using only the specified sources and programs which are referred.

Weimar, 16.08.2019

Abstract

This paper elaborates flutter analysis of 3rd Bosphorus Bridge. In parallel, two analysis methods were used: computational fluid dynamic (CFD) using VXFlow and experimental tests. Quantities that were considered for determination and comparison are static wind coefficients and critical flutter speed. From literature, cross section dimensions were found, which were used to numerically model cross section, as well to make small scale model for wind tunnel testing. In addition, from literature, first vertical and torsional frequencies were found, which were used as target values to obtain in wind tunnel test.

Keywords: CFD, VXflow, experimental test, flutter, static wind coefficients

1 Introduction

Yavuz Sultan Selim Bridge, or as it was initially named, 3rd Bosphorus Bridge, is hybrid suspension and cable–stayed bridge over the Bosphorus strait in Turkey. Location of bridge can be seen on Figure 1, marked with red dot

Figure 1. Location of 3rd Bosphorus bridge [1]

Construction started on 29 May 2014 and opening ceremony was held on 26 August 2016. Bridge is suspended on two pylons on its main span and cable stayed on two side spans. Some general facts about bridge are given in Table 1 [6].

Geometrical property	Value [m]
Deck width	58.4
Deck height above water	75
Deck depth	5.5
Total length	2164
Pylon height	320
Main span length	1408

Table 1. General facts about 3rd Bosphorus bridge

Figure 2. shows elevation view of bridge, while Figure 3. shows bridges cross section from [3].

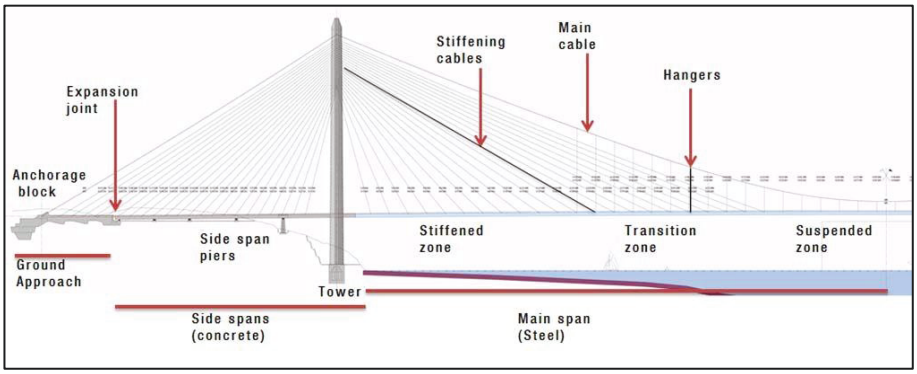

Figure 2. Elevation view of 3rd Bosphorus bridge

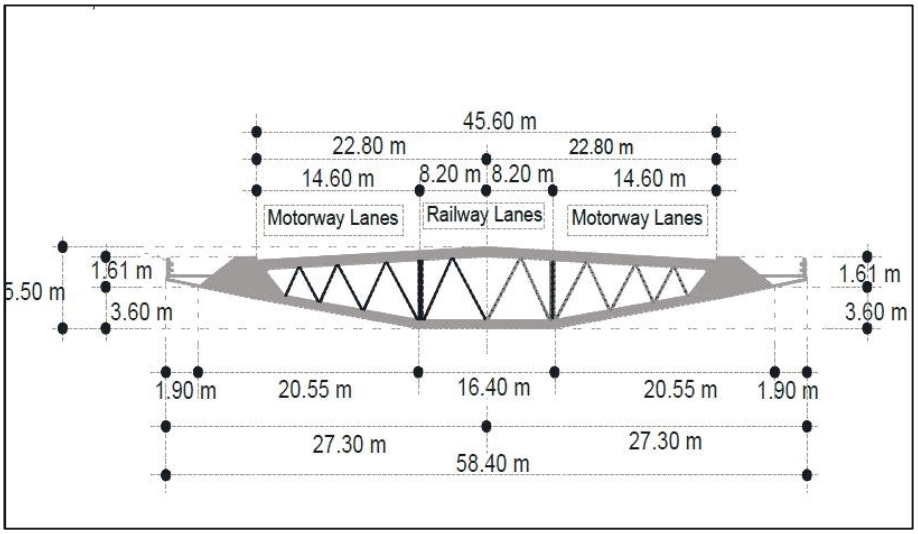

Figure 3. Cross section of 3rd Bosphorus Bridge

Fig. 2. shows first vertical mode, with frequency of 0.169 Hz, and Fig. 6. shows first torsional mode with frequency of 0.289 Hz. Both of these values were obtained from [6] and were used as target frequencies for experimental tests, which are further elaborated in Chapter 3.3.

2 Theoretical Background

Static wind coefficients can be used to express static forces that act on cross section under influence of wind. Figure 4 shows lift, drag and moment force acting on cross section under influence of wind, whose speed is U.

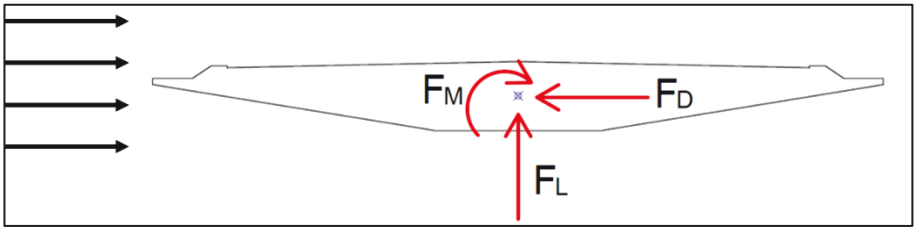

Figure 4. Static forces acting on cross section under wind load

Static wind coefficients can be expressed using static forces, cross section geometry (58.4 m represents width of cross section), wind speed and air density, ρ. Lift coefficient can calculated according to Eq. 2.1., drag coefficient according to Eq. 2.2. and moment coefficient according to Eq. 2.3 [7].

$$C_L = \frac{F_L}{0.5 \cdot \rho \cdot U^2 \cdot B} \tag{2.1}$$

$$C_D = \frac{F_D}{0.5 \cdot \rho \cdot U^2 \cdot B} \tag{2.2}$$

$$C_M = \frac{F_M}{0.5 \cdot \rho \cdot U^2 \cdot B^2} \tag{2.3}$$

Flutter is aerodynamic phenomenon, which occurs when aerodynamic forces on bridge deck couple with its motion. If aerodynamic forces, caused by strong winds, create more energy than damping of bridge can dissipate, amplitude of vibrations will increase. Those increased vibrations then amplify aerodynamic forces, which results in self-excited forces and oscillations. Vibration amplitude of bridge deck can result in bridge collapse. Self-excited forces can be expressed as lift and moment forces acting on cross section, in direction of vertical, h, and torsional, α displacement. Flutter derivatives can be used to express self – excited forces, which are shown in Eq. 2.1. for lift force and in Eq. 2.3. for moment force. Those self – excited forces are expressed as it follows, in Eq. 2.4. for lift force and in Eq. 2.5. for moment force.

$$L_{se} = \frac{\partial L_{se}}{\partial \dot{h}}\dot{h} + \frac{\partial L_{se}}{\partial \dot{\alpha}}\dot{\alpha} + \frac{\partial L_{se}}{\partial \mathrm{h}}h + \frac{\partial L_{se}}{\partial \alpha}\alpha \tag{2.4.}$$

$$M_{se} = \frac{\partial M_{se}}{\partial \dot{h}}\dot{h} + \frac{\partial M_{se}}{\partial \dot{\alpha}}\dot{\alpha} + \frac{\partial M_{se}}{\partial \mathrm{h}}h + \frac{\partial M_{se}}{\partial \alpha}\alpha \tag{2.5.}$$

where:

- L_{se} and M_{se} are self – excited lift and moment forces acting on cross section,
- h and α are vertical and torsional displacement of cross section.

From those expressions, using assumptions of small initial displacements for stable and unstable regimes, Scanlan and Tomko [8] express self – excited forces as shown in Eq. 2.6. for lift force and in Eq. 2.7. for moment force.

$$L_{se} = \frac{1}{2}\rho\overline{U}^2 B\left[KH_1^*\frac{\dot{h}}{\overline{U}} + KH_2^*\frac{B\dot{\alpha}}{\overline{U}} + K^2H_3^*\alpha + K^2H_4^*\alpha\right] \tag{2.6.}$$

$$M_{se} = \frac{1}{2}\rho\overline{U}^2 B^2\left[KA_1^*\frac{\dot{h}}{\overline{U}} + KA_2^*\frac{B\dot{\alpha}}{\overline{U}} + K^2A_3^*\alpha + K^2A_4^*\alpha\right] \tag{2.7.}$$

where:

- $\overline{U}$ is mean wind velocity,
- H_i^* and A_i^* (i = 1 – 4) are flutter derivatives.

Another approach for flutter derivatives is Theodorsen circulatory function, which describes self – excited forces acting on flat plate airfoil, subjected to sinusoidal motion. Flat plate airfoil is assumption that cross section behaves like airfoil, i.e. like wing of airplane. Also, assumption in this approach is that motion is sinusoidal. Lift force expressed using Theodorsen circulatory function is shown in Eq. 2.8. and moment force is shown in Eq. 2.9.

$$L_{se} = \pi\rho b\{-b\ddot{h} - 2UC(k)\dot{h} - [1 + C(k)]Ub\dot{\alpha} - 2U^2C(k)\alpha\} \tag{2.8.}$$

$$M_{se} = \pi\rho b^2\left\{UC(k)\dot{h} - \frac{b^2\ddot{\alpha}}{8}\left[-\frac{1}{2} + \frac{1}{2}C(k)\right]Ub\dot{\alpha} - U^2C(k)\alpha\right\} \tag{2.9.}$$

where:

- b is half width of plate,
- C(k) is the Theodorsen cyclical function, which is shown in Eq. 2.10.

$$C(k) = F(k) + iG(k) \tag{2.10.}$$

where:

- F(k) is real part of function C(k),
- G(k) is imaginary part of function C(k).

When sinusoidal displacements of flat plate airfoil from Eq. 2.8. and 2.9. are taken into consideration, and then comparing this equation to equations 2.6. and 2.7., flutter derivatives for flat plate airfoil can be determined, which is in further detail explained in [7].

3 Models

Three approaches were chosen, numerical modelling using computational fluid dynamic solver, semi analytic approach based on Theodorsen cyclic function, and experimental, small scale model for wind tunnel testing.

3.1 Numerical Analysis

Objectives of numerical analysis was to obtain static wind coefficients and critical flutter speed, which will later be compared with experimentally obtained values, as well to get flutter derivatives, which will be used for semi analytic model. All numerical analysis were performed using VXFlow which is computational fluid dynamics code based on Vortex Particle Method [4].

3.1.1 Modelling of cross section

Bridges cross section, shown on Figure 3, was simplified to make it easier to produce scaled model for wind tunnel. Simplified cross section is shown in Figure 5.

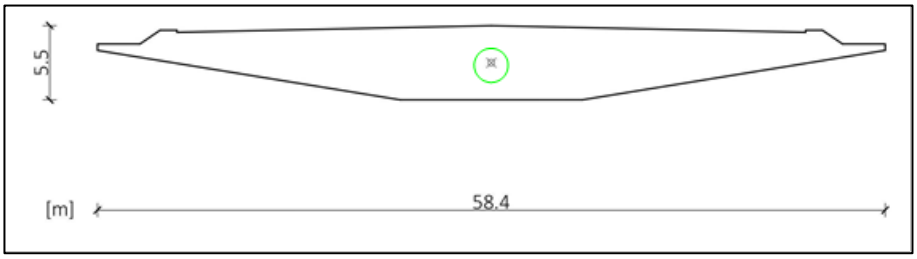

Figure 5. Simplified cross section

From simplified cross section, coordinates for each point were determined with respect to centre of coordinate system, highlighted in green circle on Figure 5. Whole cross section has 400 panels, which were divided across cross section with respect to length of each element on cross section. Purpose of panels is discretisation of cross section, and for each panel, pressure is being calculated. Pressure field is shown on Figure 6, where each red or blue line represent one panel.

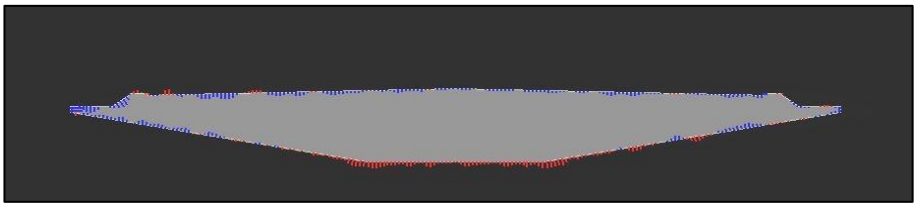

Figure 6. Pressure field on horizontal cross section

3.1.2 Static wind coefficients

First task was to determinate static wind coefficients, which were obtained using VXFlow. Simulation was ran for horizontal cross section – 0◦ angle of incidence, as well as all angles of incidence in range from -8◦ to 8◦, with step of 2. Fig. 7. Shows cross section rotated at −8◦, Fig. 8. shows cross section rotated at 8◦ and Fig. 9. display horizontal cross section from VXFlow.

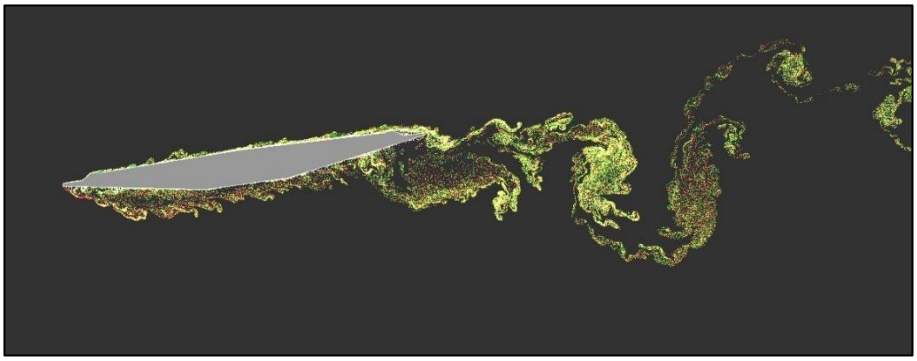

Figure 7. −8◦ angle of incidence

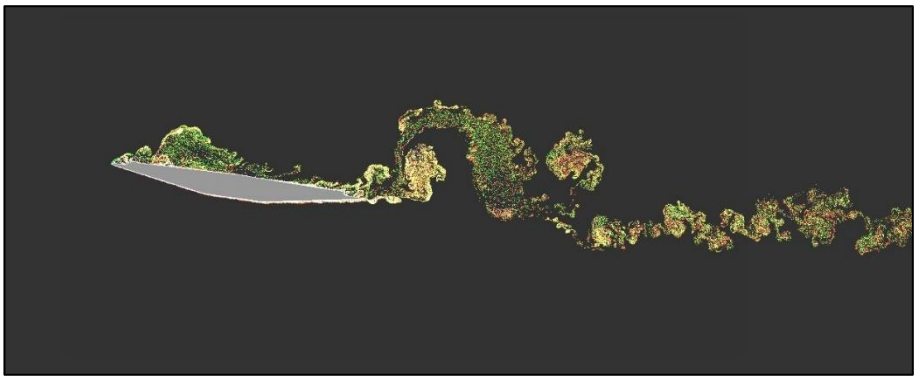

Figure 8. 8◦ angle of incidence

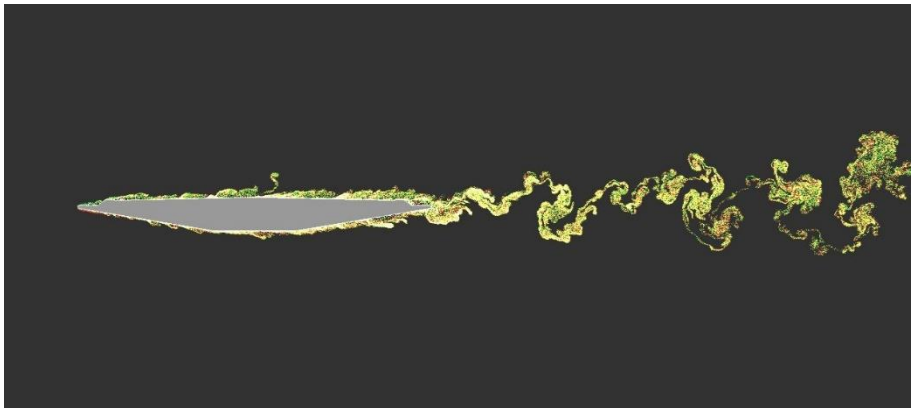

Figure 9. 0◦ angle of incidence

All simulations were ran with wind speed, U, set to 20 m/s. Air viscosity was calculated in Eq. 3.1.

$$\nu = \frac{U \cdot B}{Re} = \frac{20 \cdot 58.4}{3 \cdot 10^5} \tag{3.1}$$

where:

• ν is viscosity,

• U is wind speed [m/s],

• B is cross section's width [m]

• Re is Reynolds number.

Reynolds number was set as $3x10^5$, to match Reynolds number at which experiment will be ran. Time for static wind coefficients analysis was determined in Eq. 3.2., and according to that time, number of time steps was calculated in Eq. 3.3.

$$t = \frac{B \cdot 100}{u} = \frac{58{,}4}{\frac{100}{20}} = 292\ s \tag{3.2}$$

$$ntime\ steps = \frac{292}{0{,}012455} = 23444{,}4 \cong 25000 \tag{3.3}$$

where:

• 100 is value suggested,

• 0.012455 is value in first column of .o3 file (output file of VXFlow).

Post processing of results were done using MATLAB, where simple code was written. Code took values from second, third and fourth column of .o3 file (lift, drag and moment force), took mean value of that data, and then calculated static wind coefficient. Lift coefficient was calculated according to Eq. 2.1., drag coefficient according to Eq. 2.2. and moment coefficient according to Eq. 2.3.
Force calculation shown in Eq. 2.2., Eq. 2.2. and Eq. 2.3. were done for each angle of incidence (from −8◦ to 8◦, with step of 2◦).

3.1.3 Flutter derivatives

Flutter derivatives were determined for reduced velocities, Vr, in range from 2 to 16, with step of 2. Forced analysis was performed in VXFlow, for heave and pitch motion sepa- rately. Frequencies for heave motion was calculated for each reduced velocity, according to Eq. 3.4.

$$t = \frac{U}{V_r \cdot B} \tag{3.4}$$

With known frequencies and periods for each reduced velocity, amplitude for each reduced velocity, h_v, was calculated according to Eq. 3.5.

$$h_v = \frac{\alpha_e \cdot U}{2 \cdot \pi \cdot f} \tag{3.5.}$$

where:

• αe is effective angle (corresponds to 3◦ or 0.0524 radians).
Period for heave motion is reciprocal value of frequency, i.e. T = 1/f. Table 2 shows frequency, period and amplitude for each reduced velocity.

Vr	f [hZ]	T [s]	h_0 [m]
2	0,1712	5,84	0,9743
4	0,0856	11,68	1,9485
6	0,057	17,52	2,9262
8	0,0428	23,36	3,8971
10	0,0342	29,20	4,8770
12	0,0285	35,04	5,8524
14	0,0244	40,88	6,8358
16	0,0214	46,72	7,7941

Table 2. Frequency, period and amplitude values for each Vr [–]

For pitch motion, periods are same as in Table 2, and amplitude corresponds to 3º, or 0.0524 radians for each reduced velocity. Number of time steps was set to 35000, to ensure that for each movement and each reduced velocity minimum 6-8 periods were reached, to ensure the steady-state oscillation.

3.1.4 Dynamic numerical analysis

From small scale model that was made for experimental test, which is in more detail explained in Chapter 3.3.2., model mass per unit length and mass moment of inertia were determined, as those values correspond to vertical and torsional modal mass.

$$m_1 = \left(m_{1,sc} + m_{add}\right) \cdot \frac{1}{(\lambda_L)^2} \tag{3.6.}$$

where:

• m_l is full scale mass per unit length [kg/m],

• $m_{l,\,sc}$ is scaled model mass per unit length, which is determined in Eq. 3.7.,

• m_{add} is mass of additional elements on model (side bars), whose value is 0.96 kg.

• $(1/\lambda L)^2$ is scale factor for mass scaling with value of 22500 (further explanation in Chapter 3.3.1.)

$$m_{1,sc} = \frac{1{,}912 \cdot 1}{1.2} = 1.5933\ kg \tag{3.7.}$$

Where:
• 1.912 is weight of full model, which length is 1, 2 m
With values for all parameter required, full scale mass per unit length was calculated in Eq. 3.8.

$$m_1 = (1{,}5933 + 0{,}96) \cdot 22500 = 57450\ kg/m \tag{3.8.}$$

To calculate mass moment of inertia, rotational stiffness must be determined. It was determined using known vertical stiffness for springs used in experiment, and their distance from center of mass. Rotational stiffness was determined in Eq. 3.9.

$$k_r = \frac{k_1 \cdot x}{\frac{1}{x}} = \frac{0{,}07 \cdot 0{,}31}{\frac{1}{0{,}31}} = 0.006727\ kN\ m/rad \tag{3.9.}$$

Where:

• k_l is vertical stiffness of one spring [kN/m],

• x is distance from spring to mass centre [m].

As our dynamic setup had 8 springs, whole rotational stiffness corresponds to 0, 053816 kN m/rad. From experimental test, torsional frequency (for small scale model) was obtained as 3, 2427 Hz, which corresponds to angular frequency of 20, 3744 rad/s. Using those values, rotational mass for small scale model, $m_{r,sc}$, was calculated in Eq. 3.10.

$$m_{1,sc} = \frac{k_r}{w^2} = \frac{0{,}053816}{20{,}3744^2} \cdot 1000 = 0.129641\ kg/m \tag{3.10.}$$

To transform rotational mass of model to rotational mass per unit length, rotational mass was divided with models length, which is 1, 2 m, and rotational mass per meter length was obtained as 0,10803 kg/m. That value was then multiplied with scaling factor for mass moment of inertia, which is defined as $1/(\lambda L)^4$, as it is further explained in Chapter 3.3.1. Eq. 3.11. shows calculation of mass moment of inertia, m_r, for full scale model.

$$m_r = 0{,}10803 \cdot \frac{1}{\frac{1^4}{150^4}} = 0{,}10803 \cdot 506250000 = 54690187.5\ kgm^2/m \tag{3.11.}$$

Using critical flutter speed obtained from experimental test for Set-up 5, which is elaborated in more detail in Chapter 3.3.5. as reference point, dynamic simulations were set–up from 100 m/s to 140 m/s, with increment between them of 5 m/s, and increment of 2 m/s from 110 m/s to 120 m/s. Two mode shapes were observed, first vertical and first torsional, with frequencies that were obtained during experimental test for set–up 5. Air viscosity was calculated for each wind speed, to maintain Reynolds number of $3x10^5$.

3.2 Semi-analytic model

For semi analytic calculation of critical flutter speed flutter derivatives calculated in Chapter 3.1.3. were used. Model was based on Theodorsen's cyclic function, which is explained in Chapter 3.1. Main input parameters for semi analytic model are presented in Table 12.

Parameter	Unit
Cross section width	58.4 m
Mass per unit length	57450 kg/m
Mass moment of inertia per unit length	54690187.5 kgm^2/m
Vertical frequency	-
Rotational frequency	-
Damping ratio	-

Table 3. Input parameters for semi analytic model

Reason for why rows with frequencies and damping are empty lies in fact that semi analytic model was used to calculate critical flutter speed for each experimental test, which is further elaborated in Chapter 4.3.

3.3 Experimental test

Purpose of experimental tests were to obtain true vertical and torsional frequencies of small scale model, whose preparation will be discussed, as well to obtain static wind coefficients and critical flutter speed, to later be compared to semi analytic and numerical model.

3.3.1 Literature review on scaling laws

In long – span bridges, the rigid body modelling techniques are not sufficient. Aerodynamic influences on supporting towers and cables, which are not included in the section model, may have significant effect. Thus, we can use scaling laws, which are based on dimensional analysis, to design models whose stiffness at least partially can correspond to full size bridge. Full model testing of suspension bridges, where stiffness is, at least partially, provided by gravitational forces, requires equality of Froude Number, F r, which can by calculated as shown in Eq. 3.12.

$$Fr = \frac{U}{\sqrt{L \cdot g}} \tag{3.12.}$$

where:

- L is length of bridge [m],
- g is gravitational acceleration (9.81 m/s^2).

Froude number is going to be constant for numerical model as well as for small scale model, so those two values can be equaled, as it is shown in Eq. 3.13.

$$\left(\frac{U_m}{\sqrt{L_m \cdot g}}\right)_m = \left(\frac{U_p}{\sqrt{L_p \cdot g}}\right)_p \tag{3.13.}$$

In Eq. 3.13. m refers to small scale model and p refers to numerical, full size model. Mentioned equation was then developed, g was removed from both sides as it is constant, and rest of calculations are shown in Eq. 3.14.

$$\frac{U_m}{U_p} = \left(\sqrt{\frac{L_m}{L_p}}\right) \tag{3.14.}$$

Eq. 3.15. shows calculation for velocity scale.

$$\frac{U_m}{U_p} = \sqrt{\frac{L_m}{L_p}} \tag{3.15.}$$

Length scale is simply Lm/Lp, which for this project was chosen as 1/150. With that into consideration and using Eq. 3.15., velocity scale was determined as 0.08165. As check of hand calculation, from [7] equations were obtained to calculate length, velocity and frequency scale, as well as scale for mass and mass moment of inertia. Length scale was calculated in Eq. 3.16.

$$\lambda_L = \frac{D_m}{D_p} = \frac{0.3893}{58.4} = \frac{1}{150} = 0.00667 \quad (3.16.)$$

where:

• Dm is width of small scale model's cross section [m],
• Dp is width of full scale cross section [m].

Frequency scale, λf, for our project was determined in Eq. 3.17.

$$\lambda_f = \frac{1}{\sqrt{\lambda_L}} = \frac{1}{\sqrt{\frac{1}{150}}} = 12.247 \quad (3.17.)$$

Velocity scale, λU , for our project was determined in Eq. 3.18.

$$\lambda_U = \sqrt{\lambda_L} = \sqrt{\frac{1}{150}} = 0.08165 \quad (3.18.)$$

Mass scale was, per [2], determined as $1/(\lambda L)^2$, and mass moment of inertia, also per [2], was determined as $1/(\lambda L)^4$.

3.3.2 Wind tunnel prototype model design

Chosen scale for model was 1:150, based on scaling laws explained in Chapter 3.3.1., and also to accommodate available space inside Wind Tunnel, provided at Bauhaus-University. Figure 10 Shows mentioned wind tunnel.

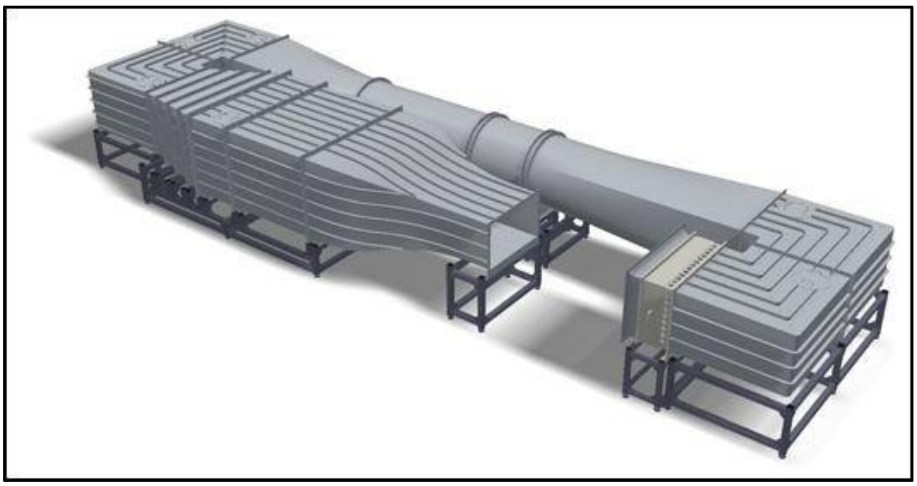

Figure 10. Wind tunnel [8]

From original cross section, which is displayed in Fig. 3, scaled version was drawn in AutoCAD, with final measurements shown in Figure 11.

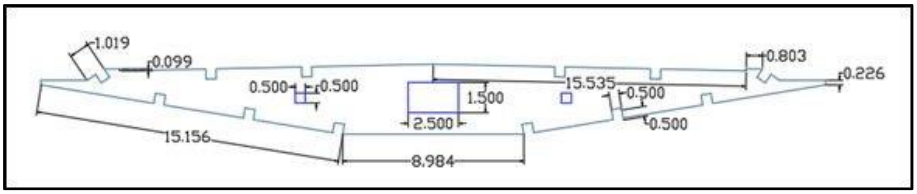

Figure 11. Scaled cross section (measurement in cm)

This scaled cross section was then cut from plywood using laser cutter and assembled with help of Modellwerkstatten and VTE. Laser cut cross section is shown in Fig. 12a., and fully assembled model is shown in Fig. 12b.

(a) **(b)**

Figure 12. Preparation and assembled model

Model's mass was determined as 1, 912 kg, and with known cross section dimensions, numerical model in SOFiSTiK was constructed to obtain spring stiffness. Spring stiffness was determined so that model would have same scaled frequencies as calculated in 3.3.1.

3.3.3 Finite element model

To determinate stiffness of springs for experimental part of project, a finite element model was prepared in SoFiSTiK. FEM model is the same as one which is prepared for testing in wind tunnel and is assembled from deck (simple section), end plates and outer and inside bars. On the ends of outer bars, springs are modelled, that connect bars and movable supports.

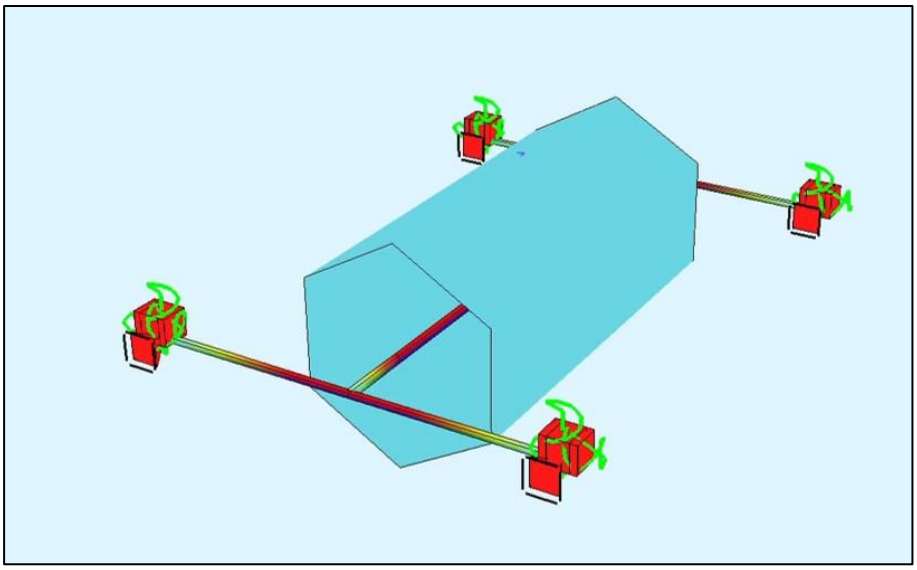

Figure 13. FEM model prepared in SOFiSTiK

One thing that deserves attention is that cross section shape does not resemble real cross section, which can be seen on Fig. 3. Reason for that is simple, our goal with FEM model was to obtain stiffness which corresponds to target frequencies, and cross section shape doesn't affect that. After scaling frequencies from literature, target vertical and torsional frequencies were obtained. In SoFiSTiK model iterative process was done, where stiffness of springs and distance between them have been iterated and observed in same time frequency. After few iterations, stiffness of vertical springs was obtained as 0.16 N/mm, with distance between them as 58 cm, whose place and properties correspond to target frequencies of system (0.169 Hz for vertical and 0.286 Hz for torsional frequency). To this purpose, eight springs were ordered. To cover possible deviations from experimental to numerical model, stiffer springs with stiffness of 0.25 N/mm and more flexible springs with stiffness of 0.07 N/mm were ordered. Figure 14 shows scheme of springs installation on experimental model.

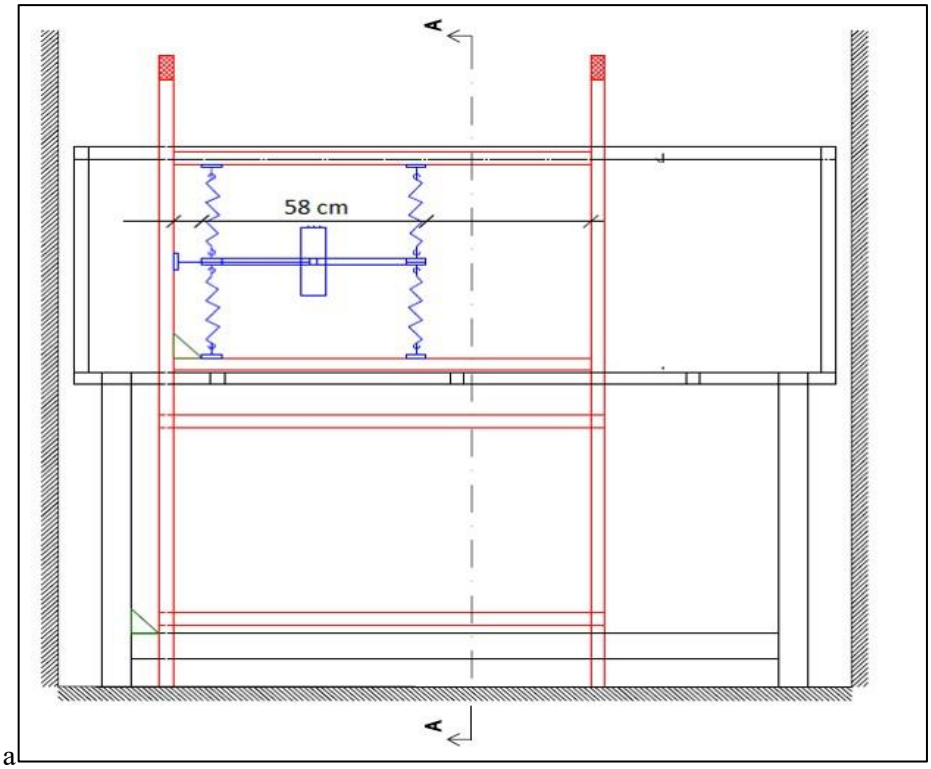

a

Figure 14. Spring installation scheme

3.3.4 Determination of static wind coefficients from static experiment under laminar flow

Static wind coefficients were determined in the wind tunnel. First step was model installation, which should be done precisely, as model, sensors for measuring and all other equipment is very delicate. Finished setup is shown in Fig. 15a. and Fig. 15b.

(a) **(b)**

Figure 15. Model setup in wind tunnel for static wind coefficient test

Test was conducted in three stages:

1. Measurement without wind,
2. Measurement with wind tunnel working,
3. Measurement without wind.

Reason for this measurement sequence is that goal was to obtain clean data, without noise. Therefore, noise was recorded and wind flowing throughout the bridge. Fig. 16. shows recording process for test conducting.

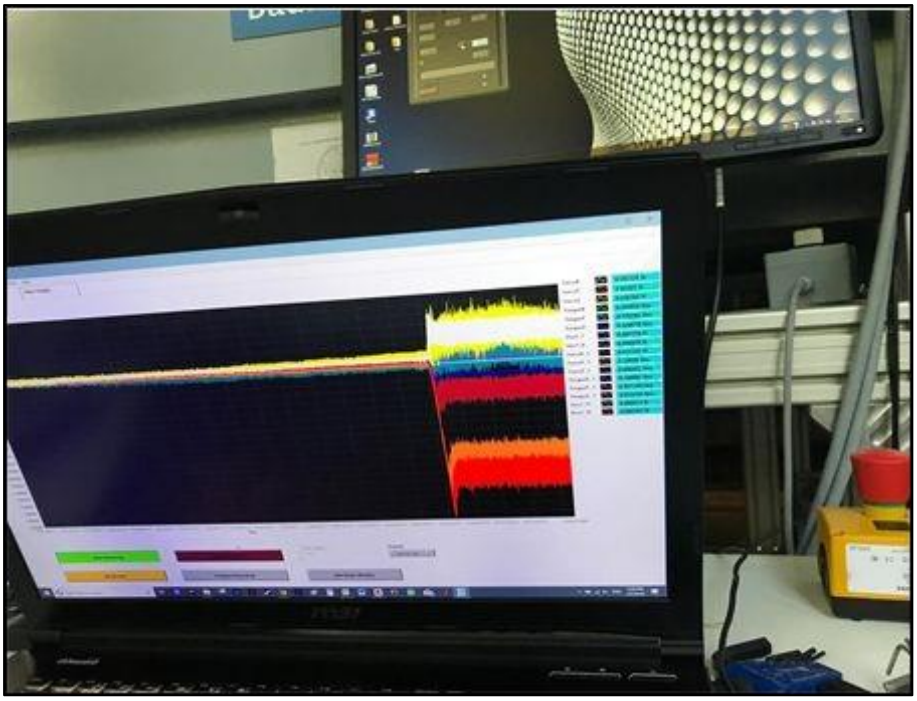

Figure 16. Recording process

To get static wind coefficients at different angles of incidence, three stage process was repeated for angles from −8◦ to 8◦, with 2◦ differential between them. Test with rotated cross section is shown in Fig. 17a. and Fig. 17b.

(a) **(b)**

Figure 17. Static wind coefficients test at various angles of incidence

Results for static wind coefficients are shown in Fig. 18.

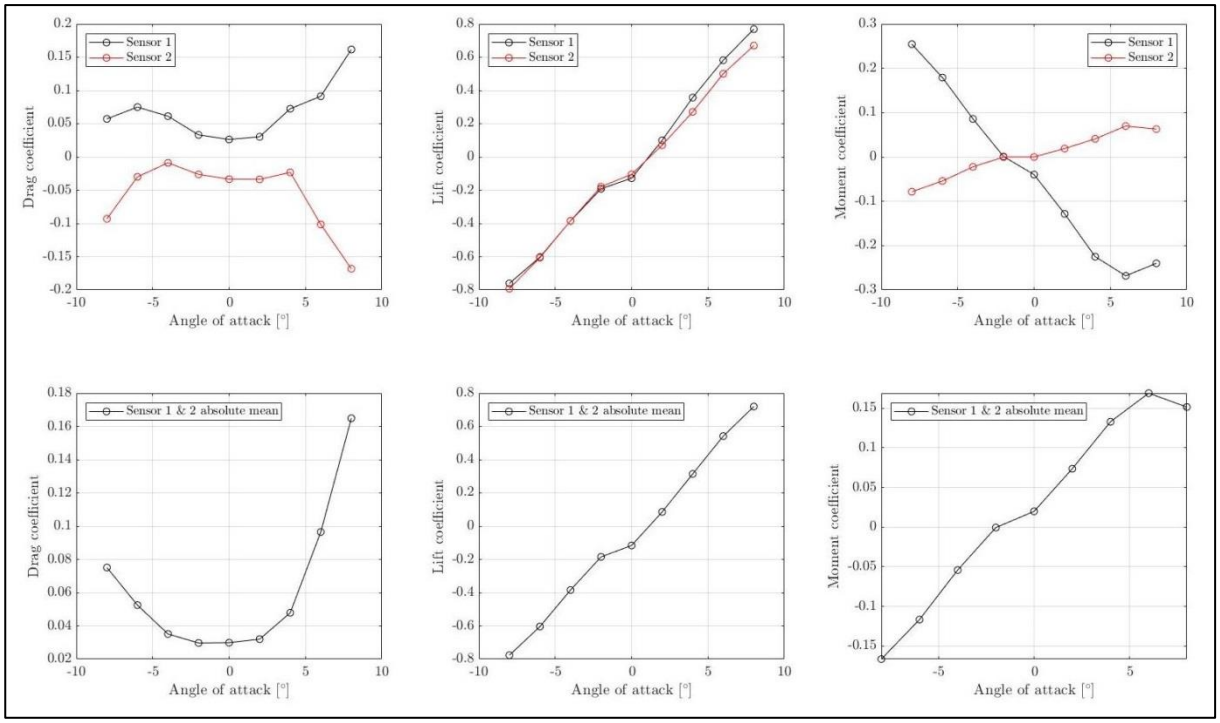

Figure 18. Static wind coefficients obtained in wind tunnel

3.3.5 Determination of critical wind speed for section model

As it was elaborated in Chapter 3.3.3., three set of springs with different stiffnesses were ordered, and using them, 5 set-ups were created. Small-scale model was manually excited in vertical direction to determinate vertical frequency, and rotated to determinate torsional frequency. Once those measurements were done, various wind speeds were tested to determinate at what wind speed each set-up starts to flutter. Data was measured using 4 (2) accelerometers, and on that data Fast Fourier Transform was preformed to determinate dominant frequency. Damping was determined from logarithmic decay of acceleration data. 5 set-ups were made, and each of them is further elaborated in following pages.

Setup 1 was made using 8 springs with stiffness of each spring 0.25 N/mm. Specifically for this test, two torsional excitations were measured, which were labeled as 2a and 2b, respectively, and one just vertical. For all tests for setup 1, frequencies and damping obtained are shown in Table 4.

Test ID	f_l [Hz]	f_r [Hz]	Vertical damping [-]	Torsional damping [-]
$2_{a,1}$	0.3168	0.4668	0.01983	0.00512
$2_{a,2}$	0.3186	0.4668	0.01969	0.00445
$2_{a,3}$	0.3184	0.4503	0.21952	0.01056
$2_{a,4}$	0.3182	0.4659	0.01946	0.00404
$2_{b,1}$	0.3168	0.4672	0.01983	0.00465
$2_{b,2}$	0.3186	0.4671	0.01969	0.00456
$2_{b,3}$	0.3184	0.4506	0.21952	0.00682
$2_{b,4}$	0.3182	0.4664	0.01946	0.00452

Table 4. Frequencies and damping for set-up 1

Fig. 8. displays acceleration time history and FFT for Test 2b, from set–up 1. Purpose of FFT was to obtain natural frequency of model from acceleration time history.

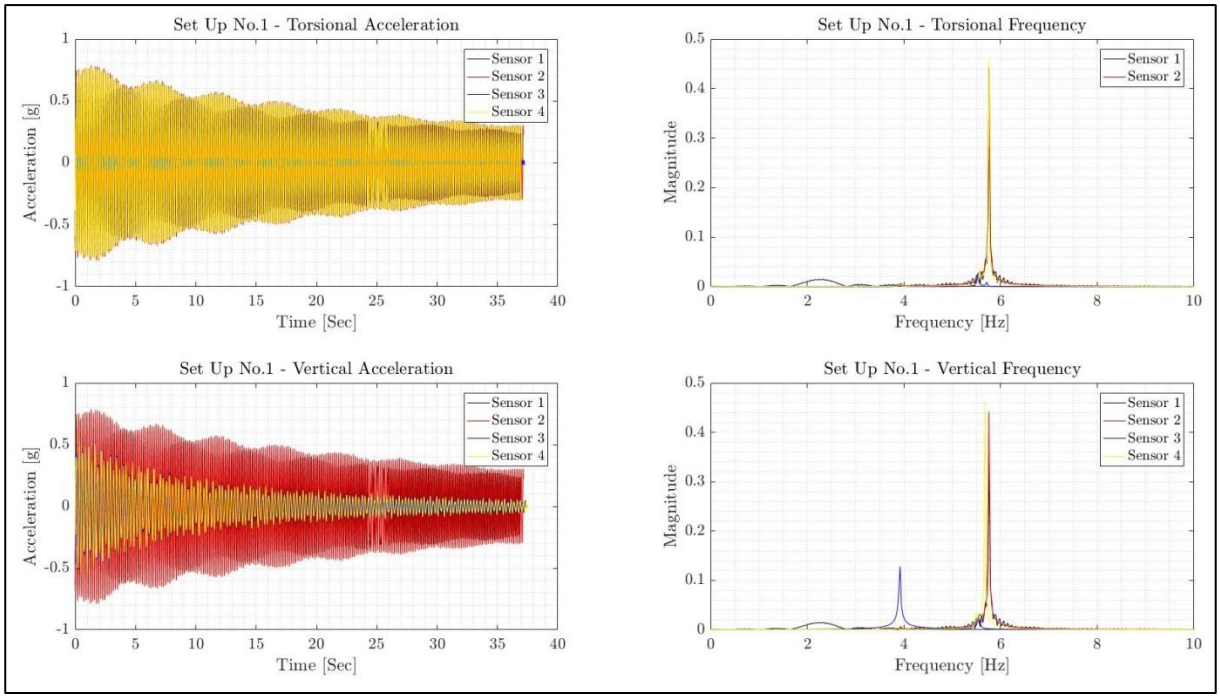

Figure 19. Acceleration time history and FFT for set-up 1

After free vibration test was done, it was observed that at wind speed of 15 m/s, which is 183.71 m/s when scaled back to full scale, using scaling laws from Chapter 3.3.1.

Setup 2 was made using 8 springs with stiffness of each spring 0.16 N/mm. For all tests for setup 2, frequencies and damping obtained are shown in Table 5.

Test ID	f_l [Hz]	f_r [Hz]	Vertical damping [-]	Torsional damping [-]
4_1	0.2461	0.3609	0.002986	0.000902
4_2	0.2468	0.3612	0.002779	0.000877
4_3	0.2469	0.3481	0.002943	0.000718
4_4	0.2473	0.3614	0.002894	0.000842
5_1	0.2471	0.3612	0.002392	0.000970
5_2	0.2465	0.3616	0.002516	0.000940
5_3	0.2464	0.3487	0.002432	0.001163
5_4	0.2465	0.3618	0.002341	0.000893

Table 5. Frequencies and damping for set-up 2

Fig. 20. displays acceleration time history and FFT for Test 4, from set–up 2. Purpose of FFT was to obtain natural frequency of model from acceleration time history.

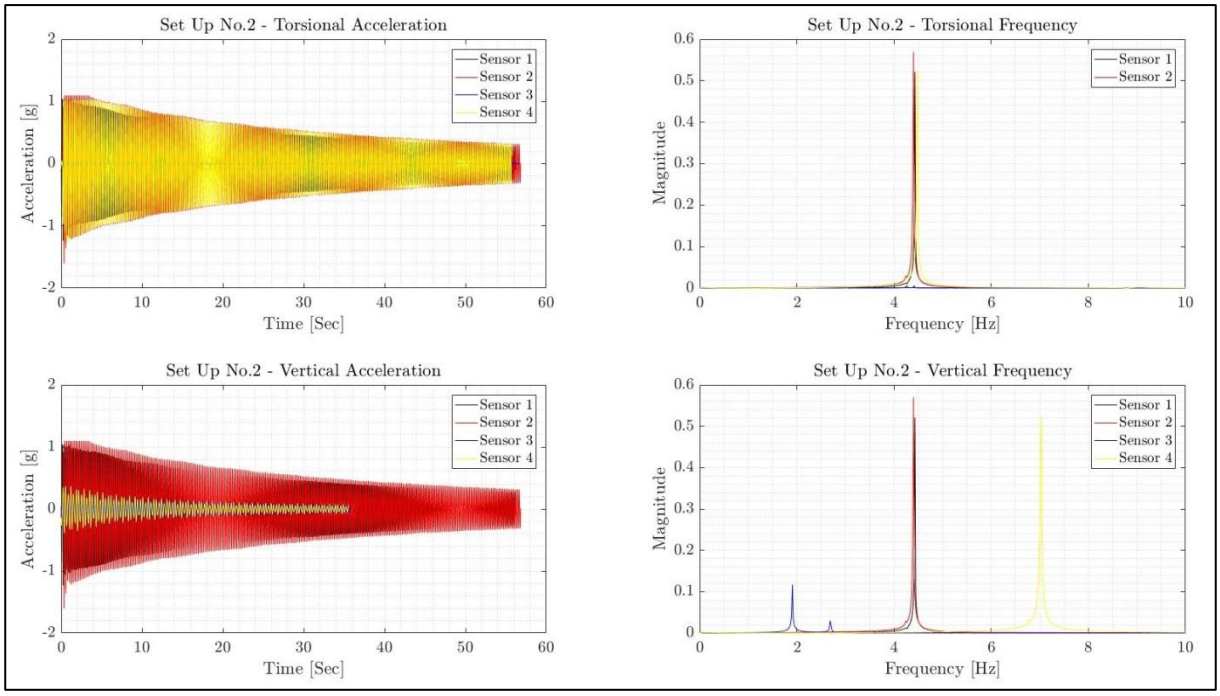

Figure 20. Acceleration time history and FFT for set–up 2

After free vibration test was done, it was observed that at wind speed of 12 m/s, which is 146.97 m/s when scaled back to full scale, using scaling laws from Chapter 3.3.1.

Setup 3 was made using 8 springs with stiffness of each spring 0.07 N/mm. For all tests for setup 3, frequencies and damping obtained are shown in Table 6.

Test ID	f_l [Hz]	f_r [Hz]	Vertical damping [-]	Torsional damping [-]
6_1	0.1719	0.2528	0.002466	0.001410
6_2	0.1722	0.2521	0.002553	0.000914
7_1	0.1725	0.2520	0.002691	0.001459
7_2	0.1725	0.2428	0.002742	0.001329

Table 6. Frequencies and damping for set-up 3

Fig. 21. displays acceleration time history and FFT for Test 7, from set–up 3. Purpose of FFT was to obtain natural frequency of model from acceleration time history.

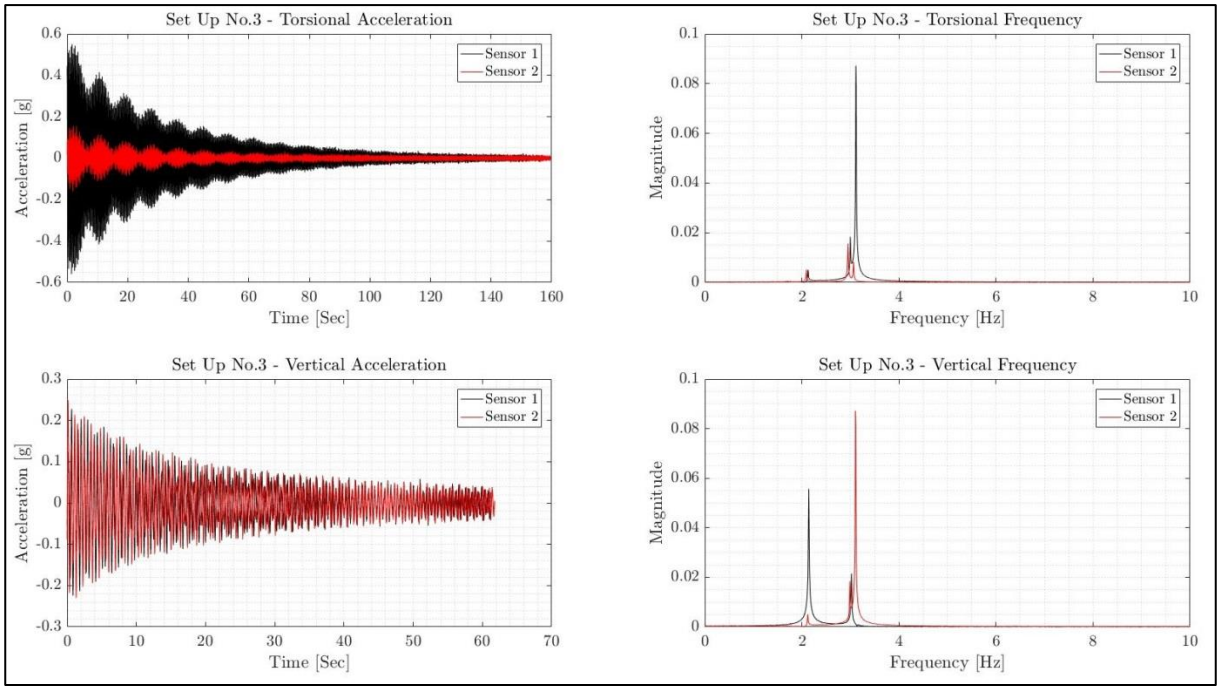

Figure 21. Acceleration time history and FFT for set–up 3

After free vibration test was done, it was observed that at wind speed of 8.5 m/s, which is 104.10 m/s when scaled back to full scale, using scaling laws from Chapter 3.3.1.

Setup 4 was made using 4 springs with stiffness of 0.07 N/mm at top side bar and 4 springs with stiffness of 0.16 N/mm at bottom side bar. For all tests for setup 4, frequencies and damping obtained are shown in Table 7.

Test ID	f_l [Hz]	f_r [Hz]	Vertical damping [-]	Torsional damping [-]
8_1	0.2117	0.3098	0.003169	0.001521
8_2	0.2117	0.2997	0.003111	0.002031
9_1	0.2127	0.3109	0.002592	0.001437
9_2	0.2127	0.2995	0.002842	0.001831

Table 7. Frequencies and damping for set-up 4

Fig. 22. displays acceleration time history and FFT for Test 9, from set–up 4. Purpose of FFT was to obtain natural frequency of model from acceleration time history.

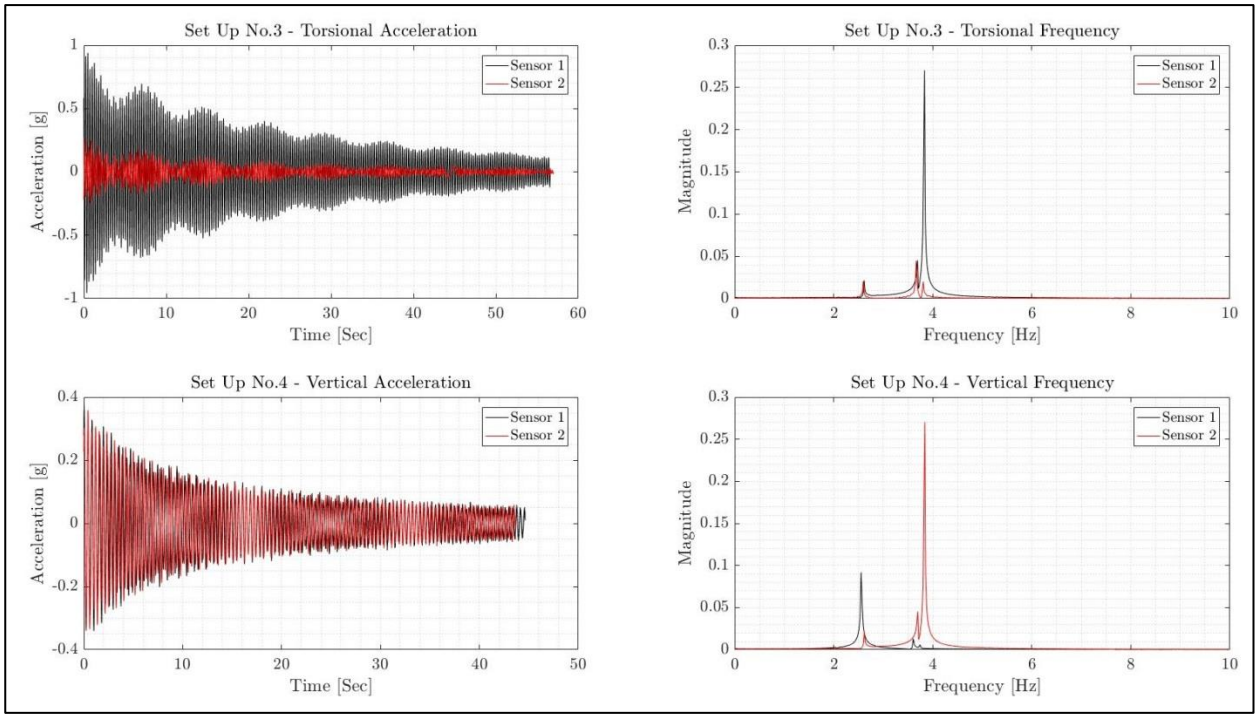

Figure 22. Acceleration time histroy and FFT for set–up 4

After free vibration test was done, it was observed that at wind speed of 10.5 m/s, which is 128.60 m/s when scaled back to full scale, using scaling laws from Chapter 3.3.1.

Setup 5 was made using 8 springs with stiffness of 0.07 N/mm, and with theirs distance from cross section centre increased to 31 cm. For all tests for set-up 5, frequencies and damping obtained are shown in Table 8.

Test ID	f_l [Hz]	f_r [Hz]	Vertical damping [-]	Torsional damping [-]
10_1	0.1711	0.2650	0.001806	0.001806
10_2	0.1713	0.2534	0.002404	0.002404
11_1	0.1721	0.2648	0.001812	0.001816
11_2	0.1722	0.2420	0.001883	0.001883

Table 8. Frequencies and damping for set-up 5

Fig. 23. displays acceleration time history and FFT for Test 11, from set–up 5. Purpose of FFT was to obtain natural frequency of model from acceleration time history.

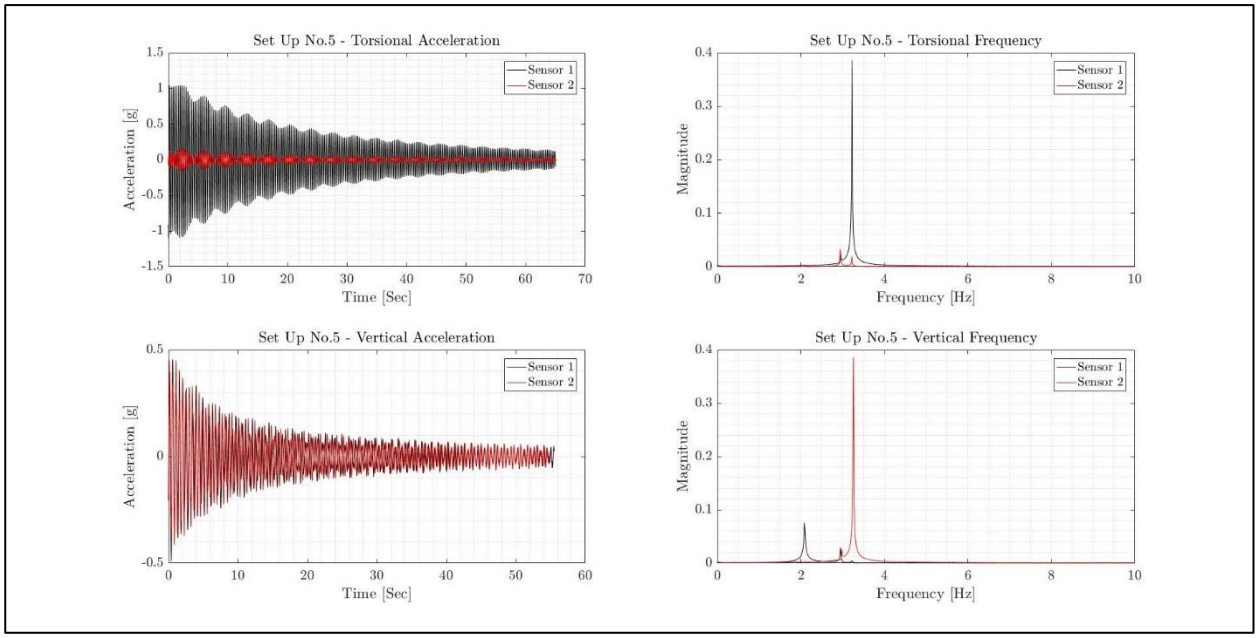

Figure 23. Acceleration time histroy and FFT for set–up 5

After free vibration test was done, it was observed that at wind speed of 9.5 m/s, which is 116.35 m/s when scaled back to full scale, using scaling laws from Chapter 3.3.1.

4 Results

4.1 Static wind coefficients

Table 9. shows values of each static wind coefficient from numerical analysis for angles of incidence from -8° to 8°, with step of 2°.

Angle of incidence [°]	$C_{L,num}$	$C_{L,exp}$	$C_{D,num}$	$C_{D,exp}$	$C_{M,num}$	$C_{M,exp}$
-8	-0.8355	-0.7766	0.0920	0.0751	-0.1669	-0.1665
-6	-0.5765	-0.6042	0.0577	0.0525	-0.1228	-0.1166
-4	-0.4255	-0.3846	0.0398	0.0351	-0.0757	-0.0541
-2	-0.3309	-0.1851	0.0239	0.0297	-0.0409	-0.0005
0	-0.2028	-0.1162	0.0158	0.0299	0.0030	0.0199
2	-0.0353	0.0855	0.0142	0.0320	0.0505	0.0737
4	0.1603	0.3143	0.0219	0.0479	0.0980	0.1329
6	0.4138	0.5415	0.0583	0.0965	0.1457	0.1690
8	0.6766	0.7197	0.1163	0.1649	0.1574	0.1515

Table 9. Static wind coefficients obtained from numerical analysis

Fig. 24. shows values for drag coefficient, Fig. 25. shows values for lift coefficient and Fig. 26. shows values for moment coefficient.

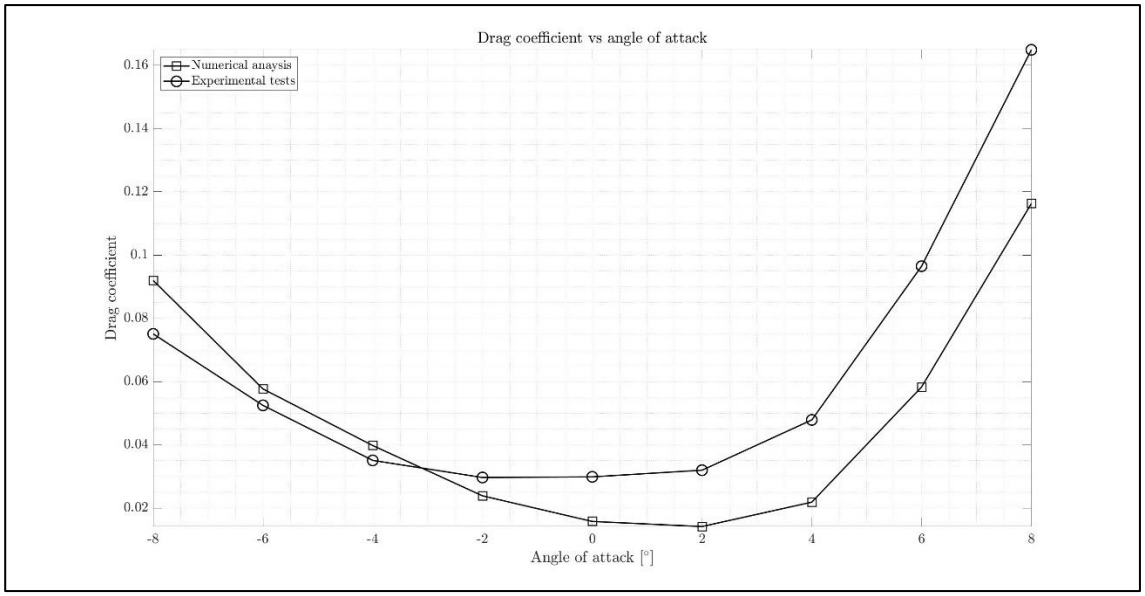

Figure 24. Comparison of drag coefficient

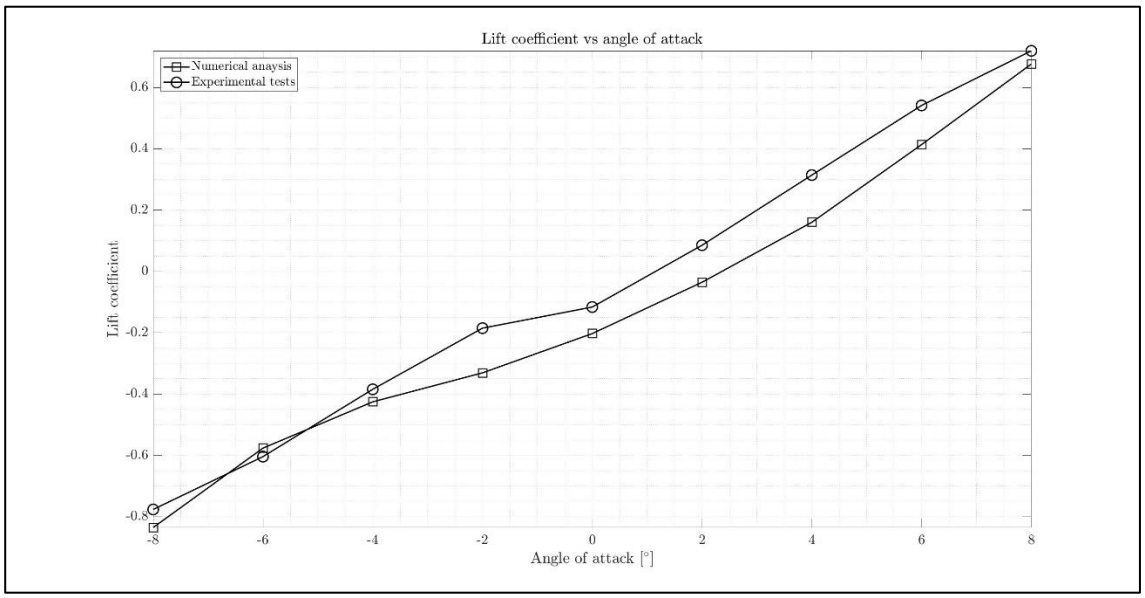

Figure 25. Comparison of lift coefficient

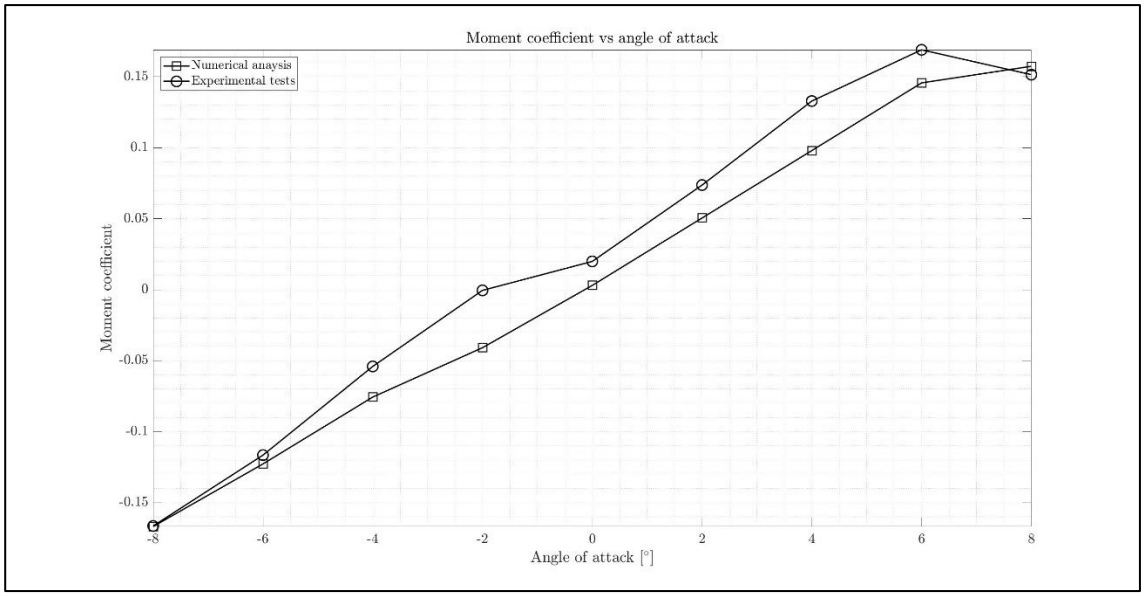

Figure 26. Comparison of moment coefficient

4.2 Flutter derivatives

After forced simulations were done, post processing of results was done in VXPost, and Fig. 27. shows each flutter derivative plotted against reduced velocity. For comparison, using VXPost, flutter derivatives for flat plate were calculated, as it was mentioned in Chapter (ref. theoretical part).

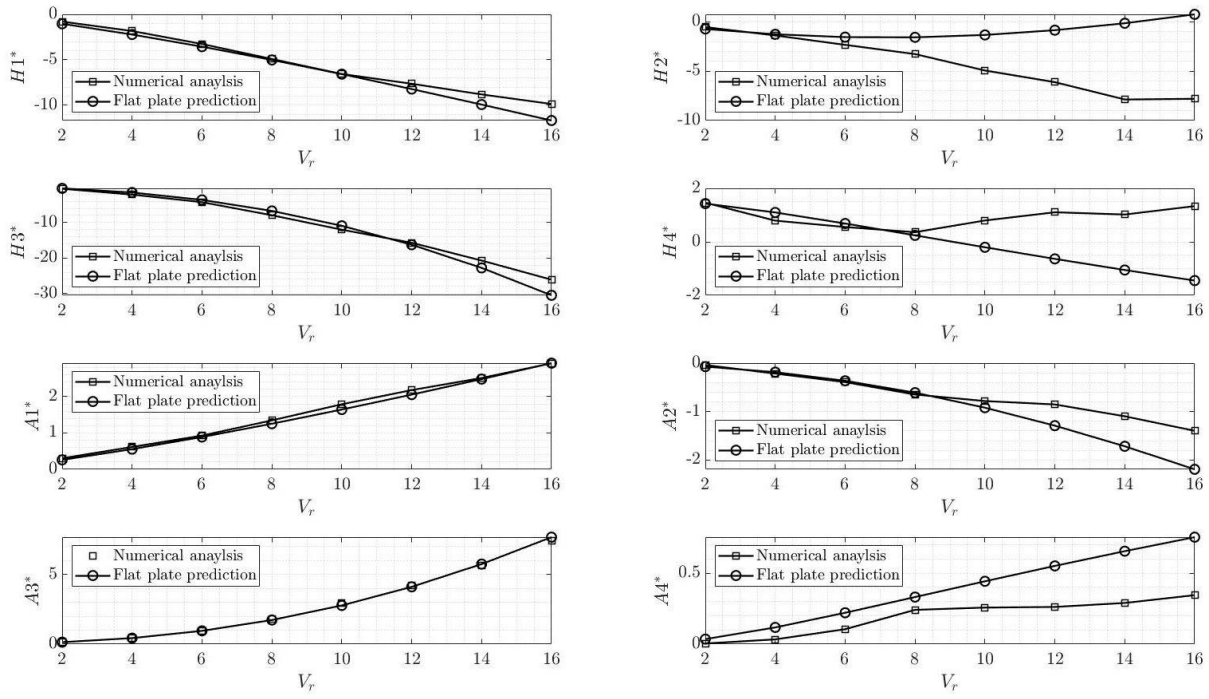

Figure 27. Flutter derivatives

From Fig. 27. it is clear that prediction that cross section behaves like flat plate is somewhat correct, as flutter derivatives are in same range of values for cross section as they are for flat plate of those dimensions.

4.3 Critical flutter speed

For each set of frequencies and damping values, as well as mass per unit length and mass moment of inertia per unit length, which were calculated earlier, critical flutter speed† was calculated using semi analytic calculation based on Theodorsen's circulation function. Table 11. gives critical wind speed for data of each of tests.

Test ID	U_{cr} [m/s]	Test ID	U_{cr} [m/s]
$2_{a,1}$	203.15	4_1	147.40
$2_{a,2}$	201.70	4_2	147.20
$2_{a,3}$	215.40	4_3	137.60
$2_{a,4}$	199.50	4_4	147.50
$2_{b,1}$	202.35	5_1	147.30
$2_{b,2}$	201.55	5_2	147.80
$2_{b,3}$	195.95	5_3	139.25
$2_{b,4}$	201.15	5_4	147.80

Table 10. Semi analytic critical speed for setup 1 and 2

Test ID	U_{cr} [m/s]	Test ID	U_{cr} [m/s]	Test ID	U_{cr} [m/s]
8_1	127.60	8_1	127.60	10_1	113.85
8_2	121.45	8_2	121.45	10_2	106.65
9_1	127.75	9_1	127.75	11_1	113.40
9_2	120.50	9_2	120.05	11_2	97.30

Table 11. Semi analytic speed for setup 3,4 and 5

Data for test 11_1 gives best results, as wind speed at which those frequencies were determined (116, 35 m/s, explained in more detail in Chapter 3.3.5.) is closest to value obtained from semi analytic calculation for test 11_1, and also those frequencies best match with one used as reference, from Chapter 1.

As it was elaborated in Chapter 3.3.5., for each of five different set–ups, different critical flutter speed was obtained, and all of those speeds (scaled to full scale) are presented in Table 12.

Set–up No.	$U_{cr,exp}$ [m/s]	$U_{cr,semi\ analytic}$ [m/s]
1	183.71	202.60
2	146.97	145.23
3	104.10	101.89
4	128.60	124.33
5	116.35	107.80

Table 12. Critical flutter speed obtained from semi analytic and experimental tests

All speeds calculated with minimum value of damping for each test, as that gives lower wind speed.

After dynamic simulations were done, it was observed that first wind speed at which flutter realizes is 120 m/s. Fig.28. shows divergence in vertical and rotational displacement for mentioned wind speed, which is associated to instability. By that, it was concluded that critical flutter speed obtained with dynamic model is 120m/s.

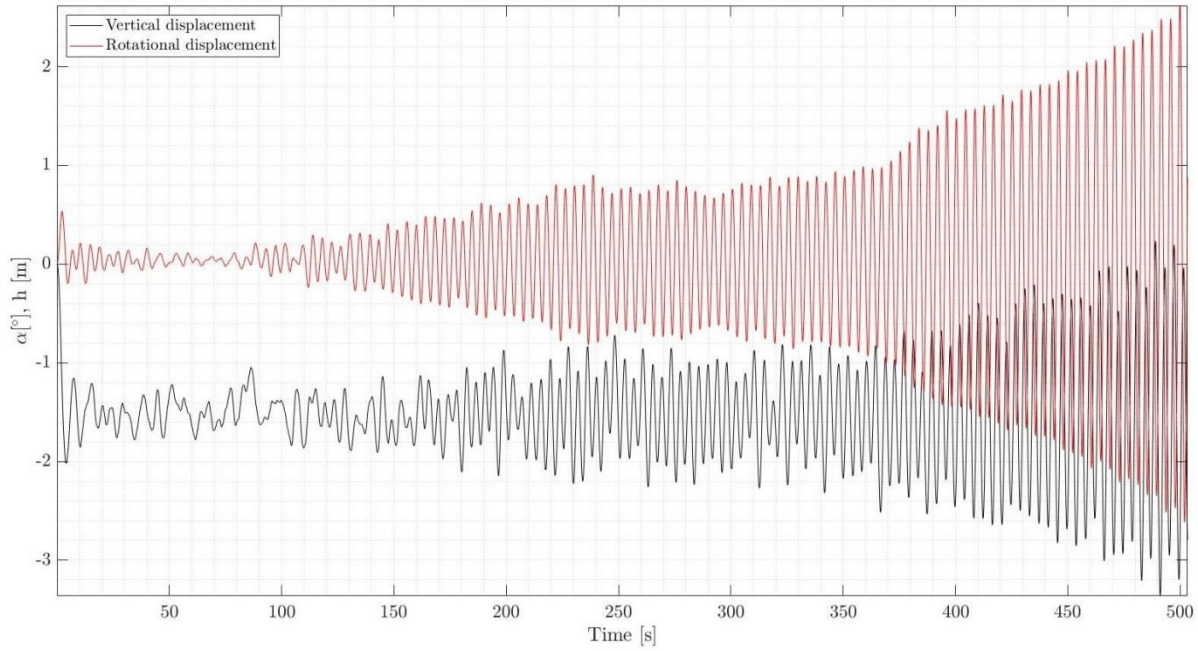

Figure 28. Numerical model displacement for wind speed of 120 m/s

On Fig. 29 bar graph is presented which shows critical flutter speed obtain through semi analytic model, numerical dynamic model and experimental test.

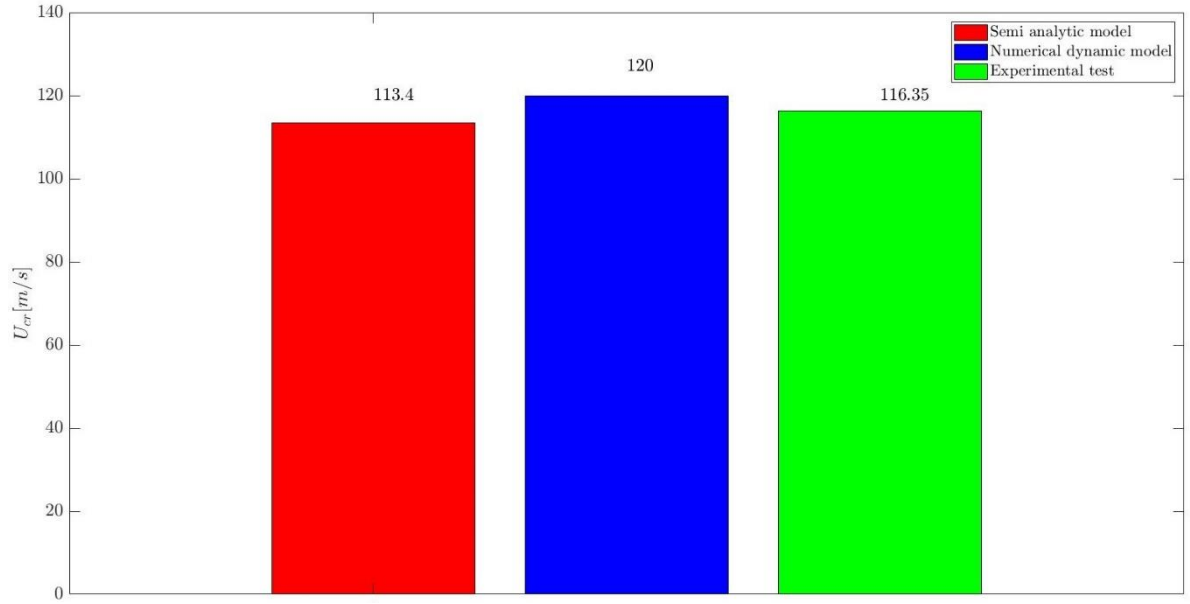

Figure 29. Comparison for critical flutter speed

On Fig. 29. for semi analytic value for comparison value from test 111 is used, as for that test frequencies obtained were closest to target ones.

5 Discussion and conclusion

The occurrence of flutter phenomenon on the Third Bosphorus Bridge has been researched. Three different methods were performed: numerical, experimental and semi-analytical analysis. The numerical analysis was successfully performed with the help of the computational fluid dynamics thorough the software of VXflow. Static wind coefficients were obtained as well as flutter derivatives. The prototype of the bridge was scaled using scaling laws [7] and the final model was taken to the wind tunnel of the Bauhaus Universität in order to determine the static wind coefficients. In addition, the vertical frequencies, torsional frequencies and the damping ratio were determined within the different five configurations of springs. Spring stiffness already calculated with a finite element software SOFiSTiK. Experimental flutter wind speed was calculated with an iterative process with the different spring configurations, obtaining the results as was estimated with the fifth configuration. Moreover, with calculated properties of the model of the bridge, the semi-analytical analysis was performed, obtaining the desire flutter wind speed. With the modal masses of the bridge, dynamic simulations were set. The model was running in between different velocities, obtaining the results for the critical flutter speed for the Dynamic numerical method. The results were compared in order to study their precision and accuracy within the different methods and the real bridge values. Over all, it can be stated that for the numerical methods, the semi analytical results, based on flutter derivatives, do not demand much computational analysis; nevertheless, they show relatively lower accuracy in representing the real scenario. The dynamic flutter analysis performed for a single slice shows good result in representing the real scenario, but it is high computational demanding; that is the reason why, for a good representation of the real scenario more slices should be used, as well as computational analysis with the demand required. Finally, the experimental sectional flutter analysis gave realistic and a good representation for the real scenario but it involves an elevated cost. Further steps that could be done to expand flutter effects on 3rd Bosporus Bridge could be to do multi slice dynamic analysis, by which we would observe behavior of more cross section at once.

List of Figures

List of Tables

Bibliography

[1] Yavuz Sultan Selim Bridge. (Accesed on: 25 August 2019). Obtained from Wikipedia (https://en.wikipedia.org/wiki/ Yavuz Sultan Selim Bridge)

[2] Andrianne, V.d (2017). The Third Bosphorus Bridge from a card-board model to the reality by the way of the wind tunnel laboratory. Engineering Office Greisch Liege University - Belgium: ACWE.

[3] Bas, N. M. (2018). Long-Span Orthotropic Steel Deck Bridges of Turkey. Department of Civil Engineering, Faculty of Engineering, Bartin University, 74100, Bartin, Turkey : IOP ebooks.

[4] Morgenthal, G. (2016). VXflow v20160310 Primer.

[5] Vincent de Ville de Goyet, Y. D. (2017). The dynamic behaviour of the third Bosporus Bridge . Copenhagen, Denmark : Eurosteel.

[6] Vincent de Ville de Goyet, Y. D. (2017). The Third Bosphorus Bridge its wind behavior during the different erection stages and in final configuration. Bureau Greisch Belgium : EACWE

[7] You-Lin. (2013). Wind Effects on Cable-Supported Bridges .Wiley.

[8] Morgenthal, G. (2019). GMTIB-Guido Morgenthal Technologien in Bauwesen.

[9] Scanlan, R.H. and Tomko, J.J. (1971) Airfoil and bridges deck flutter derivatives. Journal of the Engineering Mechanics Division, 97 (6).

VI. PROJECT ASSIGNMENT 4

Vortex-induced vibration analysis on Tokyo Bridge

(a) Study and literature review about the vortex induced vibration (VIV) phenomenon.
(b) Modelling and simulation of the reference bridge cross-section (basic cross section) using CFD tool VXflow.
(c) Determination of the critical wind speed for the VIV. Determination of the static wind coefficients.
(d) Build the main span of the bridge model using FE software and perform the modal analysis.
(e) Compare the CFD simulation results with the observed/measured values of VIV displacements.
(f) Build the section model and test it in the Wind Tunnel (Laser Cut technique for creating the model).
(g) Submission of the reports and presentation of the results.

Tokyo Bridge (Source Image: https://www.wired.com/2008/12/dec-18-1997-360-seconds-under-tokyo/)

Following report with the pages from 1 to 44 correspond to pages 136 to 179 of the report at hand

Vortex-induced vibration analysis on Tokyo Bridge

OTHMAN, Reyadh
Faculty of Civil Engineering, Bauhaus-Universiy Weimar

PERIĆ, Ana
Faculty of Civil Engineering Osijek, J. J. Strossmayer University of Osijek

SHARMA, Alok
Faculty of Civil Engineering, Bauhaus-UniversityWeimar

TERRA, Ranieri
Faculty of Civil Engineering,University of Aviero

VRDOLJAK, Ivan
Faculty of Civil Engineering Osijek, J. J. Strossmayer University of Osijek

Weimar, August 2019

Contents

List of figures

List of Tables

Abstract

The static forces are generated by the wind actions on structures, particularly bridges, in the combination of other loads. Further, these wind actions can also generate structural dynamic response translated into oscillations experienced by bridge structural elements during a certain duration of time. This report presents the detailed study of Vortex Induced vibrations phenomenon on Tokyo bay bridge. How the aerodynamic actions that induce oscillations on the bridge structural elements are studied in detail. The study is done to find the vertical vibrations based on experimental data from wind tunnel tests, numerical simulations, and analytical methods along with the literature review. This report ends with a motivation which gives rise to further studies on this subject.

1. Introduction

Wind, by its nature is extremely powerful force. In some extreme cases, with great wind speeds, it can cause natural disasters. However, even on low velocities, wind can cause damage on structures as well as people using said structure. When wind is causing deformations on a structure for a long time, it can collapse due to fatigue. Also, those vibrations cause psychological effect on people using structures, because they aren't feeling secure on bridge that goes up and down. As bridges, unlike most other structures, are usually being built in an open space, they are extremely vulnerable when it comes to wind induced vibrations.

Since wind induced vibrations are occurring under a broad spectrum of velocities, there are a lot of wind phenomena, such as vortex induced vibrations, buffeting and flutter. In scope of this research, focus was put on vortex induced vibrations that occur under lower wind velocities. When wind strikes the structure, vortexes force the structure to move. Wind velocity dictates frequency of vortexes, and since structure has it´s own natural frequency, resonance can occur when those two frequencies meet. From that moment on, movement of structure takes control of vortex shedding, as oppose to before resonance, when vortex shedding depended on shape of cross section. That phase is called lock-in, since structure "locks" vortexes.

It is also important to note as how crucial aerodynamics of cross section is. If aerodynamics is taken into consideration during the design process, vortex induced vibrations are much less expected to occur, since there is more shedding, which is more regular. Matters of aerodynamical analysis comprises of analytical, numerical and experimental approach. In scope of this research, focus was put on numerical and experimental analysis. For both parts of analysis, static and dynamic models were tested. In static analysis, cross section was excited with one wind velocity, which causes static wind forces, such as drag, lift and moment to arise. Out of static wind forces, static wind coefficients could be calculated. Also, from FFT, Strouhal number was determined and after that, resonant wind velocity could be predicted, to be used in dynamical analysis. For dynamical analysis, cross section was suspended with two sets of springs, which helped mimic dynamic behavior of structure. Section was excited with range of wind velocities, with respect to approximated resonant wind velocity. Results gathered were maximal amplitude and actual resonant wind velocity. In scope of this research, multi slice (pseudo-3D) simulation was also performed, for better understanding of how the whole bridge behaves.

2. Vortex-induced vibrations

Vortex-induced vibrations (VIV) represent serious problem to the structure. While those kinds of vibrations are considered a response problem (as opposed to flutter which is stability problem), one can also consider them as a serviceability problem because level of vibrations of structure

must be limited to ensure user comfort, otherwise psychological effect on the users can occur, and to avoid long term fatigue damage followed by premature failures (2).

VIV are motions induced on bodies facing an external flow by periodical irregularities on this flow, and, in general, occur with resonance of structure, schematically shown in Figure3.Since wind is in general non-linear fluid, complete analytical models that can accurately describe vortex-induced vibrations have yet not been obtained. However, as VIV are usually occurring under a moderate wind it is crucial to determine which wind velocity is critical for causing vortex-induced vibrations. For that matter, wind tunnel testing using full and sectional models in the only reliable method to predict the performance of structures in the wind. To complement those results, computer fluid dynamics (CFD) technique has been developed in great matter in recent years, and it had been used as supplement for tunnel testing. (3). One of the basic and important issues in the bridge aerodynamics is whether the phenomena observed in wind tunnel testing matches those in teal bridges, which is one of issues involved in research presented. (1)

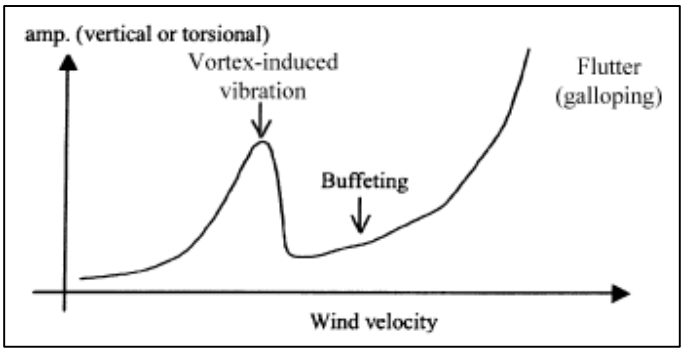

Figure 1: Wind-induced vibrations (3)

VIV, among other types of dynamic excitation, appear to be the most critical for long-span bridges and often serve as obstacle for safety and serviceability of bridges of such. In particular, girders with box sections exhibit large amplitude due to vortex-induced vibrations, as oppose to truss girders which rarely show large vortex-induced vibrations. In bridges girders, VIV can be managed by aerodynamic or mechanical measures, first being flaps and fairings that modify air flow around the girders, while second provides damping to the girders. As the aerodynamic forces are very sensitive to the geometry, even a small change of the section by adding flaps and fairings can stabilize the girder. However, it is often difficult to find aerodynamic control devices that are effective, and control of wind-induced vibrations relies on mechanical means, e.g. tuned mass dumpers (TMDs) (3).
VIV may occur in the completed bridges, but can cause even more significant problem in erection stage of bridges. During erection phase, components of bridge (pylons, girders before closing) are extremely flexible and under great influence of wind-induced vibrations, especially the vortex-induced vibrations (3).

3. Description of the Tokyo Bridge

The Trans-Tokyo Bay Bridge completed in 1997 crosses the centre of Tokyo Bay from the NW to SE, as shown in Figure 1.

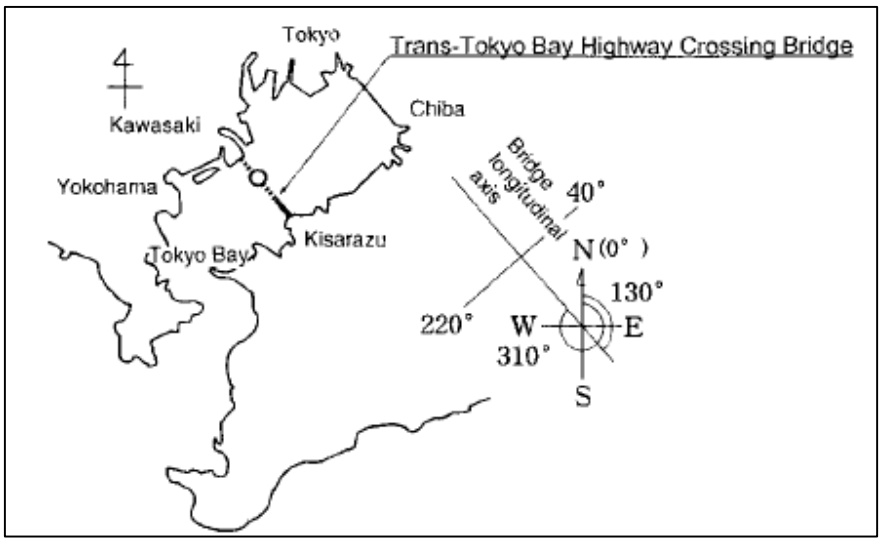

Figure 2: The placement of the Tokyo Bridge (1)

The bridge, shown in the Figure 2, is a part of the bridge portion whose total length is 4384 m. It is a straight ten-span continuous steel box-girder bridge, with three cells in the cross section. The overall length is 1630 m (from P3 to P13 – section observed in this research), with the longest span measured 240 m (1).

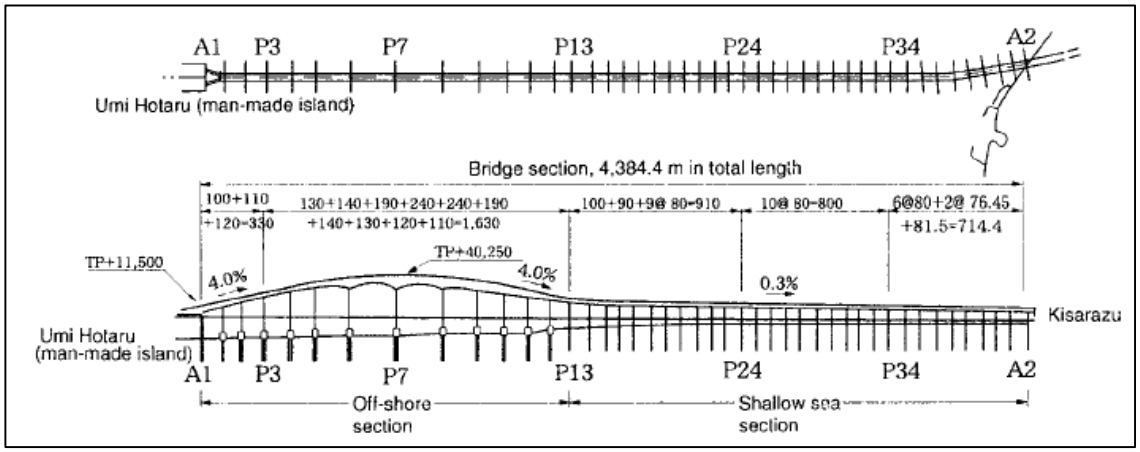

Figure 3: Longitudinal view of the Tokyo Bridge (1)

The bridge has four lanes for a total width of 22.9 m, with plan to widen the bridge with two more lanes, to meet an anticipated future increase in traffic volume, the highway will measure 29.9 m in total length (1).

The bridge has changing cross section, with 9.6 m depth in the mid span and 7.65 m depth in in the support. That way, overall forces on structure are smaller, since shedding is broken and not all forces act in the same time.

3.1 Vortex-induced vibrations of the Trans-Tokyo Bay Bridge

In the design phase of the bridge, various wind tunnel tests were performed on two-dimensional and three-dimensional models, and revealed that vortex-induced vibrations would develop in the bridge under the wind normal to the bridge axis (1).
During the construction of the crossing, significant vibration due to vortex shedding was observed in the bridge under prevailing winds, as first mode peaked at a wind velocity around 16-17 m/s, with maximum amplitude exceeding 50 m. The comparison between predictions based on wind tunnel testing and the observed response showed significant correlation (3).
After vortex-induced vibrations were observed in the field, further tests were also conducted and it was decided to install 16 TMDs in the girders to control first and second mode of vibrations. The TMDs were designed specifically for bridge in question, to allow the control of vertical girder vibration using installation that would fit in the limited space inside the girders. In addition to that, vertical plates were attached to the post of crash barriers in the girders, to aerodynamically control vibrations in higher modes (3 and greater) (1).

4. Numerical simulations

4.1 Finite Element Model

The modelling has been done in Sofistik Software as a beam model to perform dynamic analysis. The spans and piers are modelled as beam model. The springs are considered at the bottom of piers with stiffness of 10^8 kN/m.

It includes 10 spans, 1630m length continuous steel box girder. Fig. 4 and fig. 5 displays an overview of the bridge. The two 240m main spans are situated on both sides of the P7. Its cross section is of variable depth being 10.5m at abutment and 6.0m at mid span.

4.1.1 Units and sign convention

The table (1) shows the respected properties with units going through the report tasks.
Moreover, Technical document provided observe the following sign convention:
X – Longitudinal axis along the bridge

Y – Transverse axis

Z – Vertical axis

Table 1: Properties and their units respected in the report

Property	Units
Distance, displacement	m; mm
Force	kN; MN
Uni weight	kN/m^3
Area	m^2
Modulus of inertia	m^4
Frequency	Hz
Speed	km/h
Acceleration	m/s^2
Rotation	rad

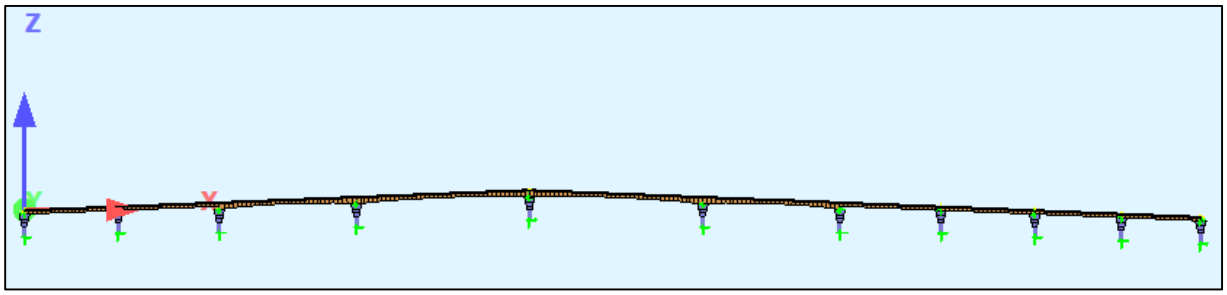

Figure 4: Full bridge from P3 to P13

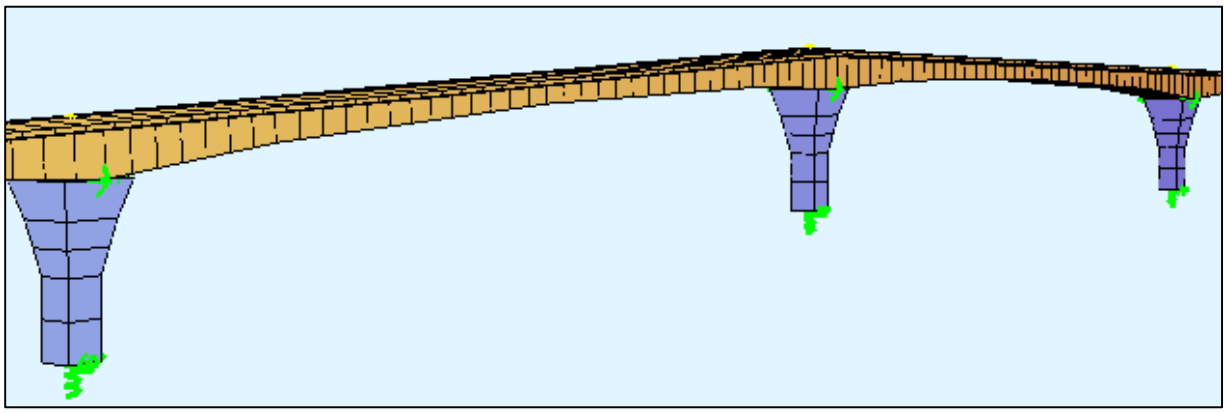

Figure 5: Main spans P6 to P8

4.1.2 Cross section properties

Cross section No. 1 - Steel Box girder-Mid

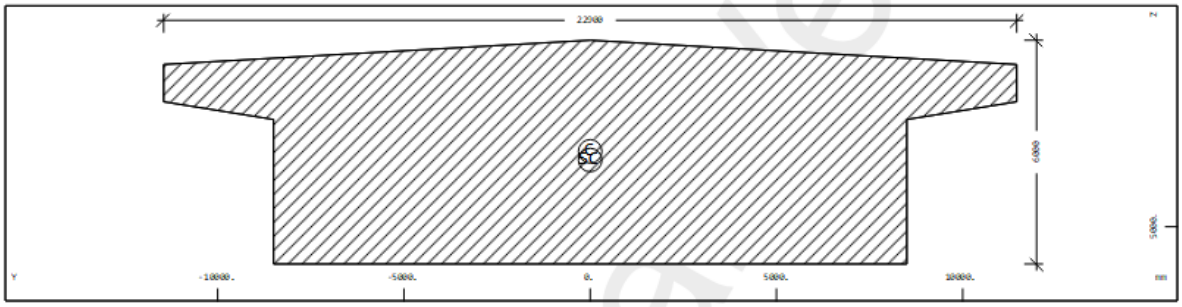

Cross section No. 1 - Steel Box girder-Mid

Static properties of cross section

SNo	Mat	A[m2]	Ay[m2]	Iy[m4]	yc[mm]	ysc[mm]	E[N/mm2]	g[kg/m]	I-1[m4]
	MRf	It[m4]	Az[m2]	Iz[m4]	zc[mm]	zsc[mm]	G[N/mm2]		I-2[m4]
			Ayz[m2]	Iyz[m4]					α[°]
1	2	1.0569E+02	9.182E+01	2.984E+02	0.0	0.0	4900	19283.9	3.071E+03
		8.869E+02	7.518E+01	3.071E+03	2979.9	3213.8	1885	(BEAM)	2.984E+02
				1.055E-14					-90.00

= Steel Box girder-Mid

SNo	section number	yc[mm],zc[mm]	ordinate of elastic centroid
Mat	material number	ysc[mm],zsc[mm]	ordinate of shear centre
A[m2]	sectional area	E[N/mm2]	Young's modulus
Ay[m2],Az[m2],Ayz[m2]	transverse shear deformation area	g[kg/m]	weight per length
Iy[m4],Iz[m4],Iyz[m4]	bending moment of inertia		
I-1[m4],I-2[m4],α[°]	principal moments of inertia and angle of the principal axes		
MRf	reinforcement material number		
It[m4]	torsional moment of inertia		
G[N/mm2]	Shear modulus		

Cross section No. 2 - Steel Box girder-Intermediate

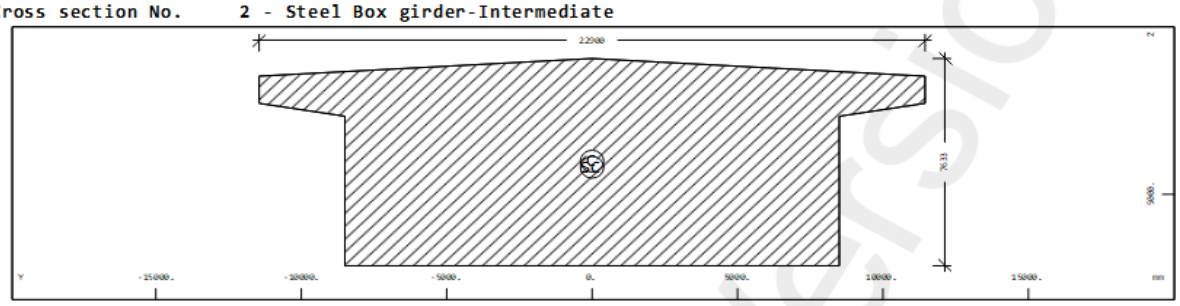

Cross section No. 2 - Steel Box girder-Intermediate

Static properties of cross section

SNo	Mat	A[m2]	Ay[m2]	Iy[m4]	yc[mm]	ysc[mm]	E[N/mm2]	g[kg/m]	I-1[m4]
	MRf	It[m4]	Az[m2]	Iz[m4]	zc[mm]	zsc[mm]	G[N/mm2]		I-2[m4]
			Ayz[m2]	Iyz[m4]					α[°]
2	2	1.3345E+02	1.150E+02	6.282E+02	0.0	0.0	4900	24349.0	3.740E+03
		1.715E+03	9.975E+01	3.740E+03	3778.0	4005.1	1885	(BEAM)	6.282E+02
				1.285E-13					-90.00

= Steel Box girder-Intermediate

SNo	section number	yc[mm],zc[mm]	ordinate of elastic centroid
Mat	material number	ysc[mm],zsc[mm]	ordinate of shear centre
A[m2]	sectional area	E[N/mm2]	Young's modulus
Ay[m2],Az[m2],Ayz[m2]	transverse shear deformation area	g[kg/m]	weight per length
Iy[m4],Iz[m4],Iyz[m4]	bending moment of inertia		
I-1[m4],I-2[m4],α[°]	principal moments of inertia and angle of the principal axes		
MRf	reinforcement material number		
It[m4]	torsional moment of inertia		
G[N/mm2]	Shear modulus		

Cross section No. 3 - Steel Box girder-End

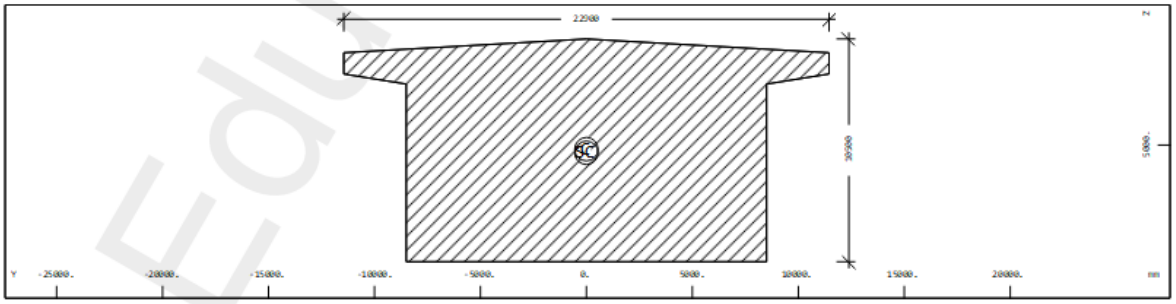

Cross section No. 3 - Steel Box girder-End

Static properties of cross section

SNo	Mat	A[m2]	Ay[m2]	Iy[m4]	yc[mm]	ysc[mm]	E[N/mm2]	g[kg/m]	I-1[m4]
	MRf	It[m4]	Az[m2]	Iz[m4]	zc[mm]	zsc[mm]	G[N/mm2]		I-2[m4]
			Ayz[m2]	Iyz[m4]					α[°]
3	2	1.8219E+02	1.556E+02	1.660E+03	0.0	0.0	4900	33241.4	4.913E+03
		3.901E+03	1.428E+02	4.913E+03	5192.7	5366.1	1885	(BEAM)	1.660E+03
				1.360E-13					-90.00

= Steel Box girder-End

SNo	section number	yc[mm],zc[mm]	ordinate of elastic centroid
Mat	material number	ysc[mm],zsc[mm]	ordinate of shear centre
A[m2]	sectional area	E[N/mm2]	Young's modulus
Ay[m2],Az[m2],Ayz[m2]	transverse shear deformation area	g[kg/m]	weight per length
Iy[m4],Iz[m4],Iyz[m4]	bending moment of inertia		
I-1[m4],I-2[m4],α[°]	principal moments of inertia and angle of the principal axes		
MRf	reinforcement material number		
It[m4]	torsional moment of inertia		
G[N/mm2]	Shear modulus		

4.1.3 Modes shapes

The dynamic analysis is performed in Sofistik to get the modal participation of the bridge in the various modes. The first five vertical modes are considered for our study. The mode shapes with the respective Eigenfrequencies are presented below.

Mode 1 with Natural frequency 0.329Hz

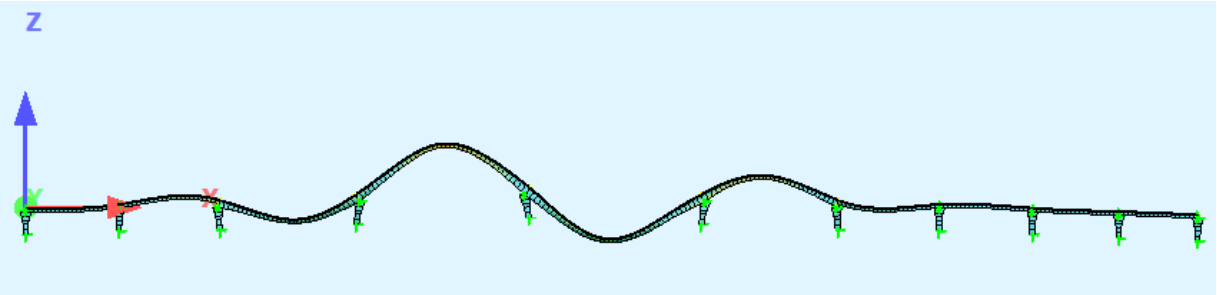

Figure 6: Vertical Mode 1

Mode 2 with Natural frequency 0.489Hz

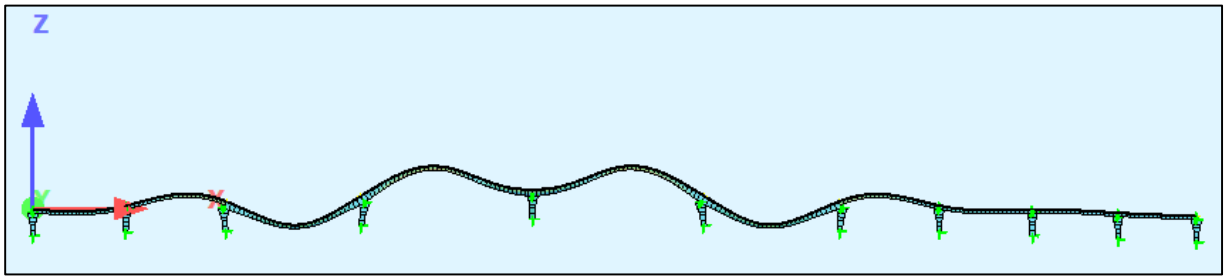

Figure 7: Vertical Mode 2

Mode 3 with Natural frequency 0.673Hz

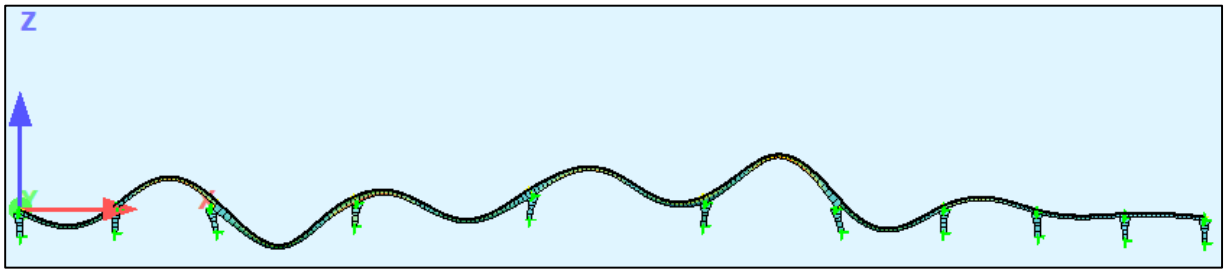

Figure 8: Vertical Mode 3

Mode 4 with Natural frequency 0.769Hz

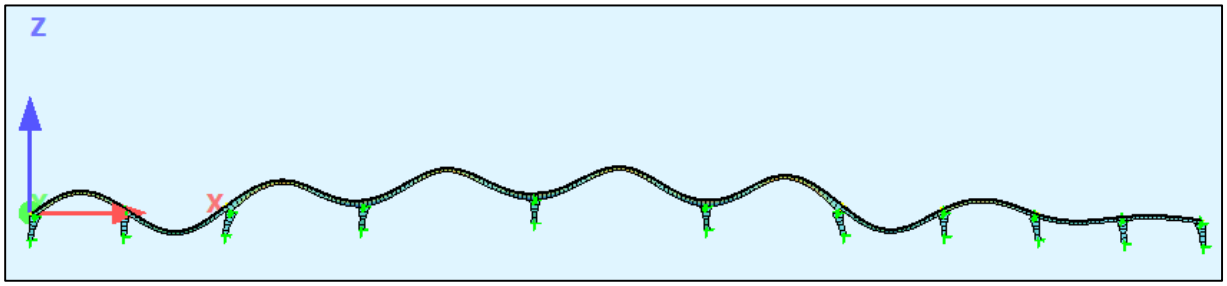

Figure 9: Vertical Mode 4

Mode 5 with Natural frequency 0.914Hz

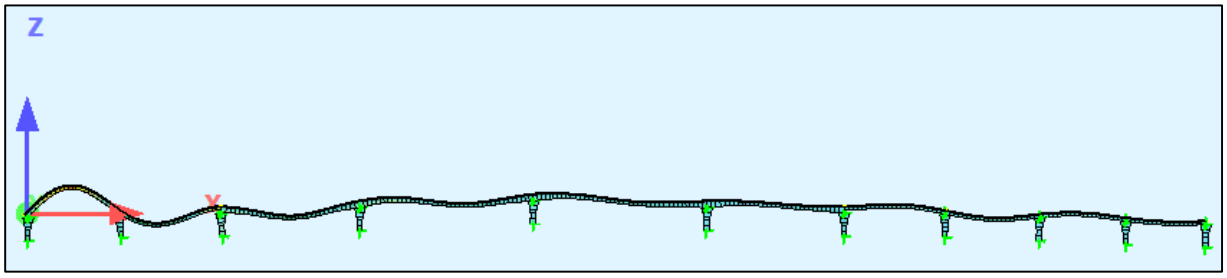

Figure 10: Vertical Mode 5

4.1.4 Modal Mass calculation

Modal Mass $=\sum$ (Mass x $\varphi_{normalised}^{2}$)

Table 2. Frequency and modal masses

Mode	Frequency (Hz)	Modal Masses (ton)
1	0.329	5643
2	0.489	7956
3	0.673	5866
4	0.769	8152
5	0.914	7962

4.2. Modelling of the cross-section using CFD software (VXflow)

Cross section with characteristics gathered from literature was modelled using house CFD software VXflowv.20160310. VXflow is a flow software based on the Vortex Particle Method (VXflow v.20160310 Primer).

Static and dynamic simulations were run for original as well as scaled cross section. In addition, multislice simulation, for five slices along part of span from 460 to 700 m, was run as well. From said simulations information on static wind Strouhal number, coefficients, resonance wind speed and amplitudes were collected and compared with literature and experimental results. Every model has around 300 panels and has been run for 25 000 steps.

4.2.1 Original cross section – Static model

Static model has been done first for determining wind coefficients and Strouhal number, so resonance frequency can be predicted. After finding Strouhal number, it was known at which wind speed resonance will occur. Originally, we know that vortex shedding will occur at Strouhal number between value 0.1 and 0.2. One of the peaks was chosen, with the value of Strouhal number. After analysing fD/U – $S(C_L)$ diagram, Strouhal number was found at value of 0.1435. [4]

After finding Strouhal number, it could be predicted at which wind speed will frequency of the bridge and frequency of vortex shedding meet. Resonance wind speed is calculated with equation (1), depending on geometry of girder as well as wind frequency and velocity.

$$U_{res} = \frac{f \cdot D}{St} \tag{1}$$

From equation (1), predicted resonance speed will be around 16 m/s.

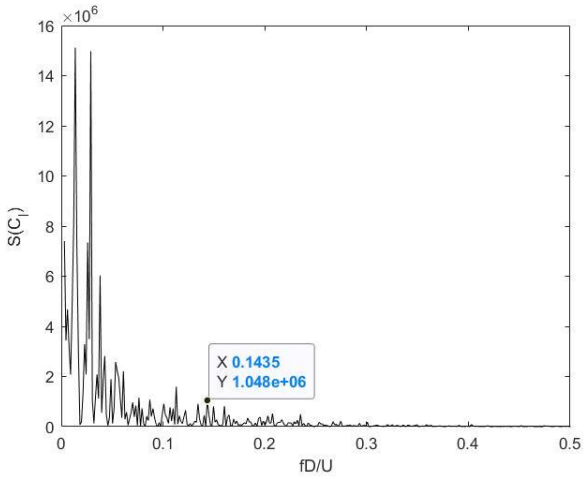

Figure 11. Predicting Strouhal number [4]

The second reason of doing static model is getting the wind coefficients and comparing them to the ones that we got from literature. Static model is modeled with wind speed of 17 m/s, because value of wind speed does not affect the wind coefficients results. Wind coefficients were determined as mean values from the graph below (5):

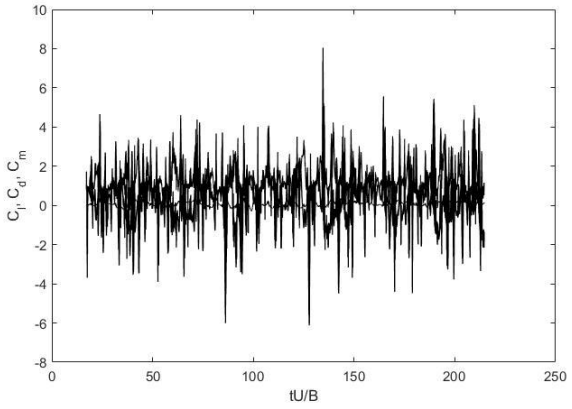

Figure 12. C_L,C_M,C_D coefficients

Values for the wind coefficients are shown in the table (1):

Table 3. Coefficients results taken from Matlab

C_L	C_D	C_M
-0,163	1,130	0,09

After getting wind coefficients for 0˚, new models were run with different angles of attack. Different angles of attack that were analysed are: 4˚, 8˚, 12 ˚, -4˚, -8˚, -12˚. Results are given in table below (3):

Table 4. Numerical wind coefficients results

Degrees	**CL**	**CD**	**CM**
-12	-1,05	2,39	-0,01
-8	-0,95	1,92	0,03
-4	-0,60	1,15	0,07
4	0,57	1,18	0,08
8	0,79	1,63	0,04
12	0,94	2,20	0,02

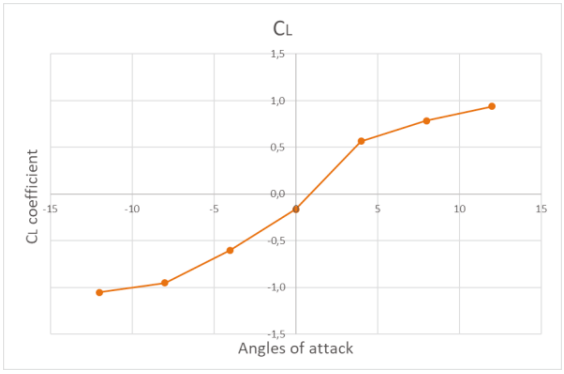

Figure 13. Coefficients of lift

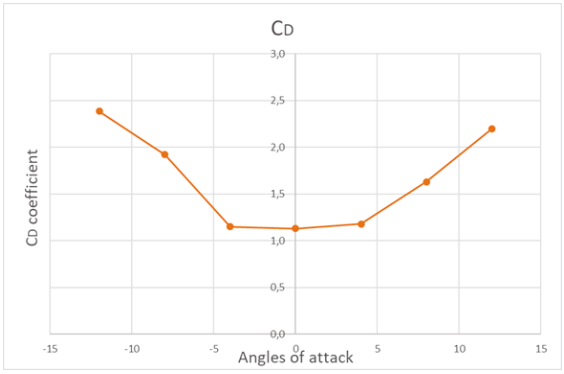

Figure 14. Coefficients of drag

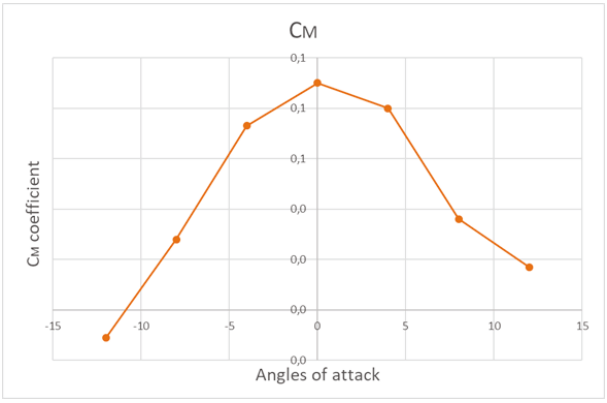

Figure 15. Coefficient of moment

4.2.2 Original cross section – Dynamic model

After making static model and getting wind coefficients, next target is finding correct speed at which wind induced vibrations will appear. This will occur when frequency of the bridge meets vortex shedding frequency. To find resonance wind speed, 8 different models with 8 different wind speeds were made. Different wind speed values that have been used are: 14 m/s, 15 m/s, 16 m/s, 17 m/s, 18 m/s, 16.8 m/s, 17,2 m/s. Targeting values for post-processing is Strouhal numbers from which we can calculate frequency.

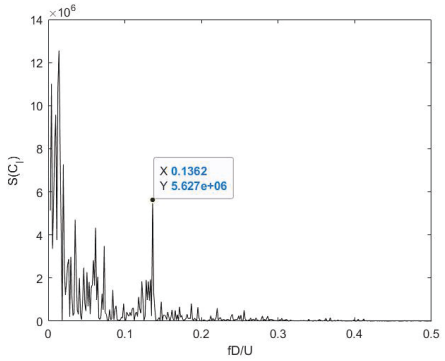

Figure 16. Strouhal number taken from Matlab

Frequency is determined from equation (1):

$$f = \frac{0.1342 \cdot 17.2}{6.9} = 0.335\ Hz$$

Results with other wind speeds were also analysed, and maximum amplitude for each wind speed can be shown at the figure below (17):

The Reynolds number is important to help predict flow patterns in different fluid situation. The Reynolds number is gotten from equation (2):

$$Re = \frac{U \cdot D}{v} \tag{2}$$

Re – Reynolds number
U – Wind velocity (m/s)
D – Width of cross section of the midspan (m)

With respect to said values, Reynolds number was determined in value of $6{,}40 \cdot 10^6$.

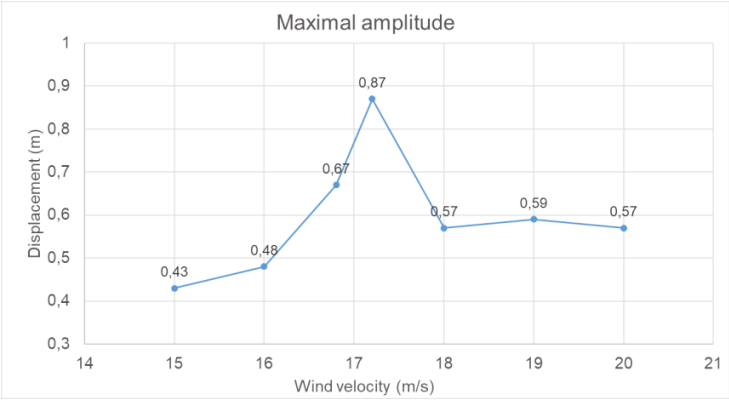

Figure 17. Maximum displacements for different wind velocities

In figure 18, for wind velocity 17.2 m/s it can be seen that vortex shedding has occurred.

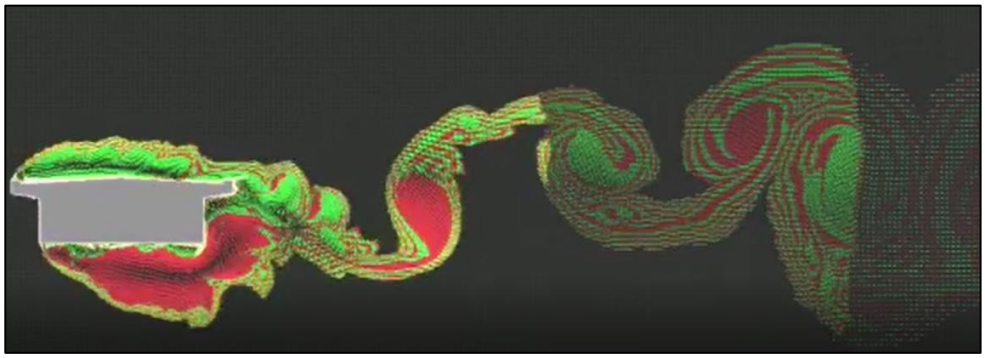

Figure 18. Vxflow visualization

4.2.3 Scaled cross section – Dynamic Model

While doing experiment, there is always insecurities about some parts and some values. For example, stiffness of the springs or mass of the bridge, also Reynolds number was also much lower. Because of said, one scaled dynamic model was made. Dynamic model has been done to compare its results with experiment. Dynamic model has been modelled with the same data as model in experiment. Frequency used in calculation is 2.24 Hz, damping is 0.0015 and calculated weight is 2.92 kg. Wind speed has been used with the value 0.9, because that was wind speed where wind induced vibration occurred. Firstly, Strouhal number is determined so the resonance speed can be found.

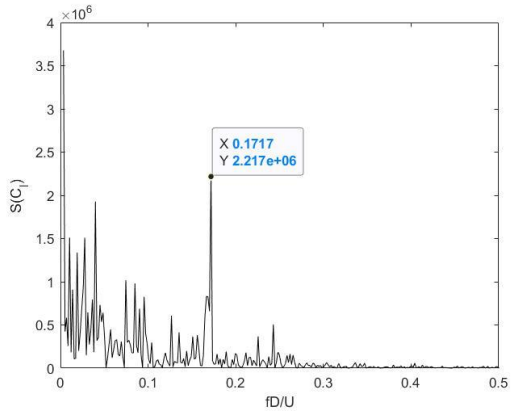

Figure 20. Strouhal number for scaled dynamic model

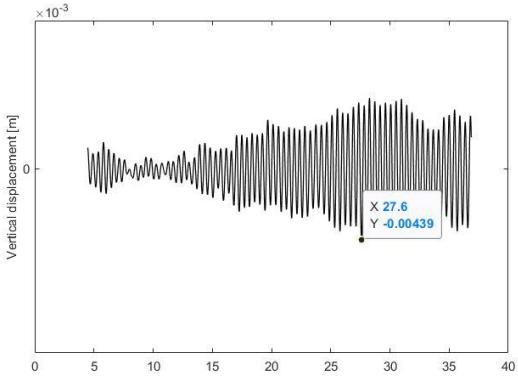

Figure 19. Maximum amplitude during resonance wind speed

Resonance wind speed is calculated from equation (1). With respect to said values, resonance wind speed is determined in value of 1.1 m/s.

4.2.4 Original cross section – multislice

Until now, the modelling was done only with 1 slice models. Tokyo Bay bridge doesn't have same cross section per length, and because of that, other cross section has been taken into consider. This was made with pseudo-3D model, known as multislice. 5 cross section were taken into consider, first was at mid span, 2 were at support, and 2 were at L/6 length.

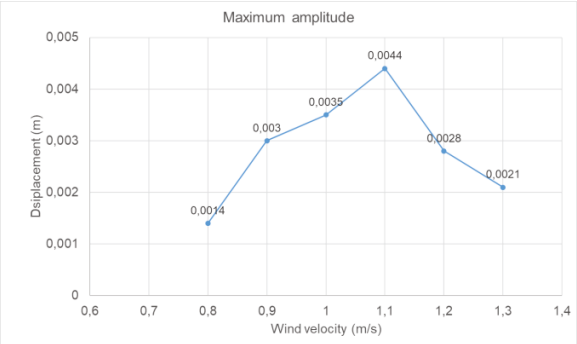

Figure 22. Maximum amplitudes for different wind speeds

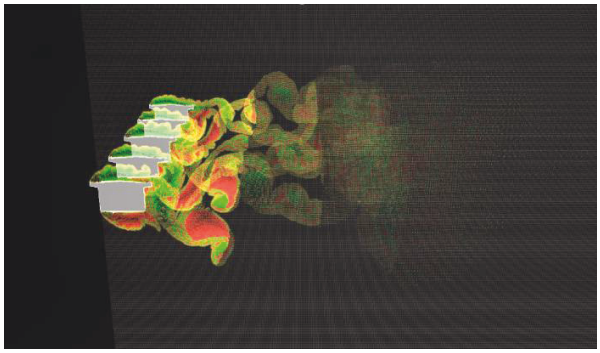

Figure 21. Multislice visualisation

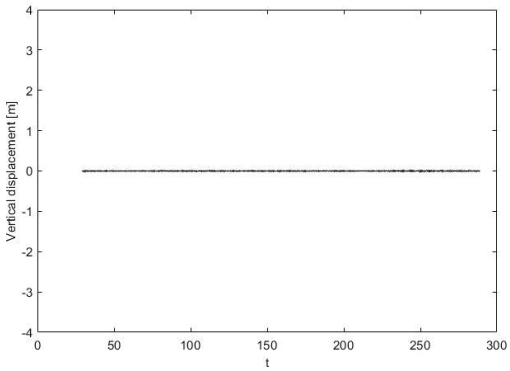

Figure 24. Time history of displacements at support

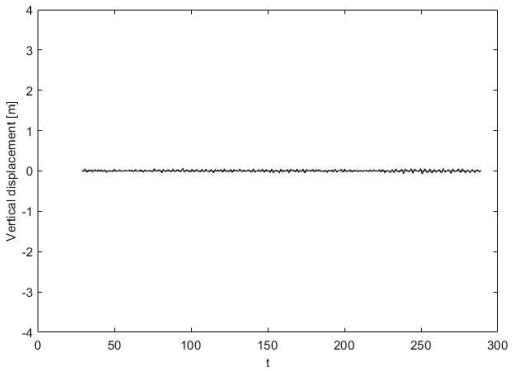

Figure 23. Time history of displacements at L/6

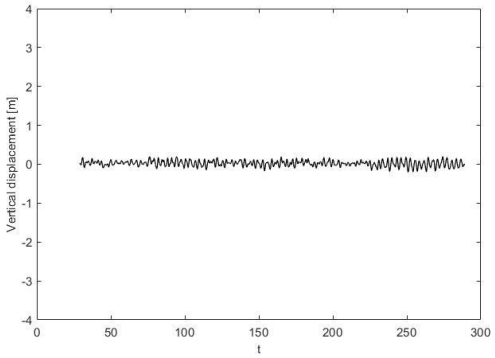

Figure 25. Time history of displacements at mid span

In the figures below [23], [24], [25], we can see time histories of displacements. At support, maximum displacement is 2.8 cm, at L/6 it is 7.2 centimeters, and at mid span it is 21.1 cm.

5 Experimental tests

5.1 Scaling laws and scaled properties of structure

Geometry scale ratio
The geometry scale ratio is taken as 1:100. And, this ratio was coming from two considerations:

1. Tunnel test geometry
2. The suitable cross section of the bridge model

Velocity scale ratio
The scale ratio of velocity is decided depending on similarity of Froude number as following:

$$F_r = \frac{V}{(Dg)^{1/2}},$$

For full scale:

$$F_r = \frac{17\ m/s}{(6.0\ m\ X\ 9.81\ m/s2)^{1/2}} = 2.216$$

Now, the velocity with respect to scaled geometry of depth and similar Froude number

$$2.216 = \frac{X}{(0.060\ X\ 9.81)^{1/2}}$$
$$X = 1.7\ m/s$$

Therefore, the ratio between full scale and protoytpe model

$$1.7 : 17 \approx 1{:}10$$

Mass per unit length

It is normal to fit the mass per unit length in case of uniform sections, but target cross section is not uniform. So, the equivalent mass per unit length is :

$$m_e = \frac{\int_0^l m(s).\Phi_1^2(s)ds}{\int_0^l \Phi_1^2(s)ds}$$

m_e: the equivalent mass per unit length.
m(s): the mass in terms of nodal mass vector.
Φ1(s): the first mode shape in terms on mode shape vector
This relation could be approximated by summation as following:

$$\int_0^l m(s).\Phi_1^2(s)ds = m_1.d_1^2.\ L_1 + m_2.d_2^2.\ L_2 + m_3.d_3^2.\ L_3 + \ldots..$$
$$\int_0^l \Phi_1^2(s)ds = d_1^2.\ L_1 + d_2^2.\ L_2 + \ldots.$$

The values will be getting by the numerical simulation of the bridge.
Finally, the equivalent mass per unit length is ($m_{e,\ L=240}$) = 11627 Kg/m

Calculating the mass of section prototype
The full scale mass per meter is 11,627 kg/m. And, the scale down factor of mass is $1{:}100^2$.
m (small scale) = 1.1627 kg/m
M_{model} = 1.1627 kg/m X 1.200 m = 1.39524 Kg ≈ 1.40 kg

Calculating the stiffness of the spring

$$\mathbf{f} = \frac{1}{2\pi}\sqrt{\frac{k}{m}} = \frac{w}{2\pi}$$

$k = (2\pi f)^2 m$ = 83.58 (N/m) per spring.

For the first mode, the frequency of the bridge deck is
f_1 = 3.48 Hz

And, for 1.2 m width section of the bridge, the mass will be as:

m = M_{model} = 1.40 kg

Now,

K = (2 X 3.14 X 3.48 Hz)^2 * 1.40 kg = 668.66 N/m

K should divide by 8 (no. of springs)

K (per spring) = $\frac{668.66\ \frac{N}{m}}{8\ (no.of\ springs)}$ = 83.58 N/m

Table 5. Scaling requirements for free vibration section model

Parameters	Scale ratio
Length	$1/\lambda_L$
Wind velocity	$1/\lambda_U$
Mass per unit length	$1/\lambda_L^2$
Mass inertial per unit length	$1/\lambda_L^4$
Structural frequency	λ_L/λ_U
Damping ratio	1

The scaling outcomes:

Table 6. Scaling characteristic results of the model

Property	**Full scale**	**Scale Ratio**	**Scale Down**
Length	-	1:100	1.2 m
Wind Velocity	16 m/s^2	1:10	1.6 m/s^2
Mass per Unit Length	11,627.0 kg/m	1:(100)^2	1.1627 kg/m
Frequecny	f_1= 0.348 Hz f_2= 0.483 Hz f_3= 0.630 Hz	100:10	3.480 Hz 4.830 Hz 6.300 Hz
Damping	0.03	1:1	0.03

5.2 Design of a prototype for wind tunnel testing including scaled geometry and dynamic properties

5.2.1 Model preparation for laser cutting

After achieving the target scaling properties, the AutoCAD model is prepared for laser cutting. Multiple cross-sections had been executed. The figure (26) shows multiple sections that was prepared for laser cutting machines.
In most cases we have to take care of sections dimensions as taking care of different covers of that plate. If you note figure (26), we could see that the dimensions are less from every edge by 1.0 mm because that covering sheets that will be setting up.

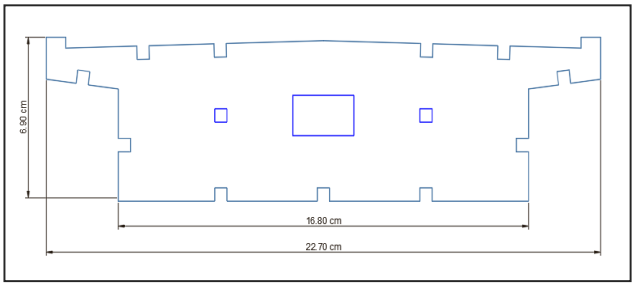

Figure 26: Model for laser cutting

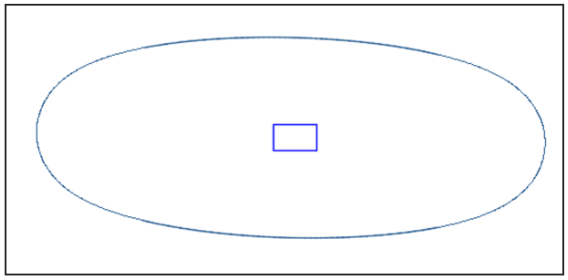

Figure 27: Outer sheet section for protection

When the wind in tunnel test is passing through the section, it should pass in stream lines. For this reason, we add protecting sheets at the end of the gross section as it is shown in figure (27).

5.2.2 Printing the model

In fact, the laser cutting machine has some rules for the way of cutting. It means that it will not work well through the prototype drawings without considering these rules on section drawings. The order of cutting is considered based on color coding, i.e., at first blue colored lines, second red lines and the finally the light blue colors. The table below shows the entered colors previously before executing the cutting.

Table 7. Laser cutting machine enters board, *TROTEC LASER GMBH,2015*

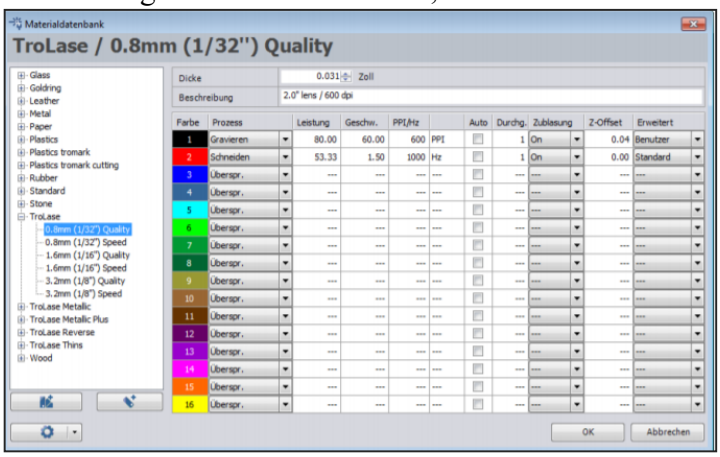

Moreover, it has color guide. They were followed during preparing the drawings. Then section is cut as shown below in figure. It looks very accurate of what has been prepared. Still the final work is to put the part of sections on each other to create the final prototype of wind tunnel test.

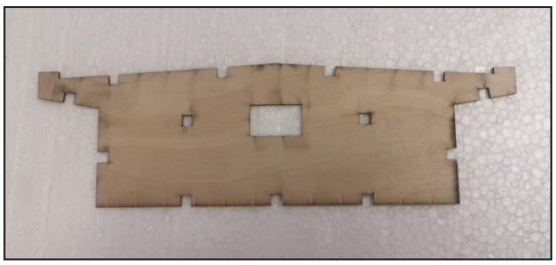

Figure 29: Section cut from laser printing

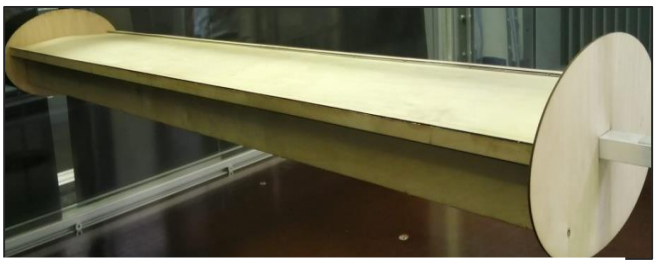

Figure 28: Prototype model of the bridge cross section

Finally, the model prototype was achieved and executed and the figure (29) shows its view.

5.3 Determination of static wind coefficients from static experiments under laminar flow

5.3.1 Setting up the model

The model was preparing in the wind tunnel with static wind force sensors located at supports on the two sides as shown in figure (30) below. The respected static forces are the lift, drag and the torsion. It was read by the two sensors to be more accurate.

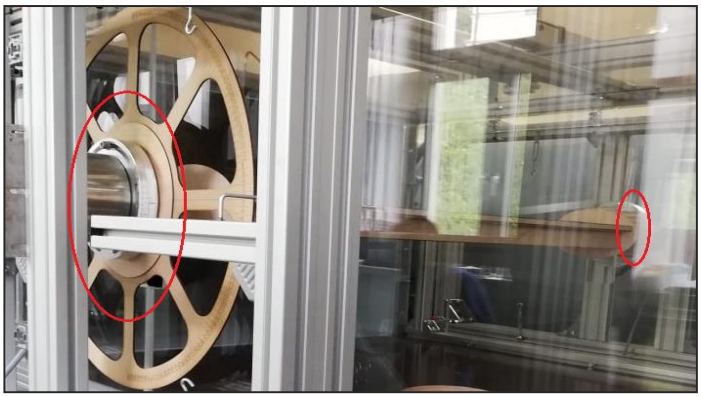

Figure 30. Setup with static force sensors

During the arrangement of the setup, it is important to be accurately measure the angles because the angles of attack are important for wind force striking the structure.

Determination of static wind coefficients from static experiments under laminar flow

In static tests, we need to flow stream laminar winds through the cross-section with constant speed. Exciting the system is required for any type of phenomena especially vortex-induced vibration. Static wind force coefficients importance comes with respect to clarifying the forces that affected on the structure which called static mean forces. The figure (31) below shows the directions of forces with respect to model cross section.

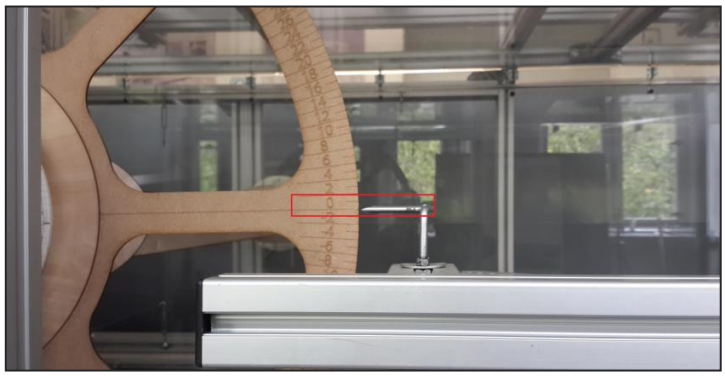

Figure 31. Leveling the model to 0 Deg angle of attack.

The resultant forces for aerodynamic phenomena on the structure could be used to calculate the coefficients. The respected equations for clarifying the procedure are the following:

Lift, $$C_L = \frac{F_L}{\frac{1}{2}\rho B U_\infty^2}$$

Drag, $C_D = \frac{F_D}{\frac{1}{2}\rho D U_\infty^2}$

Moment, $C_M = \frac{F_M}{\frac{1}{2}\rho B^2 U_\infty^2}$

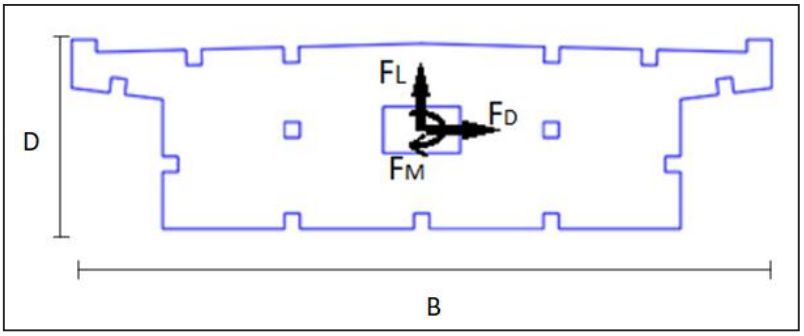

Figure 32: Static forces on the model

An experiment was performed for calculating the coefficients with respect to constant stream wind speed with multiple angles of attack. The figure below shows how the wind streams strikes the cross section.

The wind stream strikes the cross section by rotating the section at different angles from negative to positive angles (-16deg to +16deg). The results are recorded by the two sensors, the recorded data is then processed to get the wind coefficients.

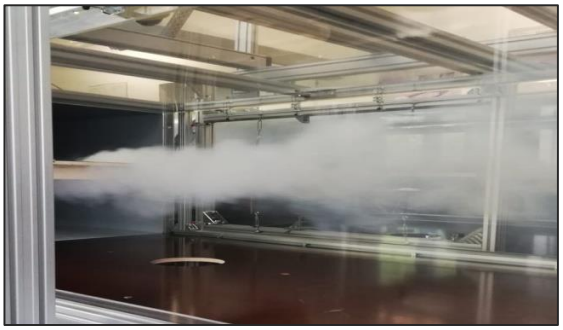

Figure 34: Wind strikes the structure in wind tunnel

Figure 33: Rotating the model to a target angle of attack

The steps followed on the executed test are prepared in the table below.

Table 8. Angle of attacks and wind speed

Sl. No.	Angle of Attack (deg)	Wind Speed (m/s)
1	0	5
2	-4	5
3	-8	5
4	-12	5
5	-16	5
6	4	5
7	8	5
8	12	5
9	16	5

For getting the coefficients values at every angle, the time history of static forces recordings was analyzed. The figure below shows the time history of vertical forces of the two side sensors with 0.0 degrees angle of attack.

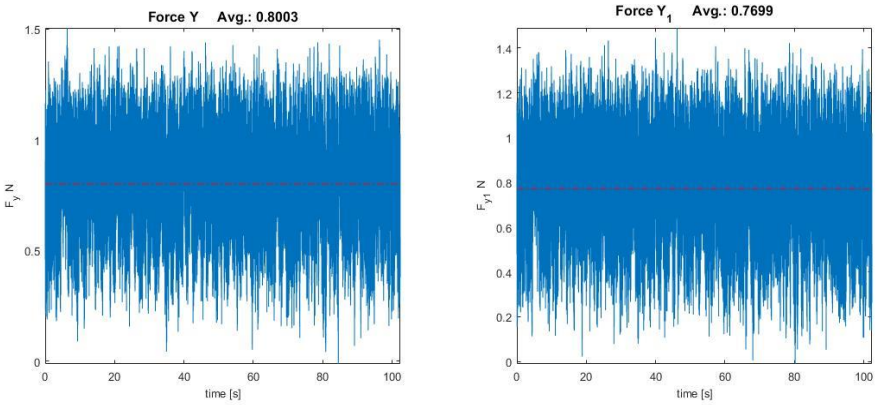

Figure 35: Time history of lift force of the sensor I (*left*) and for sensor II (*right*).

For all the coefficients figures, analyzing the time histories of all cases were verified using Malta Software. The critical part in analyzing the data is sensors reading on both sides which mean negative recordings for some files. Then, the reconsidering is taking the absolute values to get the wind coefficients. The figure below shows the clarified static forces coefficients.

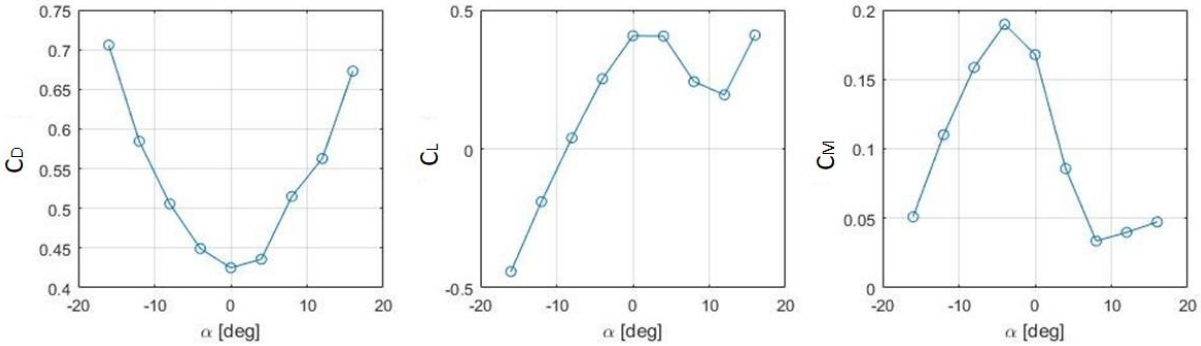

Figure 36: Static wind coefficients for multiple angles of attack for the two sensors (*top*)

5.3.2 Vortex Shedding Frequency

Vortex shedding frequency is a characteristic property that depends on the section geometry and is defined quantitatively through the strouhal number, St, as

$$\mathrm{St} = \frac{f_{shed}\, D}{U}$$

The vortex shedding frequency, f_{shed} can also be determined as

$$f_{shed} = \frac{Vc}{e}$$

where, Vc is the vortex convection velocity along the wake downstream,
e is the horizontal space covered by space covered by the vortex during one cycle.

The determination of the parameters Vc and e is more complex, as it requires visualization tools through the use of numerical simulations or other additional techniques usually employed in wind tunnel facilities.

The following equation is used for calculating the Strouhal Number in terms of frequency of shedding, depth and the wind velocity. The observed frequency of shedding is with respect to zero degree angle of attack.

Figure 37: Vortex shedding occurring during resonant.

$$\mathrm{St} = \frac{f_{shed}\, D}{U}$$

where,

f_{shed} = vortex shedding frequency.

D = the depth of the bridge cross section.

U = wind velocity.

Vortex shedding frequency is obtained by analyzing the average of lift force time history with 0 Deg angle of attack as shown below.

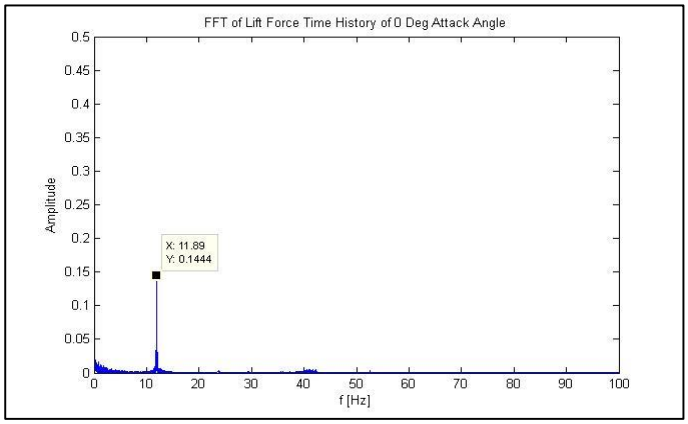

Figure 38: Vortex shedding frequency.

For our test, the St is calculating as the following:

$$St = \frac{f_{shed} D}{U}$$

$$= \frac{11.89 * 0.0617}{5} = 0.146$$

The importance of St Number is for verifying the values of resonant velocity with respect to this experiment setting. It will be more clarified in section of dynamic test.

5.4 Determination of the dynamic properties of structure

5.4.1 Calculation of target natural frequency

Natural frequency is the frequency at which the structure shows free vibrations i.e., oscillates freely when not subjected to any external force. This is also known as Eigenfrequency.

For experiment model, the spring stiffness after considering scaled mass is:
ki = 83.58 (N/m) per spring
n = 8 (number of springs)
Thus, total stiffness, k = n * ki = 8 * 83.58 = 668.64 N/m

Mass of cross section = 1.867kg
Mass of two side bars = 0.4 (kg/m) * 1.2 m * 2 = 0.96kg
Additional mass of connections = 0.1 kg
Thus, Total mass = 1.867 + 0.96 + 0.1 = 2.92 kg

Frequency, $f = \frac{\sqrt{(k/m)}}{2\pi}$ = 2.41Hz
So, target frequency of the prototype structure to be obtained in wind tunnel test is 2.41Hz.

5.4.2 Natural frequency and damping achieved in wind tunnel test

The structural model is 1.2m in length, 0.079m in depth and as wide as width of wind tunnel.
The model is suspended with 8 springs. The dynamic analysis is performed with two set of bearings in order to achieve the target frequency.

The two sensors are placed at both ends of the cross section. Then, the structure is made to vibrate vertically and the measurements are recorded by the sensors for these vibrations. The data recorded by the sensors are then post processed. Firstly, the Fourier transformation of the time history recorded is done, and then applying a band pass filter the unwanted frequencies are removed.

With the first set of springs, the resonance behavior i.e., the maximum vertical vibrations observed are at 1.2m/s. After post processing the results for this wind speed, the frequency achieved is 3.0Hz, but it was not close to target frequency 2.41Hz. So, the top four springs are replaced in order to achieve the target frequency.

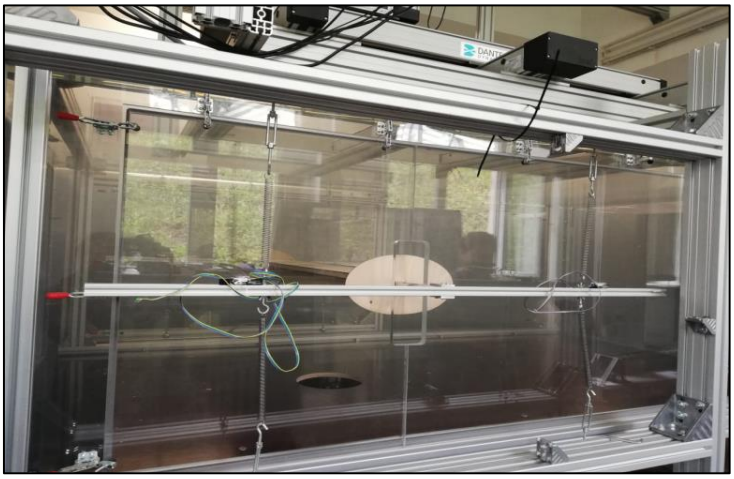

Figure 39: Arrangement of structure, springs, and sensors in Wind tunnel

The results for first set of springs are only shown for the resonant speed and are as follows. The frequency of structure measured is 2.24Hz. From manual calculation, the target frequency was 2.41 Hz, which very close to the frequency obtained for the chosen set of springs.

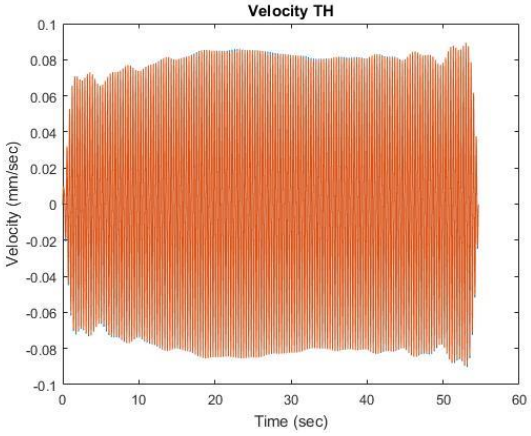

Figure 40. Time history of velocity

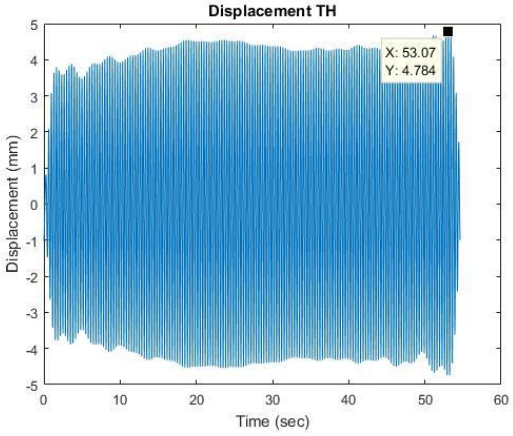

Figure 41. Time history of displacment

The damping of the structure is found nearly 0.15% from the decay of the acceleration time history.

5.4.3 Displacement and resonant wind speed due to vortex induced vibrations of wind

For the set of bearings which has shown the output frequency nearly close to target frequency, are finalized for the further wind tunnel tests.

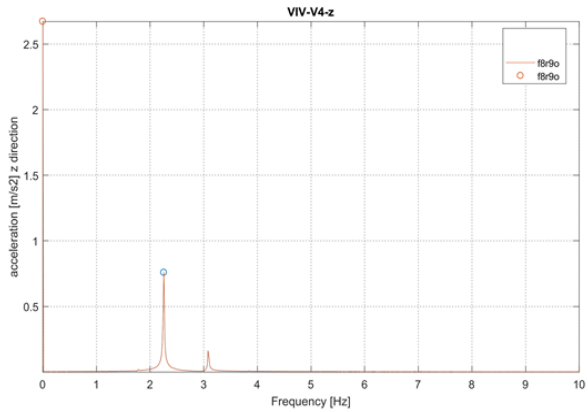

Figure 42: Natural Frequency

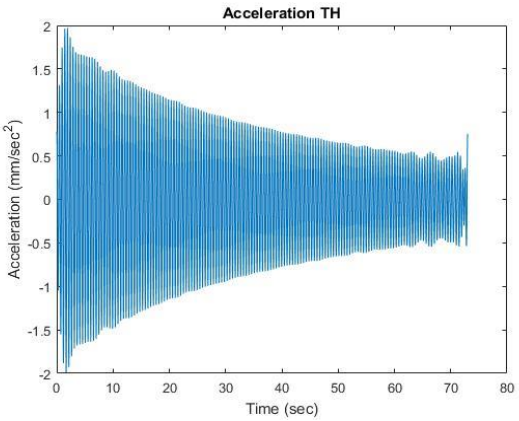

Figure 43: Acceleration TH for free vibrations

The wind is now allowed to hit the structure in the tunnel with a varying speed from 0.8m/s to 1.2m/s. The high amplitude in the vertical vibrations are observed at 1.0m/s. Thus, the resonant wind speed is 1.0m/s, at which the frequency of structure matches with frequency of wind vibrations.

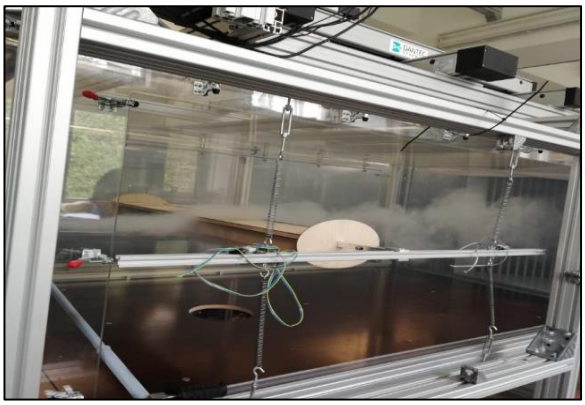

Wind speed (m/s)	Displacement (mm)
0.8	0.4808
0.9	5.538
1.0	6.523
1.1	1.658
1.2	0.2984

Table 9. Displacement for different wind speeds

Figure 44: Wind strikes the structure at different speeds

The maximum displacement observed at resonant wind speed of 1.0m/s is 6.523mm.

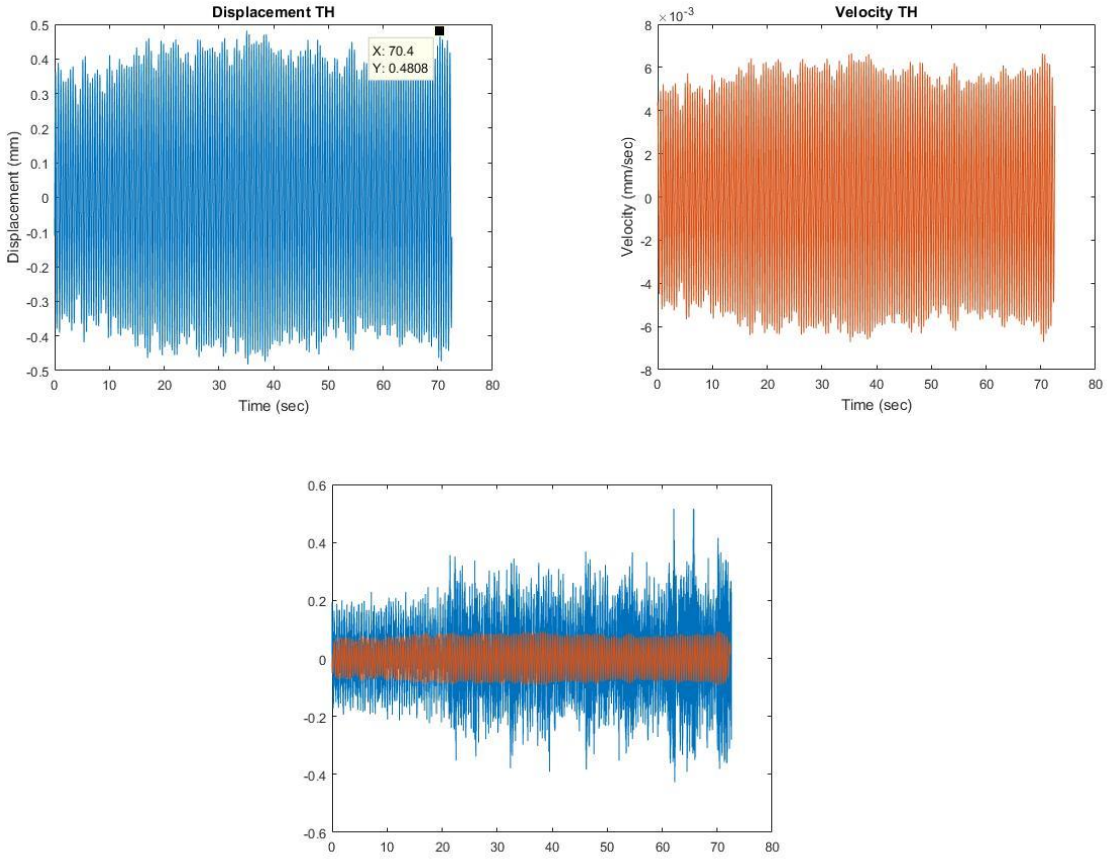

Figure 45: Time history results of model displacement (*top, left*) velocity (*top, right*) and acceleration (*bottom*) for wind speed 0.8 m/s

The displacement value is small and the acceleration increases. This is clear by the relevant figures according to data processing.

The figures (47) show the model acceleration, velocity and the vertical displacement according to wind speed of 0.9 m/s. The vertical amplitude is high compare with wind speed of 0.8 m/s. And the acceleration is increasing.

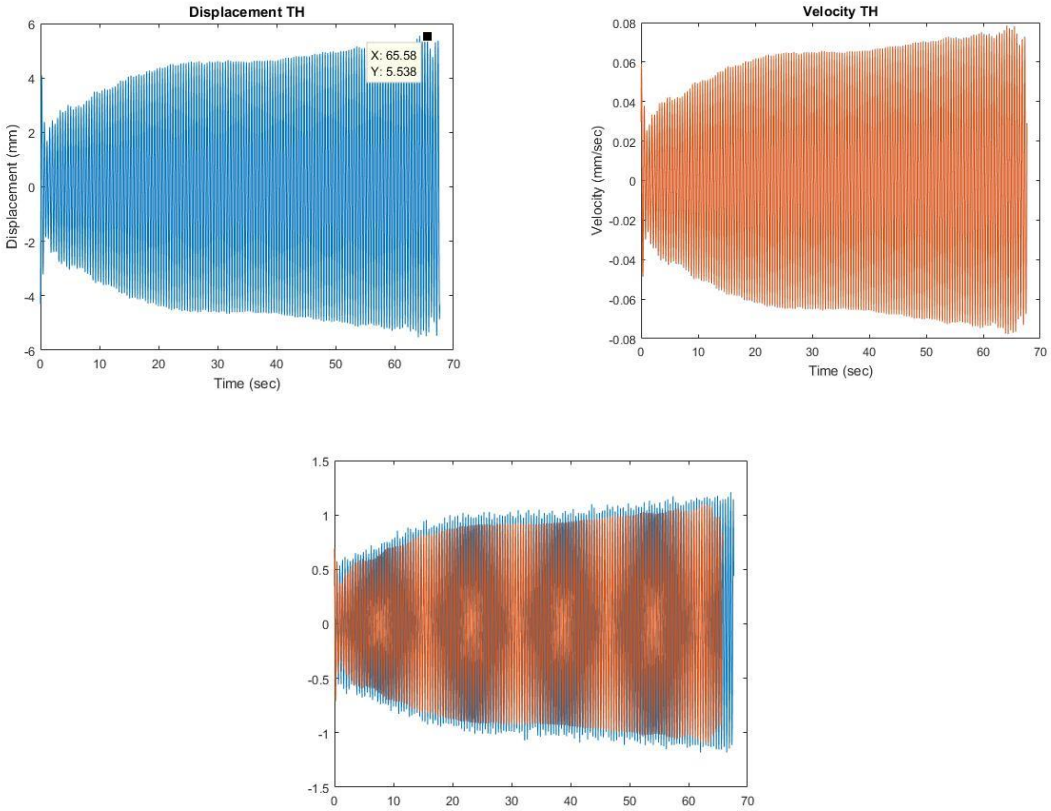

Figure 46: Time history results of model displacement (*top, left*) velocity (*top, right*) and acceleration (*bottom*) for wind speed 0.9 m/s

Moreover, the figures (47) show the model acceleration, velocity and the vertical displacement according to wind speed of 1.0 m/s. The vertical amplitude is higher than previous ones compare with wind speed of 0.9 m/s. And the filtered acceleration looks in level values.

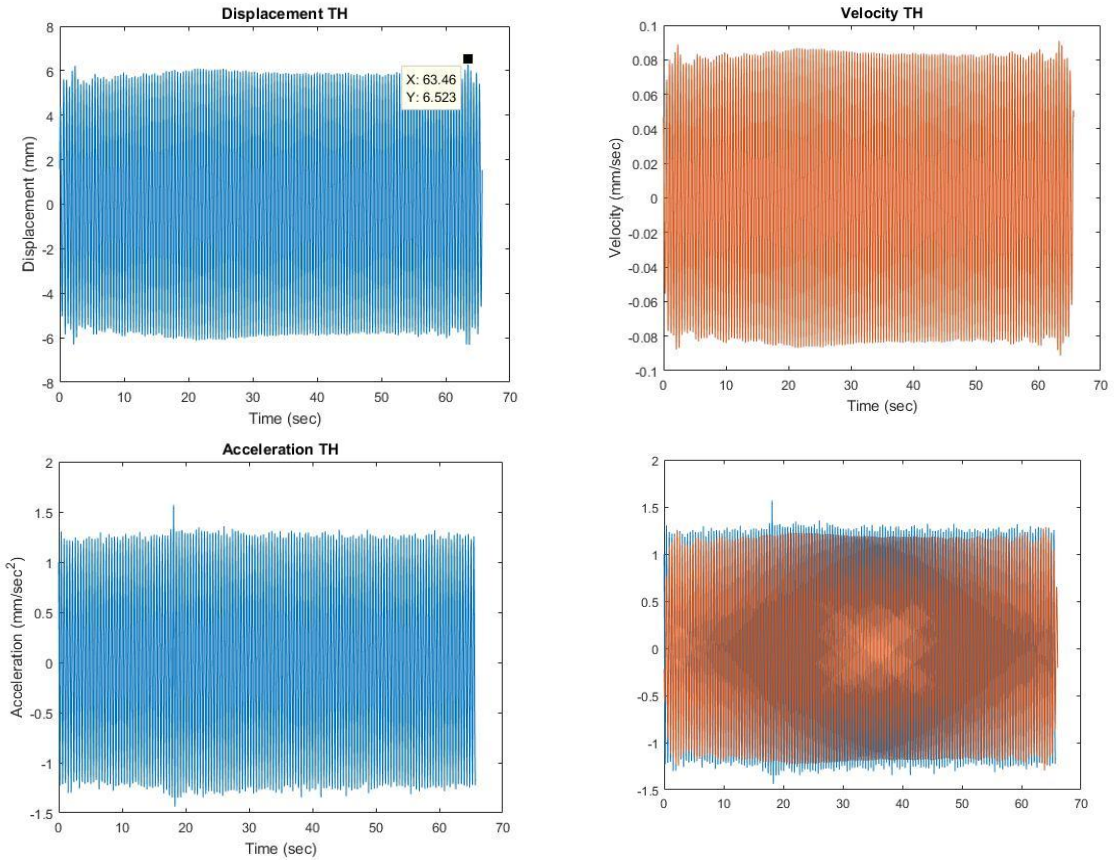

Figure 47: Time history results of model displacement (*top, left*) velocity (*top, right*) and acceleration (*bottom*) for wind speed 1.0 m/s

Furthermore, the figures (48) show the model acceleration, velocity and the vertical displacement according to wind speed of 1.1 m/s. The vertical amplitude is higher than previous ones compare with wind speed of 1.0 m/s. And the filtered acceleration looks in level values.

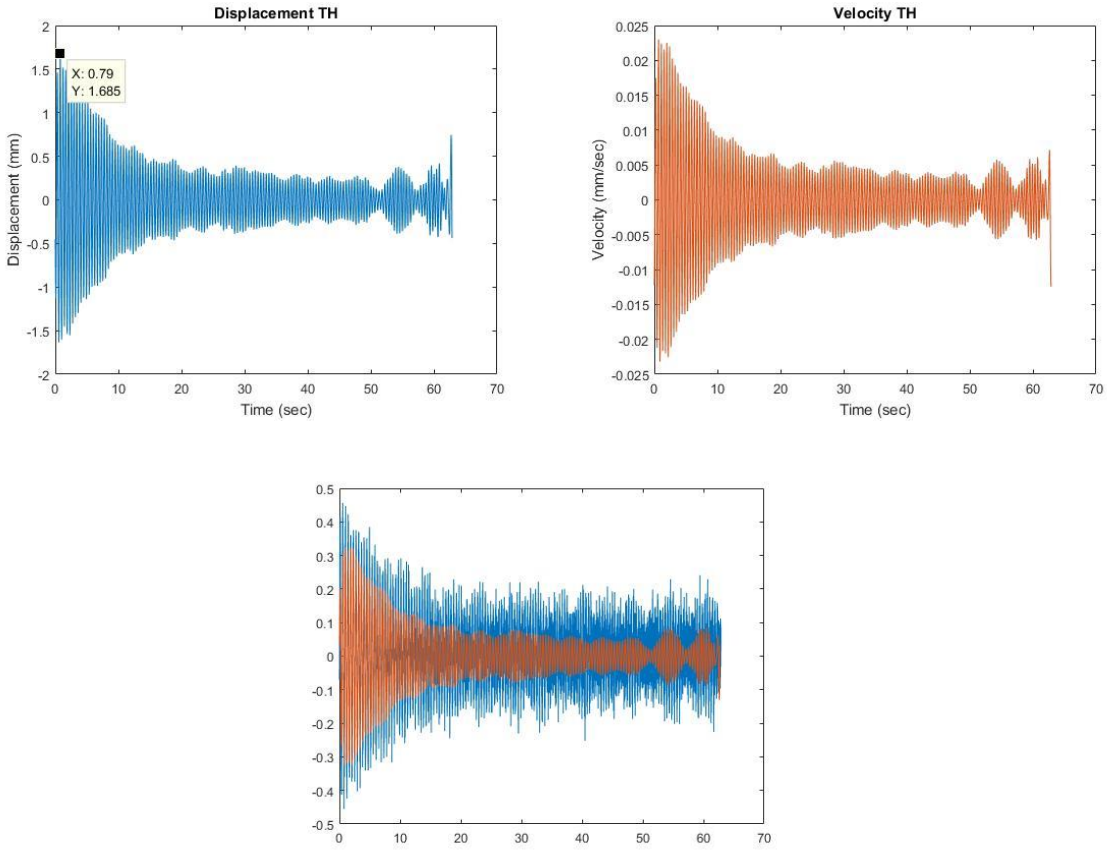

Figure 48: Time history results of model displacement (*top, left*) velocity (*top, right*) and acceleration (*bottom*) for wind speed 1.1 m/s

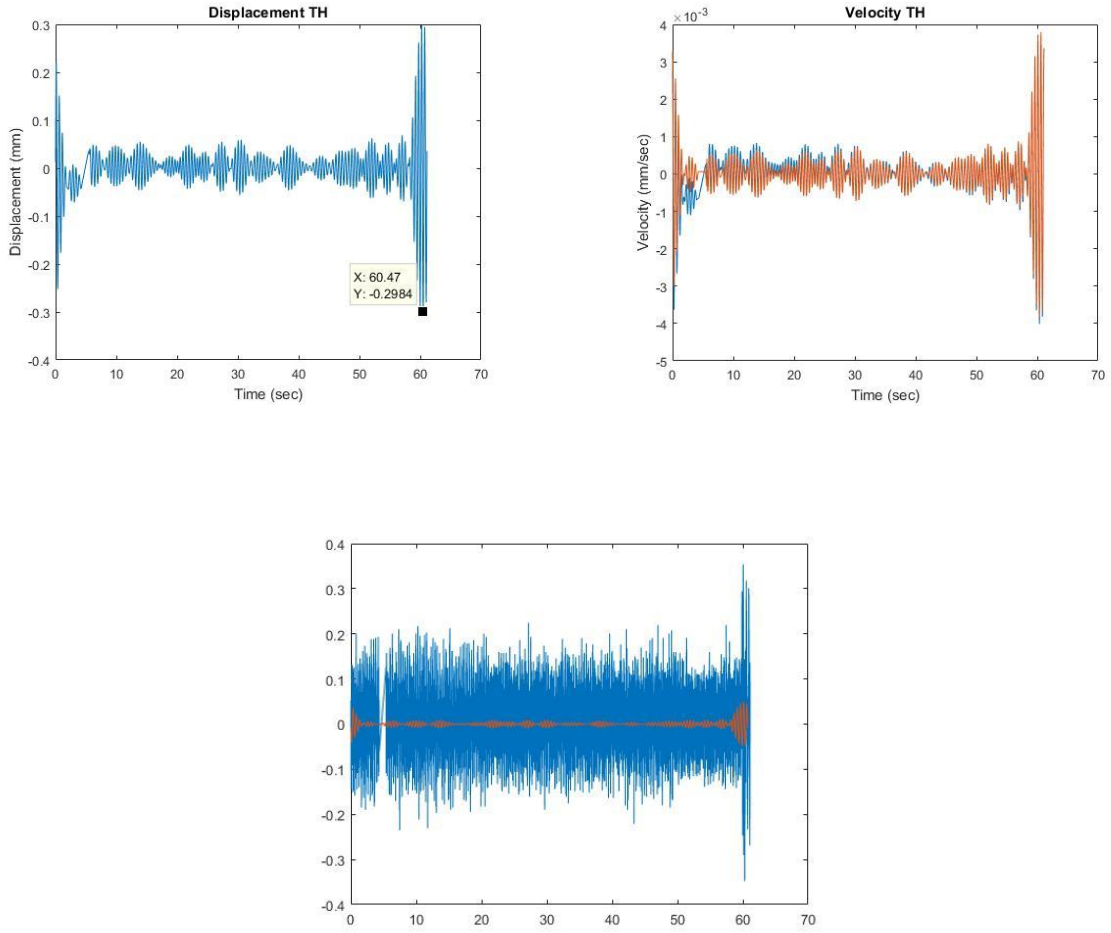

Figure 49: Time history results of model displacement (*top, left*) velocity (*top, right*) and acceleration (*bottom*) for wind speed 1.2 m/s

Finally, the figures (49) show the model acceleration, velocity and the vertical displacement according to wind speed of 1.2 m/s. The vertical amplitude is higher than previous ones compare with wind speed of 1.1 m/s. And the filtered acceleration looks in level values.

5.5 Determination of the critical/resonant wind speed analytically

Vortex induced vibrations are produced when the vortex shedding frequency, fs, coincides with or is very close in value to any of the natural vibration frequencies of the structure, fn. They are the consequence of the typical resonance phenomenon that affects only single vibration modes, mainly those associated with the fundamental frequencies excited by lower wind velocities.
The resonant wind speed is the speed at which the frequency of wind vibrations matches with the natural frequency of the structure and is given by

$$Ures = \frac{f\ D}{St}$$

Where, f, natural frequency of structure = 2.24Hz
D, depth of structure = 0.069m
St, Strouhal number calculated from static analysis using vortex shedding frequency = 0.164.

$$Ures = \frac{2.24*0.069}{0.164} = 0.942 \text{ m/s.}$$

From, experiment we found the highest vibrations were observed at wind speed of 1.0m/s.
Thus, the analytical and experimental studies are validate.

6 Comparison of the results

6.1 Static wind coefficients

In the comparison of wind coefficients, we can see that results of wind coefficients from numerical and from experimental results are slightly different. After analysis, conclusion was that an error occurred in modeling in numerical part, center of mass was not in the center of cross section.

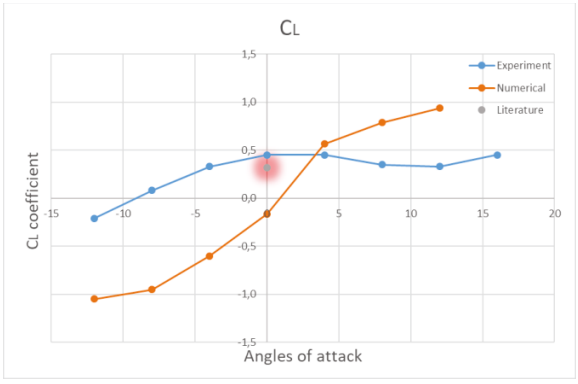

Figure 50. Coefficients of lift

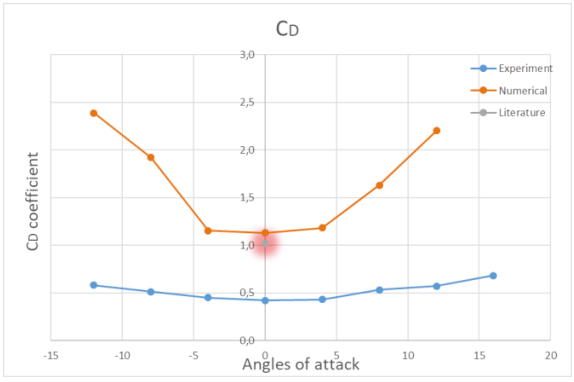

Figure 51. Coefficients of drag

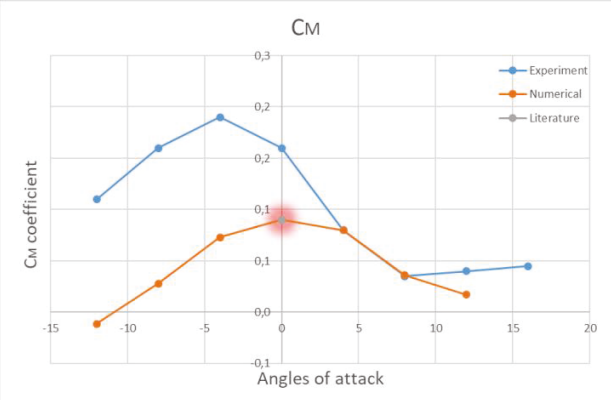

Figure 52. Coefficients of moment

The resonance velocity found in the literature was 16.8 m/s and the resonance velocity found in the numerical part was 17.2 m/s, therefore we can say that the result is close to the literature.

6.2 Resonance wind speed

After making numerical and experimental part, resonance wind speeds can be compared. For full scaled model, the result of resonance wind speed from literature and numerical part is similar. Literature value is 16.8 m/s, and numerical value is 17.2 m/s. When talking about scaled models, experimental value is determined as 0.94 m/s, and numerical results showed 1.1 m/s result.

Property	**Literature**	**Numerical**
Velocity [m/s]	16.8	17.2

Table 10: Resonance velocity of full scale

Property	**Experimental**	**Numerical**
Velocity [m/s]	0.94	1.10

Table 11: Resonance velocity for scaled model

6.3 Vertical displacment

When results from experiment was extruded from scaled dimensions, maximum amplitude was 65.23 cm. For numerical part maximum value is 86.42 cm.

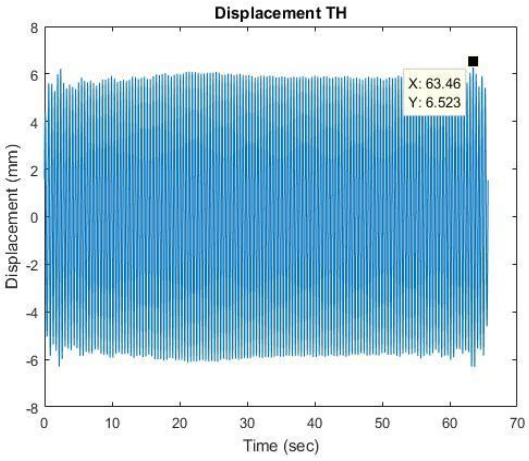

Figure 53. Experimental results

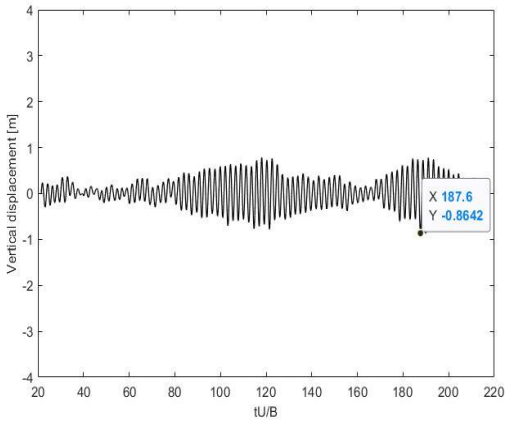

Figure 54. Numerical results

6.4 One slice and multislice comparison

After analysing results from one slice model and multislice model, we can see big differences with displacements of models. Multislice model has maximum amplitude 20.8 cm, and one slice model has maximum amplitude of 86.94 cm. When doing one slice model the only thing taken into consideration is 1 cross section, but Tokyo Bay bridge has different cross section per unit length. Because of that, multislice is much more likely to behave as original Tokyo Bay bridge then one slice model. The figures (55) and (56) show the vertical amplitude of the mid span in meter for both models, one slice model and multi-slice model. It looks that results of one slice show high values returning back to accuracy of the model comparing with the literature.

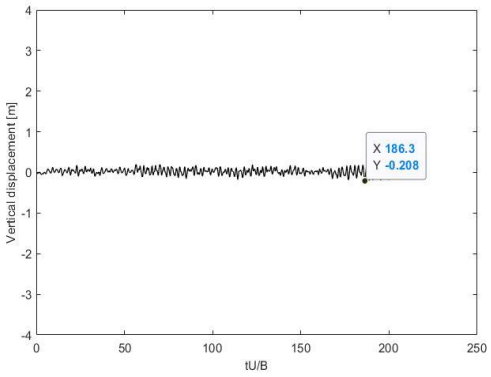

Figure 56. Multislice maximum displacement at mid span

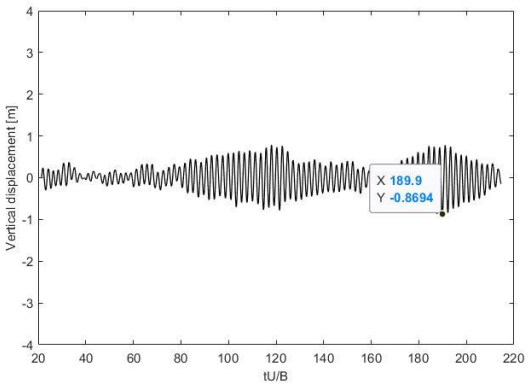

Figure 55. One slice model, maximum displacement at mid span

7 Conclusion

Vortex induced vibration phenomenon was verified experimentally and by numerical simulations resulting similarities of respected properties. What is important for conclusion is evaluating the results and go more in next future work. The experimental setting properties of scaled model are similar to the target ones. The results of static test as Strouhal number, shedding frequency and the static wind coefficients are verified well with a little difference in St number. Going ahead to the dynamic results, the most respected property is the resonant wind velocity exciting the structure causing VIV phenomena. It was different somehow comparing by guide literatures. Furthermore, the numerical simulation for the model was verified to check the full scale behaviour and the target study behaviours.

In case of respected discussed results, they still needs more simulations as to increase the number of slices and time steps. This could improve the results. Moreover, the scaled down model was done to compare with the experimental in more perfect way. Multiple identities are coming close. Finally, it could still in the same way of improving the simulations with increasing number of time step and slices.

On the other side, future work with VIV verifications and optimizing the cross-section of the bridge model are open for next work and for who are interested in. A recommendation is to optimize a suitable cross-section with little affects under wind vibrations. Finally, VIV phenomenon verifications is the most critical phenomena to study its effects on the bridges because it could be created under low speed velocity. Even though, it is not concluded for the bridges where it could be shown in many structures as chimneys, high rise buildings, nuclear structures and cold reservoirs.

References

(1) Fujino Y., Yoshida Y. (2002) Wind-Induced Vibration and Control of Trans-Tokyo Bay Crossing Bridge, Journal of Structural Engineering, August: 2002.128:1012-1025

(2) Morghenthal G. (2002) Aerodynamic Analysis of Structures Using High-resolution Vortex Particle Methods – A dissertation submitted for the degree of Doctor of Philosophy

(3) Fujino Y (2002) Vibration, control and monitoring of long-span bridges – recent research, developments and practice in Japan, Journal of Constructional Steel Research,**58**: 71-97

(4) British Standard BSI, Actions on structures-Part 1-4: General actions — Wind actions BS EN 1991- 1-4:2005. 2005.

(5) Corriols, A. Vortex-Induced Vibrations on Bridges-The Interaction Mechanism in Complex Sections and a New Semi-Empirical Model, 2015, pg. 189.

(6) You-Lin Xu, WIND EFFECTS ON CABLE-SUPPORTED BRIDGES, 2013, pg. 257.

(7) Corriols, Abraham. "Vortex induced vibrations on bridges, the interaction mechanism in complex sections and a new proposed semi-empirical model", a dissertion submitted in partial fulfillment for the doctoral of philosophy, Technical University of Madrid, November 2015.

(8) Trotec laser GMBH. "Operational Manual", December 2015.

VII. EXTRA-ACTIVITIES

The purpose of the project programme International Elective Master course, Nonlinear Analysis of Structures: Wind Induced Vibrations, is to bring knowledge and understanding of the study matter, together with other set of skills required to complete a master course in an international framework of studies. Besides that, the students had the opportunity to learn about the culture and the historical places of Weimar through guided tour around the city. In this way, the students from the partner universities and the students from Bauhaus-University were getting to know each other by trying to discover the historical places, important cultural people and their stories through a team game.

Figure 4. Pictures (top and bottom) of the course participants during the city tour

VIII. IMPRESSIONS

The students from the partner universities had the chance during their two-weeks project in Weimar to get into contact with the Bauhaus University facility and its mentors. At the end of the project, feedbacks were provided by the participants in order to understand and improve future international courses.

"The wind course was very good, I have learnt a lot of things, and working with international people helped me expand my frontiers. The lectures were fine but there is too much material to cover and not enough time. I am happy with the results and the work in international teams."

"The best experience for me was the wind tunnel experiment, as well as learning about new interesting topics, such as wind engineering. It functions well to meet in April and in August because it is enough time in between. It would be better if here we could meet in classroom like Design Room, with tables for group, so we can communicate better."

"The whole Erasmus course was a great experience."

"For me, the best part was with the tutors and prof. Morgenthal. They showed great patience, knowledge and willingness to help. Also I like the wind tunnel. The time period was fine for me. The only thing was the lack of workroom for such a great number of students, since the computer pool was too small."

"The course project was challenging and quite interesting to follow and to work on it".

"We had great mentors, they were always available for us. Best events were the Weimar tour on the first days and the barbecue party, because we get to know people much better."

"I enjoy working in a group with different background. We try to make the group works, knowing that we are too far from Weimar. I hope I can come back again to do another Erasmus+ programme."

Figure 5. Group Picture of the Course Participants